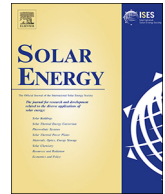




Contents lists available at ScienceDirect

## Solar Energy

journal homepage: [www.elsevier.com/locate/solener](http://www.elsevier.com/locate/solener)

## A review of solar thermal energy storage in beds of particles: Packed and fluidized beds

J.A. Almendros-Ibáñez<sup>a,b,\*</sup>, M. Fernández-Torrijos<sup>c</sup>, M. Díaz-Heras<sup>b</sup>, J.F. Belmonte<sup>a,b</sup>, C. Sobrino<sup>c</sup><sup>a</sup> Escuela de Ingenieros Industriales, Dpto. de Mecánica Aplicada e Ingeniería de Proyectos, Castilla-La Mancha University, Campus universitario s/n, 02071 Albacete, Spain<sup>b</sup> Renewable Energy Research Institute, Section of Solar and Energy Efficiency, C/ de la Investigación s/n, 02071 Albacete, Spain<sup>c</sup> Universidad Carlos III de Madrid, ISE Research Group, Thermal and Fluid Engineering Department, Avda. de la Universidad 30, 28911 Leganés, Madrid, Spain

## ARTICLE INFO

## Keywords:

Energy storage  
Packed beds  
Fluidized beds  
Thermal solar energy

## ABSTRACT

This review summarizes different solar thermal energy storage techniques from a particle technology perspective, including sensible, latent and thermochemical techniques for low- and high-temperature applications that use particles as the storage medium in the thermal energy storage system. The focus is on applications, experimental results, modeling and future trends. This review describes two different particle technologies used to store thermal energy: packed and fluidized beds. The advantages and disadvantages of both technologies are reviewed throughout different studies found in the literature for various thermal energy storage systems. Packed beds have the main advantage of thermal stratification, which increases the efficiency of solar collectors in low-temperature sensible energy storage systems and augments the exergy content in the bed. Moreover, they have been proven to be suitable as dual-media thermochemical storage systems for CSP plants. In contrast, the high mixing rates of fluidized beds makes them suitable for the rapid distribution of concentrated solar energy in particle receiver CSP systems. In addition, their high heat and mass transfer rates, compared with those of packed beds, make them the preferred particle technology for thermochemical energy storage applications. This review also notes that it is important to find new materials with an appropriate size and density that can be properly used in a fluidized bed. Additionally, more specific research efforts are necessary to improve the understanding of the behavior of these materials during the fluidization process and over a high number of charging/discharging cycles.

### 1. Introduction

The use of renewable energies, especially solar energy, requires a storage system to equilibrate the mismatch that can occur between the availability of the renewable energy and its consumption. There are different ways to store solar energy depending on the temperature, the total amount of energy to be stored, the storage time (which can vary from a few hours to several months) and of course, the final application of the energy. Low-temperature solar energy is widely used in building applications, for domestic hot water applications (Duomarco, 2015) and for building heating or air conditioning (Belmonte et al., 2016). Over the past few years, the production of electricity in CSP (Concentrating Solar Power) plants has become of great interest to the research community. The most common CSP plants are based on large parabolic trough concentrators (Gil et al., 2010), where the maximum operating temperature is typically limited to about 400 °C to avoid

thermal decomposition of the oil used as the heat transfer fluid (HTF). Another type of CSP plant is based on a field of heliostats that reflect solar beam radiation onto a central receiver. This type of plant uses molten salts as the HTF, which may allow an increase in the maximum working temperature up to 565 °C (Rodríguez-Sánchez et al., 2014). Currently, there is great interest in developing new HTFs, energy storage materials and technologies that permit even greater maximum operating temperatures, up to approximately 1000 °C (Ho, 2017), which result in a higher power plant efficiency.

Once the solar energy is collected and transferred to an HTF, the energy is usually stored in a tank or deposit. The heat storage medium can be the same HTF, a different HTF (if an intermediate heat exchanger is used), a bed of solid particles or a combination of both. Typically, solid particles store energy in sensible form by increasing their temperature. They can also be embedded or filled with a phase change material (PCM), which notably increases the energy density of

\* Corresponding author at: Escuela de Ingenieros Industriales, Dpto. de Mecánica Aplicada e Ingeniería de Proyectos, Castilla-La Mancha University, Campus universitario s/n, 02071 Albacete, Spain.

E-mail address: [jose.almendros@uclm.es](mailto:jose.almendros@uclm.es) (J.A. Almendros-Ibáñez).

<https://doi.org/10.1016/j.solener.2018.05.047>

Received 18 January 2018; Received in revised form 10 May 2018; Accepted 12 May 2018  
0038-092X/ © 2018 Elsevier Ltd. All rights reserved.

the storage system using latent energy at a nearly constant temperature. Another promising alternative is to employ a thermochemical reaction (Solé et al., 2015; Aydin et al., 2015; Prieto et al., 2016; Yadav and Banerjee, 2016). In this case, the HTF and the solid particles undergo an endothermic reaction at a certain temperature. The reversible exothermic reaction can release the energy on demand. Sensible energy storage systems require large volumes to store large quantities of energy. The use of a PCM can double or triple the energy density compared with sensible energy systems (Pardo et al., 2014b). A wide variety of PCMs have potential use in low- and medium-temperature applications (Cabeza et al., 2015), although there are still no commercially available materials that can withstand temperatures as high as those reached in CSP plants (over 400 °C). Thermochemical energy storage can store ten times more energy in the same volume (compared with a sensible energy storage system), allowing a wide range of temperatures and applications (Pardo et al., 2014b). Currently, most studies have focused on finding new materials and reactions that can reach a minimum temperature to carry out a power cycle (André et al., 2016; Prieto et al., 2016), although low-temperature applications have recently attracted much interest (Solé et al., 2015).

This paper reviews different possibilities for energy storage depending on the particle technology employed in the thermal energy storage system. Regardless of the temperature level (low, medium or high) or the form in which the energy is stored (sensible, latent or thermochemical), when particles are employed as the storage medium, they can be in a packed (also called fixed) or fluidized bed. In a packed bed, the particles or solids<sup>1</sup> are at rest, and an HTF percolates between the voids in the bed. The main characteristic of a packed bed is the use of large-sized particles typically ranging from a few millimeters up to several centimeters. In gas packed beds, the large size of the particles permits the use of high enough fluid velocities to reach turbulent flow in the fluid without notably increasing the pressure drop. In packed beds with air, which is one of the most common fluids used in packed beds, the superficial air velocity is typically around  $0.1 \text{ m/s} \lesssim u_s \lesssim 1 \text{ m/s}$ . The lower limit can lead to very low heat transfer rates between the solids and the air, whereas the upper limit can lead to an excessive gas pressure drop. Fig. 1 shows the variation in the minimum fluidization velocity, defined as the gas velocity at which the gas pressure drop overcomes the weight of the bed, depending on the particle size, assuming spherical particles with a typical density  $\rho_p = 2600 \text{ kg/m}^3$  for two different temperatures, 300 and 1000 K. The minimum fluidization velocity  $u_{mf}$  was calculated according to Kunii and Levenspiel (1991). For particles larger than approximately 1 mm, the minimum fluidization velocity is always higher than 1 m/s, which ensures that the particles in the bed are at rest.

Particles under  $d_p \approx 1 \text{ mm}$  can be easily fluidized without very high gas flow rates, which ensures a reasonable pumping cost. The fluidization process of solid particles strongly depends on the density and size of the particles. Geldart (1973) defined the fluidization regimes shown in Fig. 2, which are currently considered to be the standard classification system by the fluidization community. Geldart distinguished between four main groups of particles. The lower-left side of the diagram shows particle sizes under approximately  $50 \mu\text{m}$ , which are type C particles. These particles are very cohesive and difficult to fluidize. They tend to rise with the plug flow in beds with small diameters, or channels are formed from the distributor to the bed surface (rat holes), through which the gas can bypass the bed with little contact with the particles in beds with large diameters (see Fig. 49). Type A particles can be easily fluidized with low gas velocities and form small bubble sizes for high gas velocities. Greater particle diameters than those corresponding to the Geldart A classification lead to type B particles, which

are characterized by vigorous bubbling and mixing and are typically associated with the growth of large bubbles along the bed height. Finally, type D particles have a mean particle size  $d_p \gtrsim 1 \text{ mm}$ , which is the lower particle size limit for packed beds, as mentioned in Fig. 1. Type D particles are difficult to fluidize because very large bubbles appear at the top of the bed and the pumping cost to fluidize these large particles is very high. Therefore, type D particles are used in packed beds or, alternatively, are fluidized in a spouted bed. In this type of fluidization process, the gas is introduced to the bed through a small orifice in the center of the base of the bed. Spouted beds “...appear to achieve the same purpose for coarse particles as fluidization does for fine materials ...” (Epstein and Grace, 2011). Fig. 2 also shows a color map for the minimum fluidization velocity. For Geldart C, A and B particles, the minimum fluidization velocity is always under 1 m/s, which ensures a reasonable pumping cost during the fluidization process. In contrast, in Geldart D particles, the minimum fluidization velocity notably increases with particle size and density. Table 1 summarizes the main characteristics and differences between packed and fluidized beds, depending on the type of particle.

The original Geldart diagram was obtained for air at ambient conditions. Grace (1986) extended Geldart’s classification scheme to other gases and for a wide range of temperatures and pressures. Grace’s diagram for gas-solid contactors is represented by the following non-dimensional particle diameter and superficial gas velocity:

$$d_p^* = d_p \left[ \frac{\rho_g g (\rho_p - \rho_g)}{\mu_g^2} \right]^{1/3} \quad (1)$$

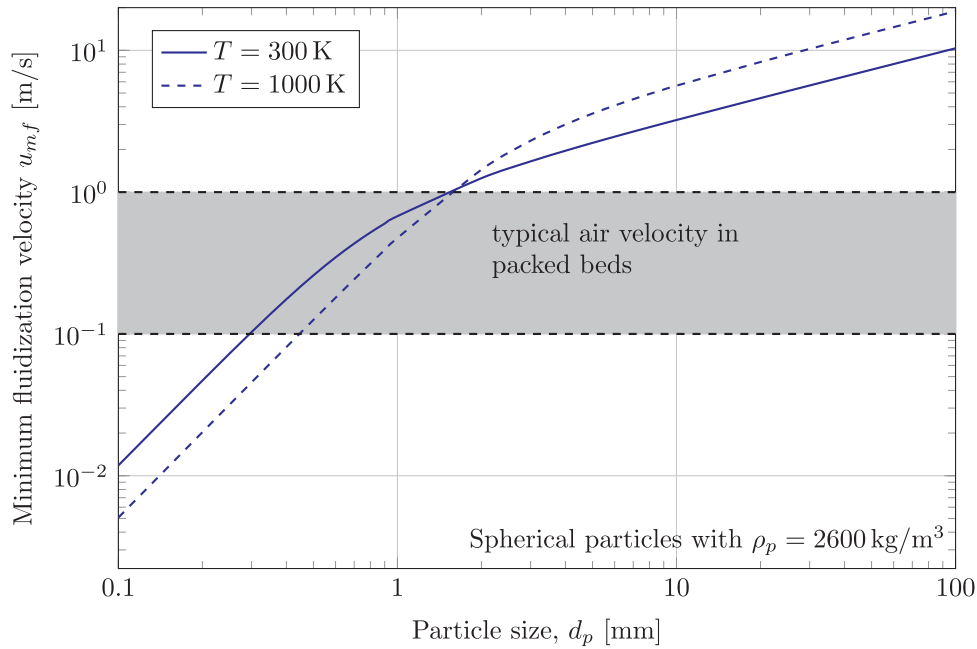
$$u_s^* = u_s \left[ \frac{\rho_g^2}{\mu_g g (\rho_p - \rho_g)} \right]^{1/3} \quad (2)$$

Fig. 3(a) shows the regions of different particle types according to Geldart’s classification and the minimum fluidization and terminal velocities of the particles. Fig. 3(b) shows the typical regions where different particle reactor types operate. Circulating bed and transport reactors operate with velocities above the terminal velocity of the particles, because in these types of reactors the solids are continuously in motion. These types of reactors are not used for thermal energy storage applications. Spouted and moving beds are contained in the region with minimum fluidization velocity and large-sized particles. The area under the minimum fluidization curve, colored in gray, corresponds to the region in which packed beds operate, whereas the region between the minimum fluidization and the terminal curves in the region of A–B particles, which is also highlighted in gray, corresponds to the region in which conventional fluidized beds operate. The regions marked in gray are the regions of interest in this review.

Although most fluidized bed applications use a gas, typically air, as the fluidizing agent, it is also possible to use a liquid, such as water, for example. Nevertheless, the behavior of a liquid-fluidized bed is completely different than that of a gas-fluidized bed. When a liquid is used to fluidize particles, once the velocity overcomes the minimum fluidization velocity, the bed expands, increasing its voidage in a homogeneous manner (Epstein, 2003). Consequently, as the liquid velocity is increased, the voidage also increases up to the terminal velocity limit. Grace (1986) also represented in a diagram the different regions observed in packed and fluidized beds using the non-dimensional variables  $d_p^*$  and  $u_s^*$ . This diagram is represented in Fig. 4. The area under the minimum fluidization curve corresponds to the region of the packed bed. Once the superficial liquid velocity is reached, the bed tends to expand, increasing the voidage until the maximum limit  $\varepsilon = 1$ , which coincides with the terminal velocity curve.

The differences between packed and fluidized beds, in addition to their different particle sizes and gas velocities, are summarized in Table 2. One of the main differences between the two particle technologies, which is of primary importance for thermal energy storage

<sup>1</sup> In this article, the only difference between “particles” and “solids” is the size. When we mention “particles” or “granules”, we are referring to small-sized particles  $d_p \lesssim 10^{-2} \text{ m}$ , while “solids” or “capsules” have larger sizes  $d_p \gtrsim 10^{-2} \text{ m}$ .



**Fig. 1.** Minimum fluidization velocity, calculated according [Kunii and Levenspiel \(1991\)](#), for spherical sand particles as a function of the particle size for  $T = 300$  K and  $T = 1000$  K. The gray region indicates the typical range of air velocities in a packed bed.

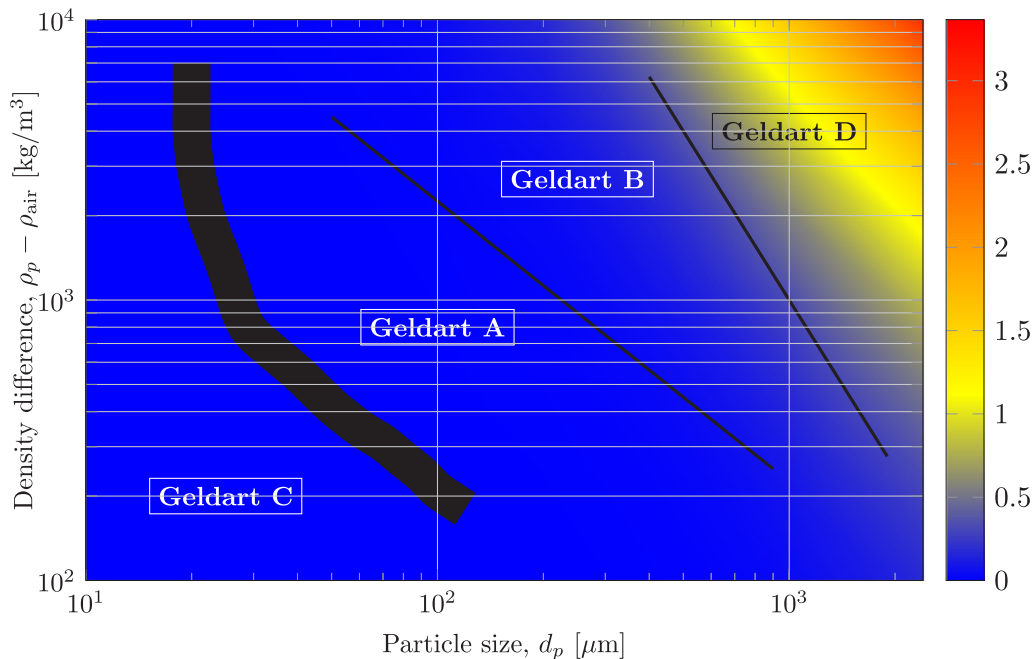


**Fig. 2.** Reproduction of the original Geldart diagram for particle classification ([Geldart, 1973](#)). The color map indicates the minimum fluidization velocity in m/s. (For interpretation of the references to color in this figure legend, the reader is referred to the web version of this article.)

applications, is the temperature distribution in the bed. In a packed bed, the temperature distribution in the bed is stratified, which is a major advantage for solar systems, as the fluid that is pumped to the solar collectors comes from the lower-temperature region of the packed bed, increasing the efficiency of the collector. [Rosen \(2001\)](#) showed that in a packed bed with the same energy content, its exergy content increases with stratification. A packed bed with a sharp thermal front, has a higher exergy content than the same bed with a lower thermal gradient in the thermocline region or a well mixed bed, because during the discharging process the HTF can be extracted at a higher temperature (higher exergy content) for longer periods of time. In contrast, fluidized beds are characterized by high mixing rates, which tend to produce a

uniform temperature distribution in the bed and therefore reduce the exergy content. The high mixing rates of fluidized beds are favorable for thermochemical reactions because the risk of hotspots is minimized and the kinetic of the chemical reactions is improved. ([Solé et al., 2015](#)).

This paper reviews the different works published in the literature that use either packed or fluidized beds as a medium for solar thermal energy storage. The review covers all the different forms of thermal energy storage, sensible, latent and thermochemical, as well as a wide range of temperature applications, from low-temperature applications used for heating, ventilation and air conditioning (HVAC) in buildings to high temperatures used in CSP plants. The main goal of this review is to compare technologies and to clearly define the advantages and

**Table 1**  
Main characteristics of the different particle types used in packed and gas-fluidized beds.

	$d_p$ [mm]	$\rho_p$ [kg/m <sup>3</sup> ]	Main characteristics	$u_{mf}$ [m/s]	Example particles
Packed beds	1–100	1000–4000	particles in rest	$\gg 1$	Rocks, sand, etc.
Fluidized beds with Geldart C particles	<0.05	100–6000	They are difficult to fluidize  There is no good contact between the air and the particles To fluidize them it is necessary to mix with type A or B particles	$O(10^{-3})$	Flour, strach
Fluidized beds with Geldart A particles	0.05–0.2	<1500	easy to fluidize with low gas velocities  Small bubbles along the bed The bed expands prior to the appearance of bubbles	$O(10^{-2})$	FCC catalyst
Fluidized beds with Geldart B particles	0.05–0.5	multicolumn111500–3000	Bubbles grow and coalesce along the bed  Vigorous bubbling and high mixing rates Bubbles appear jus after minimum fluidization velocity	$O(10^{-1})$	Sand
Spouted beds with Geldart D particles	>1 mm	100–6000	A central diluite jet region transport the particle to the bed surface Particles in the periphery moved down as in a moving bed	$\geq 1$	Drying grains, roasting coffee beans

disadvantages of packed and fluidized beds that make a particle technology more appropriate for a certain application.

## 2. Packed beds

### 2.1. Sensible energy storage

#### 2.1.1. Low-temperature applications and experiments

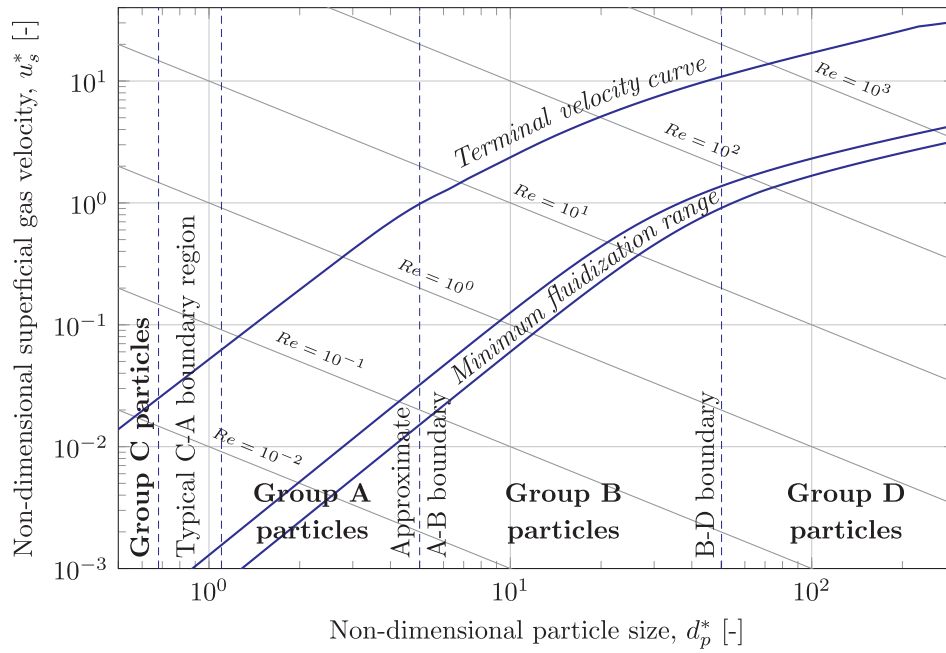
This subsection covers the current state of research in the field of low-temperature energy storage using air-based solar energy systems, based on the sensible energy stored in the thermal mass ( $\rho_p \cdot c_p$ ) of solid materials when their temperature is varied. More precisely, this subsection focuses on applications in which the temperature range of the application ranges from near ambient to values corresponding to low-pressure steam (in the range of 100–150 °C). In such applications, solar energy can be provided by nonconcentrating collectors, such as flat plate solar air heaters (SAHs). In recent years, in such temperature range, greater attention has been paid to liquid-based solar energy systems because of their higher energy density (e.g., the thermal mass of rocks is between one-third and one-half of that of water), as well as the better thermal properties of liquid HTFs compared with those of air from a heat transfer standpoint (e.g., water has a 4-times-higher specific heat and 24-times-higher thermal conductivity than air). As a consequence, greater storage volumes and pumping operation costs should be expected from solar air-based systems compared with liquid-based systems. Nevertheless, low-temperature air-based solar systems are sometimes preferred over liquid-based systems because they offer some advantages (Alkilani et al., 2011; Tyagi et al., 2012; Saxena et al., 2015), for example, SAHs are relatively simple in construction and are in general cheaper than liquid flat collectors, with high reliability for summer or winter operation. The majority of applications (except for those in which a liquid is necessary, such as for domestic hot water (DHW) applications) do not require the use of additional heat exchangers, and hence, lower SAH outlet temperatures are required for operation, which increases the SAH collection efficiency and solar utilizability (Oztop et al., 2013; Duffie and Beckman, 2013); as air is used as the HTF, problems of boiling or freezing, which water or water solutions suffer, are avoided. Additionally, the corrosion and leakage of air are not major concerns when dealing with air-based systems.

Different solid materials can be used to store sensible heat in air-based solar energy systems. The review of Singh et al. (2010) described

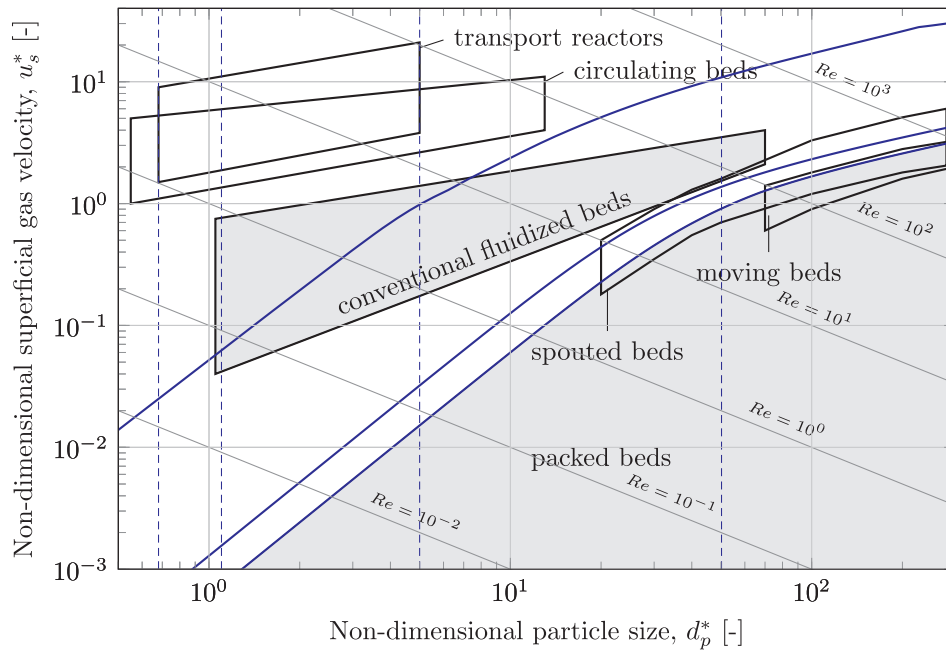
the most common materials. Table 3 lists the solid materials proposed by the authors, including water as a reference for comparison. Among them, because of their high availability and consequently low cost, pebbles and rocks (listed as stones in the table) are the most typical.

A typical rocks bed storage consists of an insulated container filled with rocks of sizes typically ranging between 0.01 and 0.05 m and a screen in the lower part of the storage bed to support the weight of the packed bed. Packed bed storage units are sized according to the load requirement and should be proportional to the collector area. Typical values found in the literature (Duffie and Beckman, 2013; Singh et al., 2015; Dincer and Rosen, 2011) recommend storage volumes per unit of collector area from 0.15 to 0.35 m<sup>3</sup>/m<sup>2</sup>. These values are much greater than those used for solar liquid systems, which are usually between 0.05 and 0.18 m<sup>3</sup>/m<sup>2</sup>. Typical design parameters for solar air-based systems are shown in Table 4. This table also includes solar liquid system parameters for comparative purposes.

Packed bed storage units usually have two (or more) openings, one in the upper part and one in the lower part of the storage bed, to promote thermal stratification. In operation, solar energy is supplied to the storage bed (charging) by hot air from the SAHs, increasing the temperature of the rocks. During this period, the airflow circulates downward through the rock bed, entering the storage unit through the upper opening so that the rocks near the top opening were heated first, leaving the storage bed by the opening located at the bottom, which is connected to the solar collector inlet ductwork. When solar energy collection is zero or small (early morning, late afternoon and during non-sunny hours), the heat recovery process (discharging) may be activated, in which the load-side fans blow cold air from the load (a building, industrial process, etc.) to the rocks bed storage. This air stream enters the storage bed through the opening at the bottom, passing upward through the rocks, leaving from the upper opening, where it is then supplied to the highest temperature level in the storage bed. In this manner the buoyancy effects maintain the shape of the thermal front and the bed has a high degree of temperature stratification. Fig. 5 plots simulation results obtained using the program TRNSYS® (Klein et al., 2017), which illustrate this concept, showing the main operation temperatures of a rock bed storage unit during a four-day operation period in winter. In this figure,  $T_{Outlet_{SAHs}}$  represents the outlet temperature from the SAH, while  $T_{Rocks_{Top}}$  and  $T_{Rocks_{Bottom}}$  are the temperatures of the rocks near the upper and lower openings of the storage, respectively. Additionally, the left axis represents the ambient outdoor



(a)



(b)

**Fig. 3.** General flow regime diagram for the whole range of gas-solid contacts (adapted from (Grace, 1986)). The minimum fluidization range reflects the difference in the mean particle diameter and the experimental scatter for different correlations. The approximate boundary for the A-B transition was calculated for  $\rho_p - \rho_g = 1000\text{--}2000 \text{ kg/m}^3$ .

temperature,  $T_{Ambient}$ . The right axis represents the airflow rates at the solar- and load-side loops, denoted in the figure as  $\dot{V}_{SAHs}$  and  $\dot{V}_{Unload}$ , respectively. These flow rates occur during charging ( $\dot{V}_{SAHs} > 0$ ) or discharging periods ( $\dot{V}_{Unload} > 0$ ), as this technology, in contrast with liquid storage systems, does not allow the simultaneous addition and recovery of heat. This figure also shows how during the charging period, the rocks at the top level are heated first, while the rocks at the bottom maintain lower temperatures. This improves the SAH efficiency, as the collector inlet temperatures are lower, and reduces the auxiliary energy needed to meet the load during the heat recovery period, as the

rocks in the upper level are the warmest. It is also shown in the figure that a uniform temperature over the entire storage volume is only achieved when it is fully discharged at night.

An example of a basic air-based solar system is reproduced in Fig. 6 (Duffie and Beckman, 2013). This schematic shows how the packed bed storage unit may link the solar resource (hot air from SAHs) and load (a building, industrial process, etc.) sides of the system in a very simple way without the need of additional heat exchangers, as air acts as the HTF and can be directly supplied to the load, permitting greater operational flexibility of the system and increasing the utilization of the

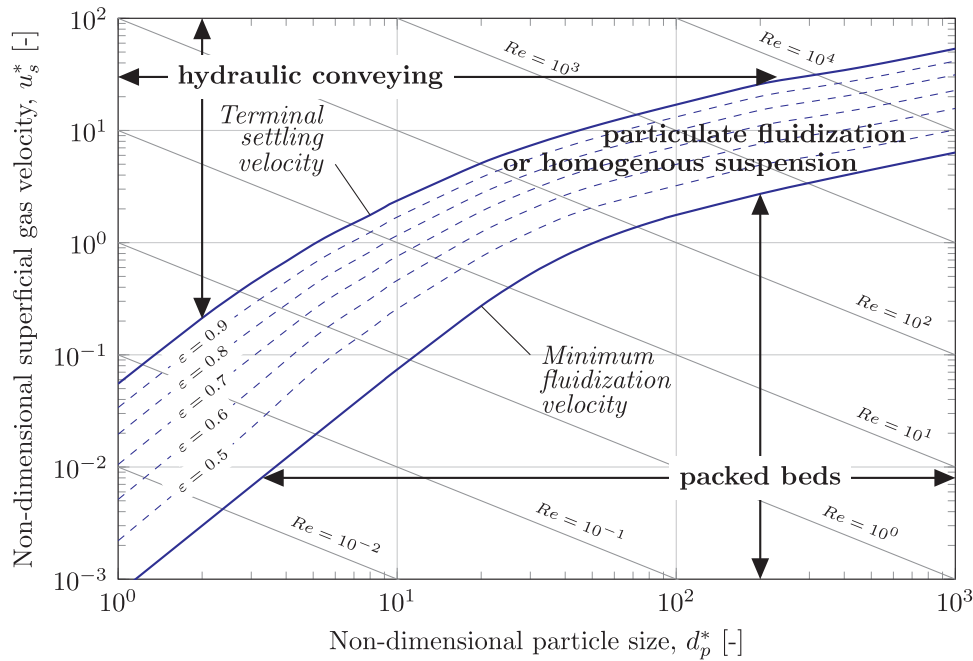


Fig. 4. General flow regime diagram of the whole range of liquid-solid contacts (adapted from Grace, 1986).

Table 2

Main characteristics of packed and fluidized beds.

	Packed beds	fluidized beds
Particle size	$\geq 1$ mm	$< 1$ mm
Temperature distribution in the bed	Plug-flow and stratified	Well mixed and homogenous
Heat transfer rate with an immersed surface	Low, $h \approx 10^{-2}$ W/(m <sup>2</sup> K)	High, $h \approx 10^2$ – $10^3$ W/(m <sup>2</sup> K)
Erosion and abrasion of the particles	Null	High
Pressure drop and pumping costs	Low-medium	Can be high for deep beds

solar energy, which is intermittent and highly variable in nature.

There is a wide variety of low-temperature applications in which this storage technology can be used, such as in greenhouses to store part of its heating needs, which will extend the cultivation period of agricultural products and thus increase their productivity. An example of this application can be found in the work of Ozturk and Bascetincelik (2003). In this work, the authors studied the energy and exergy performance of a greenhouse with a floor area of 120 m<sup>2</sup>, heated by a solar system with 27 m<sup>2</sup> of SAHs using an underground packed bed storage unit of 7.2 m<sup>3</sup> filled with volcanic stones.

Another related application is in the field of agricultural crop drying. A number of works can be found in the literature with the aim of achieving efficient drying process for long periods of time for different agricultural products, such as onions, apples, grapes or pepper, using different system configurations (Atalay et al., 2017; Abu-Hamdeh, 2003; Fohr and Figueiredo, 1987; Tomar et al., 2017; Jain, 2005; Helwa and Abdel Rehim, 1997). Fig. 7 shows an example configuration for this application, in which the trays for crop drying are located above the packed bed storage unit, which stores the thermal energy from hot air blown from the greenhouse during sunny hours to provide heating during non-sunny periods.

Another example configuration of a solar dryer integrated with a packed bed unit was proposed and experimentally tested by Atalay et al. (2017). The studied system, which was designed for drying apple

Table 3

Comparison of the thermal properties of sensible heat storage materials (Singh et al., 2010).

Medium	Density $\rho$ [kg/m <sup>3</sup> ]	Specific heat $c_p$ [kJ/kg K]	Heat capacity $\rho \cdot c_p$ [kJ/m <sup>3</sup> K]	Thermal conductivity $\lambda$ [W/mK]
Aluminum	2707	0.896	2425.47	204 at 20 °C
Aluminum oxide	3900	0.84	3276	
Aluminum sulfate	2710	0.75	2032.50	
Brick	1698	0.84	1426.32	0.69 at 29 °C
Brick magnesia	3000	1.13	3390	5.07
Concrete	2240	1.13	2531.20	0.9–1.3
Cast iron	7900	0.837	6612.30	29.3
Pure iron	7897	0.452	3569.44	73.0 at 20 °C
Calcium chloride	2510	0.67	1681.70	
Copper	8954	0.383	3429.38	385 at 20 °C
Earth (wet)	1700	2.093	3558.10	2.51
Earth (dry)	1260	0.795	1001.70	0.25
Potassium chloride	1980	0.67	1326.60	
Potassium sulfate	2660	0.92	2447.20	
Sodium carbonate	2510	1.09	2735.90	
Stone, granite	2640	0.82	2164.80	1.73–3.98
Stone, limestone	2500	0.9	2250	1.26–1.33
Stone, marble	2600	0.8	2080	2.07–2.94
Stone, sandstone	2200	0.71	1562	1.83
Water (For reference)	1000	4.186	4186	0.591 at 15 °C

slices, consisted of a drying cabin containing 10 trays, a heat recovery system, 3 SAHs with an area of 2 m<sup>2</sup> each and a packed bed thermal storage unit containing approximately 2000 kg of pebbles to provide greater stability and continuity to the drying process. The studied drying system was able to dry 7 kg of apple slices in 5–6 h through 12 experiments conducted in August and September under weather conditions typical for Turkey.

Packed bed storage units can also be integrated in buildings for DHW or space heating or cooling applications (Duffie and Beckman, 2013; Ahmed Ghoneim, 1989) to store part of their heating or cooling

**Table 4**

Typical design parameters for low-temperature solar air-based and liquid-based systems (Duffie and Beckman, 2013).

Parameter	Solar air-based systems	Solar liquid-based systems
Collector flow rate	5–20 $\frac{l}{s \cdot m^2}$	30–70 $\frac{l}{h \cdot m^2}$
Storage capacity	0.15–0.35 $\frac{m^3 \text{ of pebbles}}{m^2 \text{ of solar collector}}$	50–180 $\frac{l \text{ of water}}{m^2 \text{ of solar collector}}$
Pebble size (graded to uniform size)	0.01–0.05 m	–
Bed length, flow direction	1.25–2.5 m	–
Pressure drops:		
Pebble bed	55 Pa	–
Collectors	50–200 Pa	–
Ductwork	10 Pa	–
Maximum recommended entry velocity	4 m/s	1.5–2 m/s

needs. An example of a solar air system integrated with a packed bed storage unit, capable of providing part of the DHW, space heating and cooling needs, is reported in the work of Karaki et al. (1977). The authors presented experimental data gathered during operation of the Colorado State University House II (CSU II House) solar air system integrated with a packed bed unit during the heating season of 1976–77. This solar system had a solar field with a net area of 64.1 m<sup>2</sup> of conventional SAHs and a nearly cubic storage unit containing 10.2 m<sup>3</sup> of pebbles with sizes between 2 and 4 cm. This system required an air-to-water heat exchanger to preheat the DHW. For year-round operation, two fans were necessary, one for heating the building and a second for cooling, which also supplied hot air to the DHW preheat tank. A summary of the most relevant operating data obtained during several months of the heating season is plotted in Fig. 8. The tested solar air

system was able to deliver large solar energy contributions from the DHW and meet the space heating demand of the building. The delivered solar energy represented solar fractions between 52% and 91% in the case of DHW and between 53% and 86% of the space heating needs. Solar fraction is defined as the ratio of the solar contribution to the load divided by the load.

Finally, although it is more difficult to find, this storage technology can also be used in solar desiccant systems to allow operation during hours of inadequate solar radiation (Duffie and Beckman, 2013).

### 2.1.2. Operation of a thermocline tank

This subsection focuses on CSP storage systems, in which the thermal energy in the HTF is used to heat a packed bed of solid particles. Most packed bed systems have a single tank that acts as a thermocline, so that the tank contains both HTF hot and cold reserves and a filler material compatible with the HTF, which provides sensible heat capacity at a reduced cost. A thermocline storage system is considered to be a low-cost storage system alternative to active two-tank systems, as they use molten salt as a liquid storage medium, so that the volumes of hot and cold liquid are maintained in separate tanks. Bayon and Rojas (2013) established that the cost of the tanks and the molten salt inventory dominates the two-tank storage system cost. Thus, thermocline tanks have the advantages of using one tank instead of two tanks and having a lower volume of Solar Salt than two-tank systems (Kolb, 2011), being the cost of thermocline tanks approximately 2/3 the cost of a two-tank system for parabolic trough power plants (Pacheco et al., 2002). Moreover, Rodríguez et al. (2016) concluded that direct thermocline systems enable a reduction in the capital investment of 41.6%, while this figure was 25.3% for indirect systems (with an intermediate heat exchanger between the solar collection and the storage systems).

Fig. 9 shows the temperature profile inside a conventional rock-filled thermocline tank. Hot salt is stored at the top of the tank and is withdrawn during the discharge process to generate steam. Cold salt is stored at the bottom of the tank and exits the tank floor during the charge process to be heated in the solar receiver. During charging, the

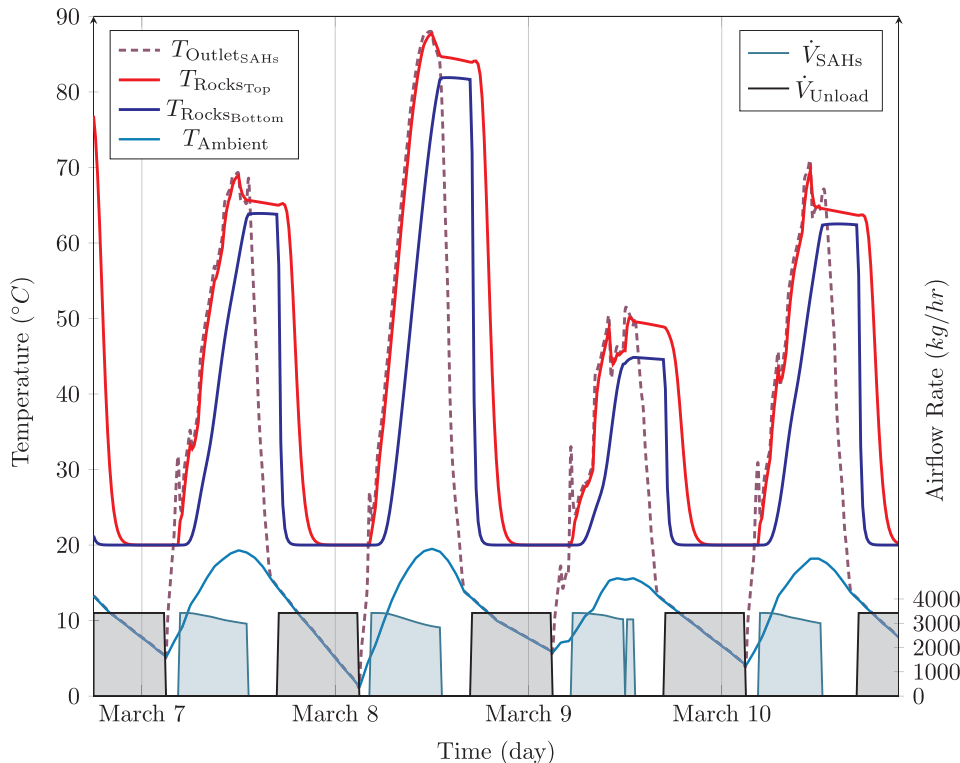


**Fig. 5.** Example of the temperature stratification in a rock bed storage unit over four days of operation. Simulation results were obtained from TRNSYS® Klein et al. (2017) using the standard component Type 10.

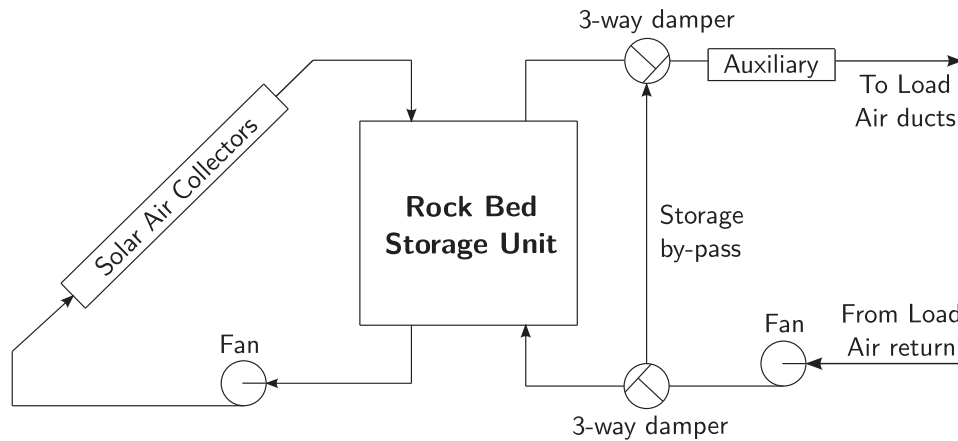


Fig. 6. Schematic of a basic air-based solar system (Duffie and Beckman, 2013).

hot HTF from the collection field enters the tank at the top, flowing down and transferring the heat through the porous bed, and leaves from the bottom of the tank, so that the heat-exchange region moves downward until the tank is filled with hot HTF. For the discharge process, the flow is reversed, so that the cold HTF enters the tank at the bottom, and is heated as the fluid flows up through the porous bed, until the heat-exchange region climbs to the top of the tank. The operation of the CSP plant entails a minimum threshold temperature ( $T_{\text{discharge, cut-off}}$ ) for the molten salt extracted from the tank during discharging that is useful for steam generation, and a maximum threshold temperature ( $T_{\text{charge, cut-off}}$ ) during charging to prevent overheating inside the receiver. Both temperature limits result in an intermediate thermal dead zone that cannot exit the thermocline tank.

In order to evaluate the degree of stratification of a thermocline tank, Zavattoni et al. (2015) defined the stratification efficiency by,

$$\eta_{str} = \frac{\Delta S_{\text{fully-mixed}} - \Delta S_{\text{real}}}{\Delta S_{\text{fully-mixed}} - \Delta S_{\text{stratified}}} \quad (3)$$

where  $\Delta S_{\text{real}}$  is the entropy change of a real system, with respect to the initial dead-state,  $\Delta S_{\text{stratified}}$  is the entropy change of a perfectly stratified TES (a packed bed with two adiabatically-separated regions, the one at the high temperature at the top and that at low temperature at the bottom) and  $\Delta S_{\text{fully-mixed}}$  is the entropy change of a fully mixed TES (considering the entire volume of the packed bed at the average temperature). According to the proposed definition, a stratification efficiency close to unity indicates that the real TES is operating with a sharp thermal stratification, and consequently the thermal energy is stored at the highest thermodynamic quality.

The particle size has a notable influence on the thermal front (White, 2011; White et al., 2014, 2016). For small particles, the heat transfer area between the HTF and the particles augments, and the

length of the thermocline region is reduced. This fact reduces the irreversibility associated with the heat transfer. In contrast, the pressure drop of the HTF along the bed increases when the particle size is reduced, and the irreversibility associated with this pressure drop augments. As a consequence, there is an optimum particles size that minimizes the sum of both effects. For example, White et al. (2014) fixed a particle size of 10–20 mm to avoid an excessive pressure loss in a thermocline tank with argon as HTF.

### 2.1.3. High-temperature applications and experiments

The most common liquid materials used for thermal storage in CSP plants are molten salts, as they present high thermal capacity, high thermal stability at high temperatures, low vapor pressure, low viscosity for reducing the pumping costs, high thermal conductivity, non-flammability and non-toxicity (Nunes et al., 2016; Pelay et al., 2017; Srivastva et al., 2017). The two leading candidates are the binary mixture Solar Salt, consisting of 60%  $\text{NaNO}_3$  and 40%  $\text{KNO}_3$ , and the ternary mixture HitecXL, formed by 48%  $\text{Ca}(\text{CO}_3)_2$ , 7%  $\text{NaNO}_3$  and 45%  $\text{KNO}_3$  (Gil et al., 2010). Solar Salt has the highest thermal stability (600 °C), the lowest cost, and the highest freezing point (221 °C), whereas HitecXL has the advantage of presenting a lower freezing point at 133 °C, but its thermal stability is limited to 500 °C (Kearney et al., 2003). According to Zhao and Wu (2011) and Kearney et al. (2003) the cost of the Solar Salt was 0.5 "\$"/kg and 1.1 "\$"/kg for the HitecXL. The major obstacle of the molten salt is its high freezing point, which demands increased operation and maintenance requirements. Zhao and Wu (2011) reported a novel ternary salt mixture of  $\text{KNO}_3$ ,  $\text{LiNO}_3$  and  $\text{Ca}(\text{CO}_3)_2$  with a low melting temperature below 100 °C, and Wang et al. (2013) presented a quaternary salt consisting of a mixture of  $\text{LiNO}_3$ ,  $\text{KNO}_3$ ,  $\text{NaNO}_3$  and  $\text{NaNO}_2$  with a freezing point at 100 °C and a higher heat capacity than both Solar Salt and HitecXL.

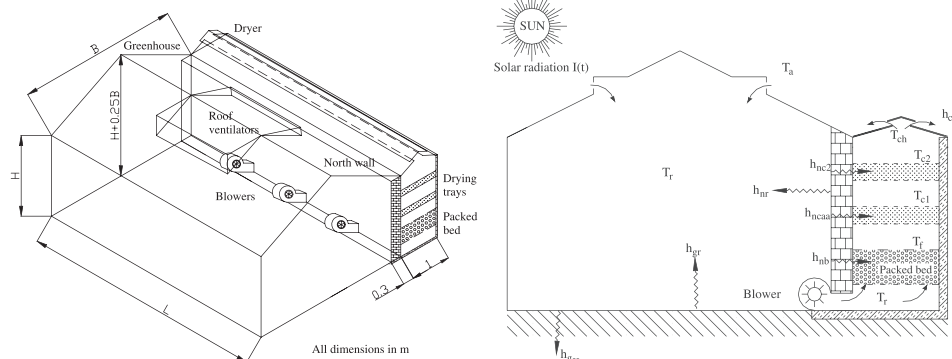


Fig. 7. Schematic views of a greenhouse and crop dryer for drying onions in trays with an integrated packed bed storage unit (Jain, 2005).

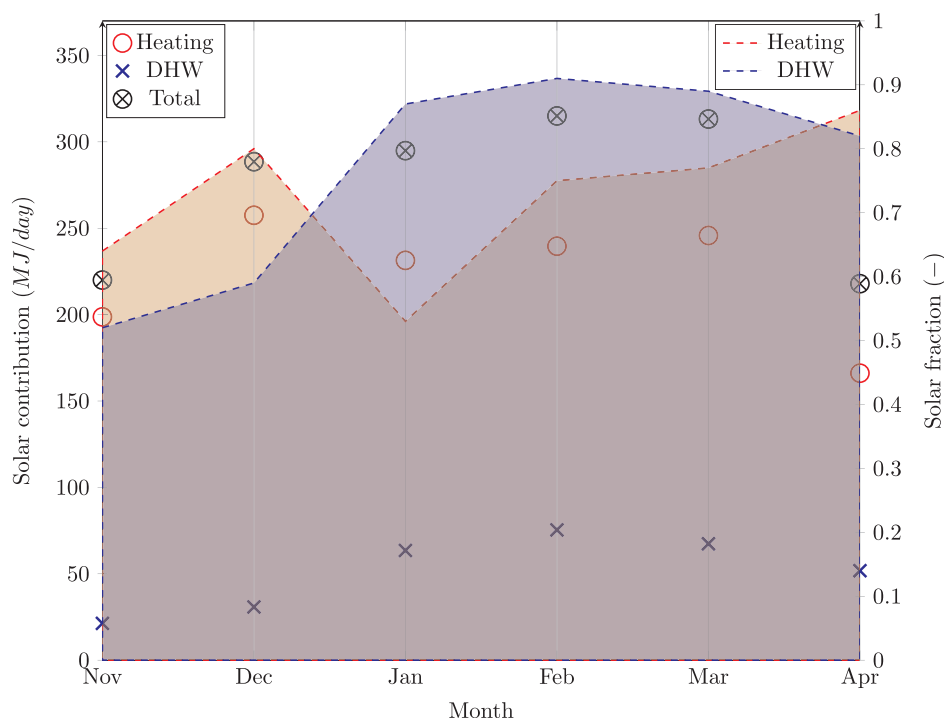


Fig. 8. Experimental results collected during 6 months of operation of the CSU II House solar air system (Karaki et al., 1977). Monthly average values for the heating season from 1976 to 77. Data from Duffie and Beckman (2013).

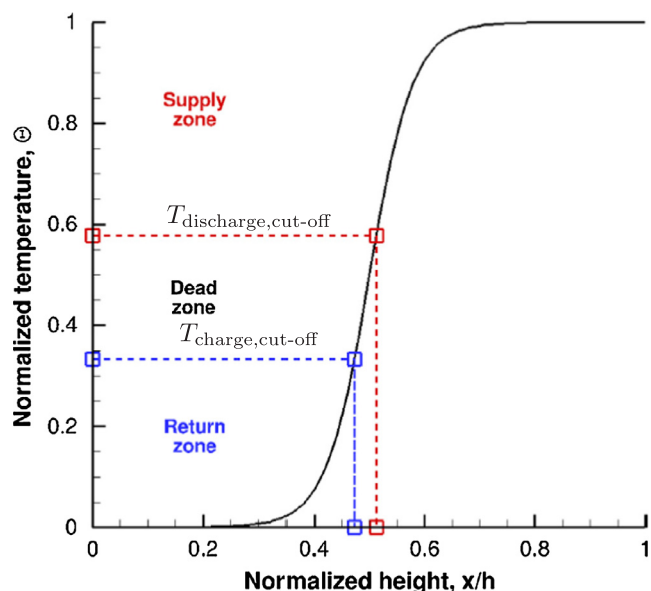


Fig. 9. Temperature profile of the molten salt inside a conventional rock-filled thermocline tank (Flueckiger and Garimella, 2014).

In a thermocline tank, the liquid HTF and the filler bed are in direct contact, so the materials must be chemically compatible. The ideal filler material must be inexpensive, widely available and non-hazardous; have a high heat capacitance and a low void fraction to reduce the amount of liquid required; and be compatible with the salt. Pacheco et al. (2002) tested the compatibility of some materials with both Solar Salt and HitecXL. They concluded that both taconite pellets and quartzite rock presented acceptable behavior under thermal cycling conditions typical of a thermocline system. In the experiments, they added filter sand to reduce the void fraction in the thermocline tank.

Sensible heat storage in a packed bed of rocks is especially suitable in air-based central receiver CSP plants, which uses air as the HTF.

Therefore, a heat exchanger between the HTF and the storage tank is not necessary, and the operating temperature constraints due to chemical instability of the HTF or the rocks are eliminated. However, higher air mass flow rates and larger surface areas are needed due to the lower volumetric heat capacity and thermal conductivity of air compared with those of other proposed HTFs (Hanchen et al., 2011).

For air-based central receiver CSP plants, Fricker (2004) studied the storage efficiency and cost of different ceramic bodies for high-temperature storage up to approximately 800 °C. They concluded that a packed bed of ceramic saddles has the lowest cost and the highest net capacity as a function of gross storage capacity, followed by a packed bed of ceramic spheres.

Meier et al. (1991) measured the transient behavior of magnesium silicate rock as the storage material at 550 °C during the charging process, and the results showed a fairly well-stratified temperature distribution.

Furnas (1930) experimentally studied the heat transfer process from a stream of air to a bed of iron balls at temperatures up to 750 °C for different particle sizes, temperatures and flow rates, and they concluded that the heat transfer coefficient increases with temperature and gas velocity and decreases for higher particle diameters. Nsofor et al. (2001) used cylindrical pellets of zirconium oxide as the heat storage material to measure the convective gas-pellet heat transfer coefficient in a packed-bed. The correlation developed is valid for temperatures up to 1000 °C and Reynolds numbers between 50 and 120.

Thermal oil is another liquid that has been employed as storage fluid in CSP plants. However, due to its higher cost in comparison to molten salt, commercial parabolic through power plants that work with thermal oil in the solar field, employ molten salt as the storage media in a two-tank system. Dual-media thermoclines, consisting of a packed bed of rocks and thermal oil, have been proposed as an alternative to reduce the cost of the storage system in plants where the oil is intended to be used both in the solar field and the storage system. For example, Bruch et al. (2014) built an experimental test loop to study the charging and discharging process of a dual-media TES system of rocks and sand and thermal oil, where the maximum inlet temperature of the thermal oil was 300 °C. In their experiments, 250 thermocouples installed inside the

tank along the radial and axial directions allowed to check the transversal temperature uniformity, with maximum temperature differences of 15 °C at a given axial position for the highest mass flux tested. In this manner, the one-dimensional assumption made in their numerical model was corroborated. Additionally they proposed a new approach, experimentally verified, for the application of the Ergun equation (Ergun, 1952) to calculate the pressure drop in a bed made of a mixture of sand and rocks of different particle size. Moreover, the model proposed was verified with experimental data, concluding that to represent accurately the experimental behavior, the thermal capacity of the tank wall needs to be considered in the model, what is done typically through the inclusion of an equivalent density in the solid energy equation, that accounts for the additional mass of the wall.

#### 2.1.4. Numerical modeling: description

Modeling the thermal performance of a packed bed storage unit is a complex task because of the complex heat transfer and fluid transport phenomena involved. When using a stream of low-temperature air (or other gas) as the HTF, some simplifications can be assumed without significant loss of accuracy. Although all heat transfer mechanisms are present during heat exchange between the air stream and the particles, they do not contribute equally, and the heat transfer process is mainly dominated by the convection term due to the low thermal conductivity of air. Radiation, as well as heat conduction within a particle (intra) and between particles in direct contact (inter), usually do not play an important role in heat exchange and are thus negligible in most models (Jalalzadeh-Azar et al., 1996). For this reason, the shape and size of particles, as well as their position and orientation in relation to the airflow direction (as these factors are responsible for the turbulent flow behavior), are major factors in analyzing heat transfer (Singh et al., 2009) in a packed bed with a low-temperature gas as the HTF.

The first attempt to model packed beds was by Anzelius (1926) and years after by Schumann (1929), with the development of the “Schumann model”. Anzelius (1926) presented the solution for the temperature difference between both phases whereas Schumann (1929) extended the previous work of Anzelius (1926) obtaining the solutions for the temperatures of the gas and solid. This model is a two-phase continuous model that neglects thermal diffusion in both phases, i.e., the interparticle conduction and the energy stored in the gas phase. This last simplification is acceptable when air is used as the HTF because its thermal capacity is several orders of magnitude lower than that of solids. To ensure energy balance between the fluid and particles, both equations can be mathematically coupled by a common convection heat transfer term. One important limitation of the Schumann model, which was treated in detail by various authors years later, is that it does not take into consideration the internal heat conduction within the solid particles. For this reason, this method is only considered adequate for low Biot numbers. The Biot number is defined as:

$$Bi = \frac{h d_p}{k_p} \quad (4)$$

where  $h$  is the convective heat transfer coefficient between the fluid and the external surface of the capsule or granule,  $d_p$  is the characteristic particle size and  $k_p$  is the thermal conductivity of the particles.

For practical purposes, some authors (Singh et al., 2009; Xu et al., 2012a; Esence et al., 2017) have established a limit for the application of the two-phase continuous model to Biot numbers less than 0.1. A different approach to model the behavior of packed beds is to extend the validity range for applications of lumped capacitance methods based on zero-dimensional (0D) models (only valid for small Biot numbers, as they are based on the assumption that the temperature of the particle is only a function of time) to greater Biot numbers. Following this approach, Xu et al. (2012a) developed an interesting method capable of accurately predicting the thermal behavior of storage units and compared their results to analytical results. The model

proposed by the authors showed good agreement with analytical results for a wide range of Biot numbers up to  $Bi = 100$ . In this study, the authors proposed a novel approach by modifying the expressions for both the heat transfer coefficient between the fluid and particles and the Biot number of the storage unit, presenting formulas for the effective expressions (for both the heat transfer coefficient and Biot number) that could be used in the lumped capacitance method to include the intraparticle heat conduction effect. However, the analytical approaches mentioned above, although useful, were still not able to reproduce the long-term thermal response of solar energy systems operating under real conditions, characterized by arbitrary time-dependent inputs (such as solar radiation, temperature, etc.); therefore, the integration of packed beds in more complex and realistic systems required the use of numerical techniques.

In packed beds at high temperature, the main difference from low-temperature modeling is the ability to account for radiative heat transfer between the HTF and the particles, which is neglected for low-temperature applications. Another important aspect is the thermal energy stored in the HTF within the tank. For packed beds with air as the HTF, the energy stored in the gas is several orders of magnitude lower than that stored in the solids and is thus usually neglected, as in the Schumann model. In contrast, when using a liquid as the HTF, because its heat capacity is similar to that of the solids in the bed, this term must be retained in the energy balance equations. Additionally, the Biot number cannot be below 0.1 in some cases, depending on the heat transfer coefficient between the fluid and the solids. The thermal conductivity of the liquids is higher than that of air, although the liquid usually flows in the bed at lower velocity, which reduces the heat transfer coefficient. For cases where  $Bi > 0.1$ , interparticle conduction should be taken into account in the model.

Apart from simple packed bed tanks, in recent years, work on the thermal modeling of tanks for high-temperature applications has focused on predicting the performance of thermocline tanks. Thermocline storage tanks for CSP plants have been simulated as packed bed systems. Most of the numerical models of thermocline tanks solve the heat transfer between the HTF and the filler by considering a volumetric interstitial heat transfer coefficient calculated from empirical correlations. Commonly, the solid filler is treated as a dispersed phase embedded in a continuous HTF phase, so the effective thermal conductivity of the HTF-filler mixture is obtained from empirical correlations. There are different correlations in the literature for both, the interstitial heat transfer coefficient (Gupta et al., 1974; Wakao et al., 1979; Dixon and Cresswell, 1979; Achenbach, 1995) and the effective thermal conductivity (Yagi and Kunii, 1957; Yagi et al., 1960; Krupiczka, 1967; Elsari and Hughes, 2002; Van Antwerpen et al., 2010; Suárez et al., 2017). Depending on the author, some discrepancies can be observed. For example Wakao et al. (1979) observed discrepancies in the heat transfer coefficient up to a factor of 4. Nevertheless, the use of different correlations for both the interstitial heat transfer coefficient and the effective thermal conductivity from the literature was studied by Xu et al. (2012b), concluding that the predictive thermal performance is relatively insensitive to the correlation chosen.

#### 2.1.5. Numerical modeling: results for low-temperature applications

Using a numerical approach to model heat transfer within a packed bed, Kuhn et al. (1980) applied a finite-difference method to numerically approximate the differential equations of the two-phase continuous model for the fluid and bed temperature. They concluded that the simplified model proposed by Hughes et al. (1976) (commonly known as the “infinite-NTU method” or the “Single-Phase Model”), based on the assumption that the temperatures of the particles and air at any point in the bed are equal, produced essentially the same results as the two-phase continuous model for the majority of situations, while requiring much lower computing costs. Such situations in which the “infinite-NTU method” was fully applicable without significant loss of accuracy were defined by Hughes et al. (1976) as those in which the

corrected values of  $NTU$  ( $NTU_c$ ) proposed by Jeffreson (1972) were much greater than ten, which in practice, corresponds to the majority of packed bed units. Using a finite-difference method, other similar approaches can be found in the literature, such as that developed by Mumma and Marvin (1976), which proposed a simplified one-dimensional heat transfer model to solve the transient response of the packed bed.

Saez and McCoy (1982) developed a basic numerical model that could be implemented in a programmable calculator of that year. Compared with the experimental and analytical results, the proposed method was able to accurately reproduce the axial heat dispersion and intraparticle heat conduction in a packed bed.

Singh et al. (2015) proposed a simplified numerical model, which demonstrated good agreement with experimental tests conducted in a packed bed heat storage system containing 8500 kg of pebbles with an equivalent diameter of 5 cm. The authors reported that the discrepancy between the predicted and experimental hot air temperatures exiting the bed varied by  $\pm 10\%$  during the tests.

To optimize the storage design and propose guidelines for the adequate sizing of energy storage units, many researchers have noted the inevitable trade-off between enhanced thermal performance and increased pressure drop related to the cost of pumping air through the packed bed. Zavattoni et al. (2015) and White et al. (2016) analysed and quantified the different exergy losses that occur in packed beds. To improve the exergy efficiency of packed beds with sensible energy storage, different works proposed to segment the bed into different layers to promote thermal stratification throughout the bed. Crandall and Thacher (2004) showed that dividing the bed into different segments and with an appropriated control scheme, stratification is preserved, getting higher temperatures during the discharging process than those achieved in a conventional bed.

Several works can be found in the literature (Maaliou and McCoy, 1985; Choudhury et al., 1995; Singh et al., 2006, 2013; Webb, 1979; Agrawal et al., 2018) that report that the storage geometry, rock size and shape, void fraction and airflow rates are the main parameters to consider in the design process to achieve an acceptable solution between the minimum friction factor (related to air pumping costs) and the maximum heat transfer coefficient (related to the thermal performance). In this direction, Maaliou and McCoy (1985) optimized, from an economic standpoint, the main operating parameters of a cylindrical storage containing steel and rock spheres, namely, its bed length, diameter, airflow rate, diameter of the particles and collection time. A similar study was conducted by Choudhury et al. (1995) for a storage bed with a square cross-sectional area by including the total energy stored in the storage unit in the economic optimization process. Singh et al. (2006) treated the trade-off between the thermal performance and pressure drop comprehensively, reporting an extensive number of correlations for the Nusselt number and friction factor as function of Reynolds number ( $Re$ ), airflow rate ( $\dot{V}$ ), sphericity ( $\psi$ ) and void fraction ( $\epsilon$ ) for different shapes. Table 5 reports the range of variation of the input variables considered in their work. Years later, these authors, in a different work (Singh et al., 2013), discussed in more detail the thermo-

hydraulic relations in packed beds among temperature stratification, thermal performance, void fraction, and the shape and packing arrangement of the particles in the bed by studying particles with different sphericity (from perfect spheres ( $\psi = 1$ ) to rectangular blocks with  $\psi = 0.65$ ) and concluded that spheres with the minimum void fraction ( $\epsilon = 0.275$  when packed in rhombohedral arrangement), exhibited the largest thermal stratification associated with the highest Nusselt numbers, demonstrating a strong correlation between them. In this work, the best hydraulic behavior, that is, the minimum friction factor, was achieved when cubic particles (with sphericity  $\psi = 0.8$ ) with the largest void fraction ( $\epsilon = 0.48$ ) were tested. Considering both thermal and hydraulic effects, the authors, using the parameter defined by Webb (1979), which combines both terms in a single parameter, concluded that the spheres with the lowest void fraction give the best packing arrangement.

#### 2.1.6. Numerical modeling: results for high-temperature applications

Flueckiger et al. (2014) developed a one-dimensional simplified model for incorporation in a system-level model of a 100 MWe power tower plant to investigate the storage performance during long-term operation. The results showed that the annual plant capacity factor was increased to 0.531 due to the inclusion of a molten-salt thermocline tank which was sized to provide 6 h of thermal energy storage. As shown in Fig. 10, power production is sustained each day after nighttime shutdown of the solar receiver. In addition, an excellent year-long storage effectiveness exceeding 99% was obtained, which is due to the short duration of standby periods when the flow is stagnant inside the tank.

Pacheco et al. (2002) developed a numerical one-dimensional model based on Schumann's equations, considering that fluid and packed bed particles have different temperatures and neglecting heat conduction in the fluid, heat exchange between the packed bed particles and thermal losses to the environment. They concluded that the thermal capacity obtained from the numerical model showed good agreement with the results obtained from a pilot-scale test. Kolb and Hassani (2006) developed a model of the Saguaro solar parabolic trough plant based on the TRNSYS simulation system, including a thermocline storage tank. This model allowed thermal conduction between control volumes and included thermal losses to the environment, so that the results show good agreement with the Solar One data recorded during a discharge test and during a multi-day cool down of the tank (Faas et al., 1986).

However, one of the problems associated with dual-media thermocline tanks is the thermal ratcheting caused by the cyclic charge and discharge processes. During the charge half-cycle, the steel tank shell expands and the filler particles collapse to fill the extra volume in the tank. During the discharge half-cycle, the steel tank shell cannot recover its original shape due to the resistance posed by the rearranged filler, which results in a gradual increase in the mechanical stress in the steel tank shell over repeated operation cycles. Flueckiger et al. (2011) developed a multi-dimensional two-temperature computational fluid dynamics (CFD) model in FLUENT, which included the energy transport in the wall, to obtain the maximum thermomechanical stress used to predict thermal ratcheting under different heat loss conditions. Hoop stresses are determined by the magnitude of the temperature fluctuation, and thus, thermal ratcheting can be reduced by maximizing the insulation between the steel shell and the filler region. Because CFD models require high computational cost to simulate a thermocline tank, considering transient state operation, a simplified dual-phase model that includes unsteady heat transfer through a multi-layer wall was developed by Fernandez-Torrijos et al. (2017), which was validated against the CFD results. They studied the influence of the molten salt flow rate on the thermal response of the steel shell and concluded that the normalized stress decreases as the Reynolds number increases because there is not enough time for the wall to be affected by the cyclic molten salt fluctuations for high Reynolds numbers, as shown in Fig. 11.

**Table 5**  
Range of variation of the main parameters studied by Singh et al. (2006).

Parameter	Studied range
Sphericity ( $\psi$ )	0.55–1.00
Void fraction ( $\epsilon$ )	0.306–0.63
Mass velocity ( $G$ )	0.155–0.266 (kg/s m <sup>2</sup> )
Reynolds number ( $Re$ )	1257–2157 (T-joint masonry tile bricks) 1047–1797 (standard masonry tile bricks) 1257–2157 (standard masonry bricks) 1558–2674 (concrete cubes) 1139–1955 (concrete spheres)

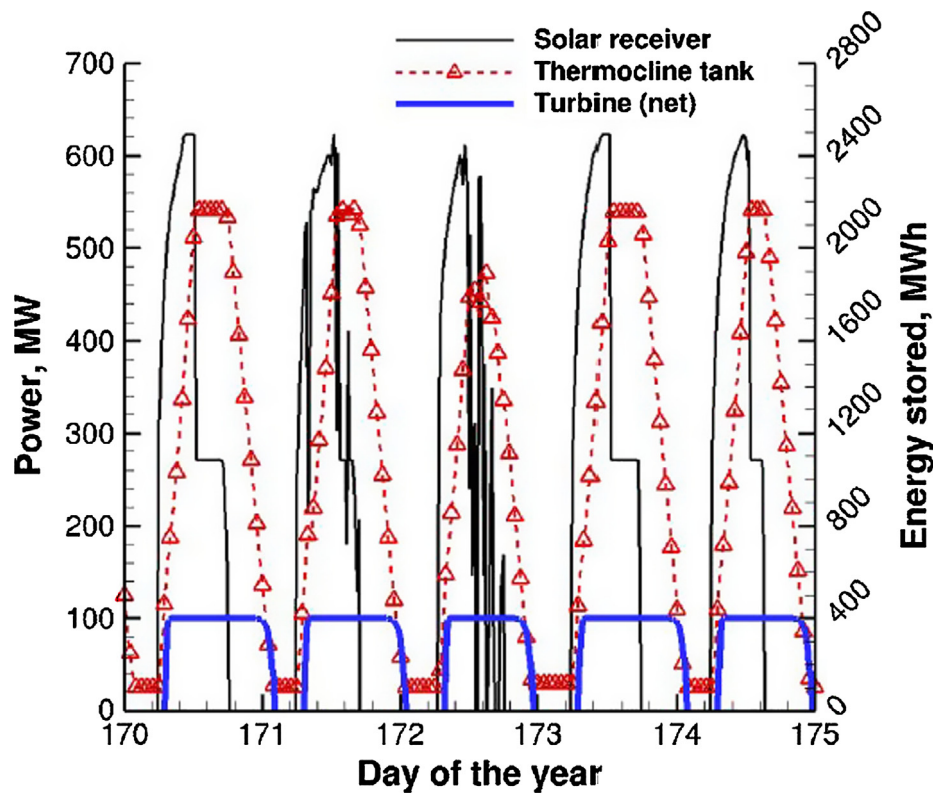


Fig. 10. Power tower plant performance for June 19–23 (Flueckiger et al., 2014).

Bayon and Rojas (2013) developed a single-phase one-dimensional model for characterizing the behavior of thermocline tanks, which was validated against experimental data found in the literature (Faas et al., 1986; Pacheco et al., 2002). They proposed a design equation to obtain the minimum tank height that ensures the maximum theoretical

efficiency of the thermocline tank, given the tank diameter, temperature interval, storage medium and thermal power.

Zhao et al. (2017) used a one-dimensional enthalpy-based dispersion-concentric model, to study the operation of a TES system composed of solar salt and different solid-filler layers configurations,

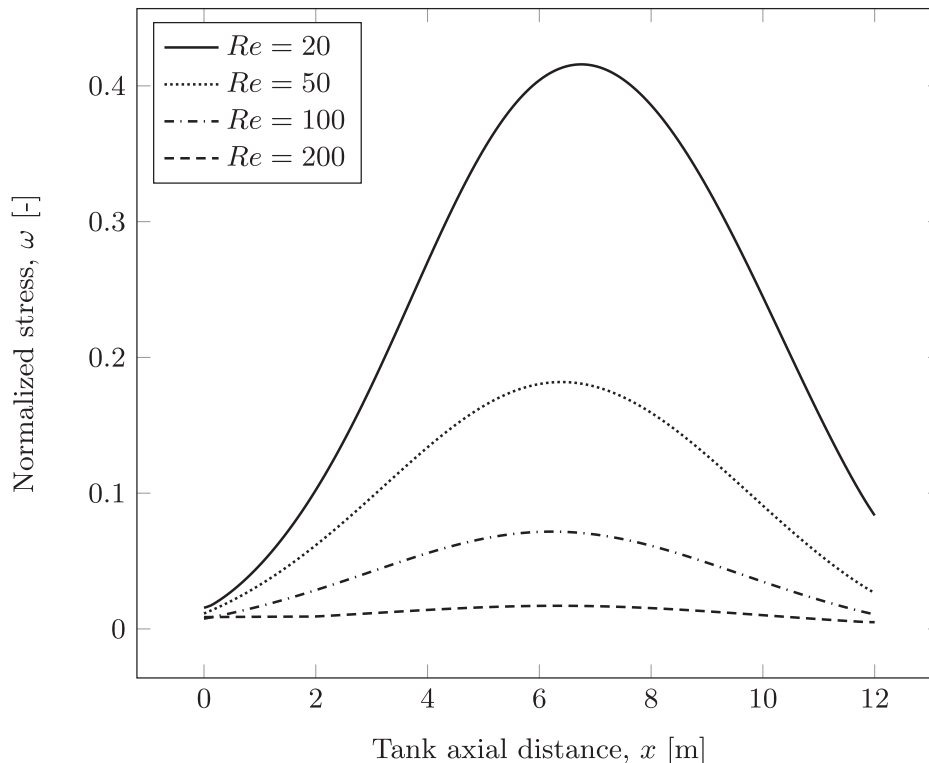


Fig. 11. Hoop stress along the tank height for different Reynolds numbers  $Re = 20, 50, 100,$  and  $200$  (Fernandez-Torrijos et al., 2017).

including both sensible materials and PCMs. The simulations conducted investigate the effect of the partial charge/discharge of the tank on the storage capacity of the system. Although in the majority of studies focused on packed beds in solar systems, the packed bed storage is considered to accomplish a full charge/discharge cycle as the outlet temperature reaches specified cut-off values, real operation typically entails partial charges caused by a lack of energy collection (e.g. as may occur in cloudy days) and partial discharging, due to low demand of power generation. According to their results, the introduction of partial charging-releasing cycles led to significant variations in the energy storage and release capacity in the subsequent full charging-releasing cycles performed afterwards.

Anderson et al. (2014) measured charging and discharging cycles of a packed bed of alumina particles, using air as HTF. The experiments were used to validate a two-phase model, which included the thermal losses to the surroundings. According to model results, wall losses have a strong effect on the temperature profile and can be mitigated by using a shorter vessel, increasing the flow velocity, increasing the heat capacity of the solid, or lowering the overall heat transfer coefficient of the vessel walls. In a different work, the authors (Anderson et al., 2015) proposed a one-phase model that assumes thermal equilibrium between the fluid and the solid phases and solves the energy equation for the packed bed, insulation and vessel considering axial and radial temperature variations. The one-equation thermal model can be adopted when the thermal conductivity and thermal capacity of the solid are high compared to those of the heat transfer fluid, which is the case for the air/alumina system presented. Using the model, the effect of temperature-dependent thermophysical properties is studied, concluding that even at a narrow range of operation the temperature dependence of the alumina and air properties need to be accounted to obtain accurate results.

Zanganeh et al. (2012) built a pilot-scale storage tank made of concrete and filled with pebbles, that was used to validate a numerical model. To this end, a 110 h charging experiment with air at 550 °C was conducted. The tank had a truncated cone shape to make use of the lateral earth pressure, for reducing the normal force on the walls during the thermal expansion of the rocks by guiding them upwards and to reduce the wall losses due to the higher volume-to-surface ratio on the top of the tank, where the temperature is highest. The quasi-one dimensional two-phase heat transfer model formulated was used to simulate the behavior of a storage tank of rocks and air for the temperature range from 20 to 650 °C. The energy balance equation was written in terms of the enthalpy for the fluid phase and in terms of the internal energy for the solid phase, to account for the temperature-dependent solid and fluid properties. Since the fluid was a gas, the radiation exchange between the particles and between the particles and the walls was considered. Moreover, the pressure drop in the packed bed was calculated using the equation presented by Ergun (1952), but conveniently modified to include a buoyancy term. According to the analysis of Zanganeh et al. (2012), the thermal losses were under 0.5% and the outflow temperature during discharging process remained over 590 °C.

White et al. (2016) numerically studied a packed bed filled with a gas and performed an exergy optimization of the system. The authors calculated the different exergy losses in the packed bed and concluded that the efficiency is maximized when the thermal losses, associated to the irreversibilities in the heat transfer process between the gas and the particles, the pressure drop losses and the conductive losses, that occur when the heat is conducted down the temperature gradient within the thermal front, are balanced. White et al. (2016) also observed that the use of segmented reservoirs can reduce the minimum loss between 25% and 50% and suggested that adjusting the ratio between the height and the diameter of the bed, the minimum loss can also be reduced. McTigue and White (2016) also proposed a segmented packed bed for a Pumped Thermal Energy Storage (PTES) system, where a heat pump works between two temperature levels, established by the energy stored

in two separated packed beds. When necessary, the energy stored is transformed into electricity by a heat engine. The authors demonstrated that segmentation reduces the conductive losses during the charging process, increasing the efficiency and the total energy stored per cycle.

Several simulation works have been dedicated to study the effect of different parameters, such as fluid flow rate, tank height or solid particle size, on the performance of thermocline tanks. To study the influence of molten-salt flow rates on the efficiency of a thermocline thermal storage system, Yang and Garimella (2010b) developed a multi-dimensional two-temperature computational fluid dynamics (CFD) model to simulate mass, momentum and energy transport inside a molten salt thermocline tank, which did not include heat losses through the tank wall. The discharge efficiency of a thermocline tank was defined in this work as the ratio between the useful energy recovered during discharging, which is the energy retrieved above a certain temperature level, and the total energy initially stored in the thermocline tank. They concluded that the efficiency decreases for higher Reynolds numbers, as increasing the Reynolds number reduces the slopes of the temperature profiles in the heat-exchange zone, so that the high-temperature zone is reduced.

Later, Yang and Garimella (2010a) studied the effects on the heat transfer and fluid flow of a non-adiabatic tank wall, considering a wall Nusselt number of  $1.6 \times 10^5$ . Comparing the results obtained for adiabatic and non-adiabatic wall boundaries of thermocline tanks, the flow field in adiabatic thermoclines was uniformly distributed, whereas that in non-adiabatic thermoclines showed distorted streamlines. Although the overall temperatures were lower in non-adiabatic thermoclines, the decrease in the outflow temperature was larger at small Reynolds number because higher Reynolds numbers result in lower discharge periods. They concluded that the discharge efficiency increases with the Reynolds number in a non-adiabatic thermocline, in contrast to the behavior of an adiabatic thermocline. Interestingly, for a non-adiabatic tank with a modest wall Nusselt number, the discharge efficiency first increases and then decreases as the Reynolds number increases, as shown in Fig. 12. The initial increase indicates that the increased discharge time has a dominant influence on the discharge efficiency, whereas the subsequent decrease shows that the expansion of the heat-exchange zone caused by the increase in Reynolds number has a more important effect on the efficiency.

Flueckiger and Garimella (2012) studied the influence of the internal granule diameter and external convection losses on the tank performance, and they concluded that the use of smaller filler particles can greatly increase the discharge efficiency, as the heat-exchange region is narrower for smaller particles, which yields higher outflow

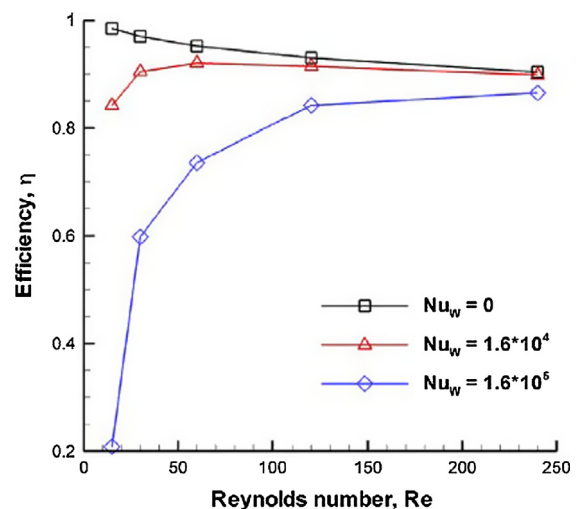


Fig. 12. Discharge efficiency as a function of Reynolds number under different wall heat transfer rates  $Nu_w$  (Yang and Garimella, 2010a).

temperatures during discharge. The same conclusion was reached by Zanganeh et al. (2015b), who simulated the charging and discharging processes of a TES unit containing rocks using air at high temperature as HTF. The results showed that the outlet temperature at the end of the discharging process increased when the rock diameter decreased due to the higher heat transfer coefficients between the solid and the fluid.

For air-based central receiver CSP plants, Hanchen et al. (2011) developed a 1D two-phase transient model, which considers uniform-temperature particles, neglects radiation heat transfer and heat conduction in the fluid phase, and accounts for heat losses through the walls. The model was validated against the experiments of Meier et al. (1991). The authors studied two different scenarios: (i) a tank, initially at ambient temperature, was charged for 6 h and then discharged for the same period of time (single charge/discharge cycle) and (ii) a series of consecutive 6-h charge and 6-h discharge daily cycles until the steady state will manifest itself (continuous operation). Different behavior in terms of the charging, discharging and overall efficiency and capacity ratio are observed for the two scenarios considered. For the continuous operation of the tank (at the 20th cycle), they concluded, that high air mass flow rates lead to superior capacity ratio (amount of energy stored compared to the theoretical maximum energy that can be stored when the solid material in the tank reaches the input temperature of the air stream). The overall efficiency (ratio of recovered energy for a single charge/discharge cycle to the input and pumping energy) showed a maximum at intermediate flow rate.

Concerning the effect of the tank height, Hanchen et al. (2011) observed a decrease in the capacity ratio and a moderate increase in the overall efficiency with increasing tank height. This last effect was attributed to the lower losses of the hot fluid leaving the tank during charging, due to its lower temperature associated with the longer tank length.

## 2.2. Latent energy storage with PCMs

The use of PCMs in solar energy storage systems has two main advantages over traditional sensible energy storage systems: first, they increase the energy density of the storage system by augmenting the energy stored in the same volume or reducing the volume required to store the same amount of energy and second, PCMs are able to store large amounts of energy at a nearly constant temperature. Some applications require the solar energy to be stored at lower temperatures than those reached in sensible storage systems. A typical example is a simple solar facility for DHW. This application requires water to have a maximum temperature of approximately 45–50 °C. A simple solar facility can reach temperatures of approximately 80–90 °C in summer. Therefore, the water has to be mixed with cold water prior to its final use. This process is very inefficient from an exergy point of view.

When using a PCM in a packed bed, it must be encapsulated, typically in a spherical geometry. Due to the change in volume that a PCM suffers during phase change, it is necessary to not completely fill the encapsulation with PCM because the walls of the container can be damaged and the PCM can leak out when it is in liquid form. Several authors explained and reviewed the different methods and processes of PCM encapsulation (Wei et al., 2018; Navarro et al., 2017; Yataganbaba et al., 2017; Milián et al., 2017).

### 2.2.1. Low-temperature applications and experiments

As previously mentioned, packed beds with sensible energy storage typically use air as the HTF. Rady (2009a,b) and Izquierdo-Barrientos et al. (2013, 2016b) experimentally and numerically studied the performance of a packed bed filled with a commercial granular PCM from Rubitherm ([www.rubitherm.eu](http://www.rubitherm.eu), 2017) with air as the HTF. This granular material consists of a porous matrix with embedded paraffin. The SiO<sub>2</sub> matrix gives mechanical support to the paraffin, maintaining the paraffin inside the solid matrix even when it is in the liquid state. This material is used commercially in a wide range of low-temperature

applications (between –10 and 90 °C) and with two different particle sizes: a finer grade, with particles between 0.2 and 0.6 mm, and a coarser grade, with diameters between 1 and 3 mm. The smaller grade is composed of Geldart B particles, which are more suitable for a bubbling fluidized bed, while the larger grade is composed of Geldart D particles, which are more suited for use in a packed bed (Izquierdo-Barrientos et al., 2016d). Rady (2009a) experimentally studied the materials GR27 and GR41 (the number represents their approximate phase change temperature in degrees Celsius) in a column with an internal diameter of 45 mm and a test section height of 200 mm, and they developed a simple two-phase numerical model for the heat transfer process. Rady (2009a) concluded that the correct determination of the phase change characteristics of the material and the voidage of the bed are the main parameters that affect the results of the numerical model. Other parameters, such as the particle-to-fluid heat transfer coefficient and the axial dispersion have a negligible impact. Izquierdo-Barrientos et al. (2016b) used materials with a higher transition temperature (GR50 and GR80), which they were tested in a facility of larger dimensions than that used by Rady (2009a), with an internal bed diameter of 200 mm and tested height of 200 mm. The authors developed a numerical model, which in non-dimensional form, can be used with the same numerical scheme for either sensible or latent energy storage. Their model also includes the energy stored in the walls of the bed and heat losses to the surroundings. Under their experimental conditions, they observed that the energy stored in the walls of the bed represents 8.2% of the energy stored in the granular PCM. Fig. 13 shows the experimental data obtained by Izquierdo-Barrientos et al. (2016b) using the material GR50 and an air flow rate of 250 L/min, together with the numerical model results. Good agreement is observed between them. They also analyzed the influence of the air flow rate and observed that the numerical model fits better with the experimental data for low flow rates because the heating rate of the process is similar to the slow heating rate ( $\approx 0.5$  °C/min) of the DSC measurements used to determine the temperature-enthalpy curve of the granular material.

Rady (2009b) also studied the possibility of mixing two granular PCMs with two different transient temperatures in different proportions. Rady (2009b) mixed GR27 and GR41 in ratios between  $m_{GR27}/m_{GR41} = 0.2$  and 5.0. The conclusions of the work indicate that the optimum mixing ratio to maximize the exergy efficiency of the system is around  $m_{GR27}/m_{GR41} \approx 1$ , independent of the Reynolds number.

With air as the HTF, Arkar and Medved (2005) experimentally study a packed bed of a PCM, but they did not use granular materials; instead, they filled the bed with 5-cm-diameter spheres filled with RT20 paraffin from Rubitherm ([www.rubitherm.eu](http://www.rubitherm.eu), 2017). The bed had a diameter of 34 cm and a height of 152 cm. The air flow rate was between 50 and 220 m<sup>3</sup>/h. They experimentally measured the temperature along the bed as well as inside the two spheres. They compared the experimental data with numerical results from a simple two-phase model and concluded that the best agreement between the experiments and the model for the apparent specific heat was measured at a heating rate of 0.1 K/min, which was the nearest value to the slow heating rate of their experiments. Beasley et al. (1989) also experimentally studied 2.1-cm-diameter polypropylene spheres filled with paraffin wax in a packed bed with air as the HTF. They compared the experimental data with two different models, one with constant temperature during the phase change and other with rising temperature during the melting process. Both models agree well with the corresponding experimental data. Karthikeyan et al. (2014) numerically studied the influence of different parameters on the performance of a packed bed with air. The packed bed consisted of spherical capsules filled with paraffin. They varied the size of the spheres between 6 and 10 cm, the air inlet temperature of the bed between 67 and 80 °C, the air flow rate between 0.05 and 0.015 kg/s and the effective thermal conductivity of the bed between 0.4 and 2 W/(m K). They observed that the charging time is more influenced by the air inlet temperature than by the ball size or the mass flow rate in

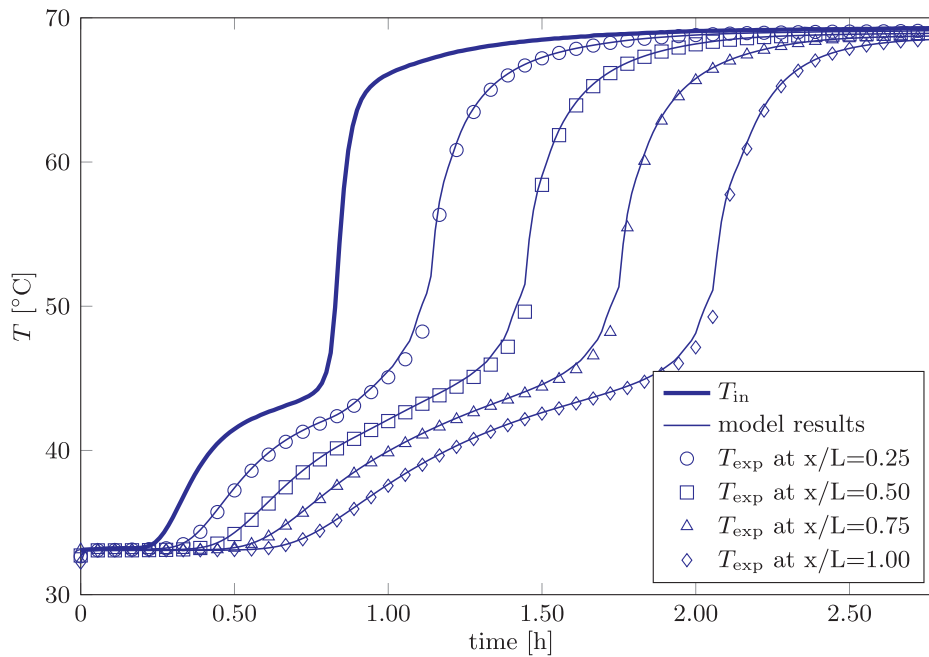


Fig. 13. Comparison of the experimental and numerical results obtained by Izquierdo-Barrientos et al. (2016b) for the granular PCM GR50 with an air flow rate of 250 L/min.

the ranges tested in their work. Karthikeyan et al. (2014) also concluded that an increase in the equivalent thermal conductivity of the bed beyond 1 W/(mK) does not improve heat transfer because the dominant resistance is associated with air convection.

The ability of the PCM to maintain a fairly constant outlet temperature for the HTF during discharging is advantageous for applications such as the drying of agricultural crops. For this purpose, Esakkimuthu et al. (2013) performed experiments using a solar-based dryer consisting of a solar air heater, a packed bed composed of a PCM storage tank and a drier. In that system, the PCM was HS58, because its melting point was suitable for the drying process, which required hot air at approximately 55 °C. The PCM was contained in spherical capsules 75 mm in diameter. The authors concluded that the selection of a PCM with a suitable phase change temperature prevented overheating of the air during the peak sunshine hours due to the absorption of heat by the PCM at a constant temperature and, consequently, reduced the spoilage of food products due to excessive heating.

Other authors proposed the integration of a packed bed energy storage system into a solar collector. For example, recently, Arfaoui et al. (2017) experimentally studied a novel solar air heater integrated with an latent energy storage system, which consists of two rows of 156 spherical particles filled with a PCM with a transition temperature of 27 °C. The diameter of the spheres is approximately 7.5 cm. During the sunny hours of the day, the system provides a flow of heated air and, at the same time, stores part of the energy absorbed in the PCM capsules. This stored energy can be released during the non-sunny hours of the day. Fig. 14 shows the results of the instantaneous powers absorbed, carried out by the gas stream (useful heat) and stored in the bed, during a typical day. The charging period is from 09:00 to 17:00. The system maintains a nearly constant power carried out by the gas stream until 07:00 the next day.

In addition to the extensive studies using air as the HTF, packed beds with spherical capsules filled with a PCM have also been studied for domestic hot water applications, using water as the HTF. Nallusamy et al. (2007) and Nallusamy and Velraj (2009) carried out experiments by varying different operating conditions in a 48-L storage tank. A total of 264 spherical capsules 5.5 cm in diameter filled with paraffin wax were placed in the tank. The resulting voidage was approximately 0.5, which indicates that half of the tank stored energy in sensible form by

increasing the water temperature and the other half stored latent energy in the spheres during the phase transition of paraffin. In their experimental study, Nallusamy et al. (2007) carried out experiments under two different conditions: first, with a controlled water inlet temperature in the tank and second, with the tank directly connected to flat solar collector, which results in a variable source. They varied the mass flow rate (between 2 and 6 L/min) and the inlet temperature of the water (between 66 and 70 °C). They observed a notable decrease in the charging time during the phase change process of the PCM, whereas the reduction in the charging time was negligible when the bed temperature was less than the phase change temperature of the PCM. Increasing the mass flow rate notably reduced the charging time under various source conditions (connected to the solar collector) due to the large amount of energy absorbed by the water in the collector. An increase in the mass flow rate from 2 L/min to 6 L/min reduced the charging time from 200 min to 140 min. Under constant inlet temperature conditions, an increase in the mass flow rate did not reduce the charging time because, over the range tested, the flow was in the laminar regime and the major thermal resistance was in the PCM capsules. Nallusamy and Velraj (2009) studied two different voidages in the bed 0.5 and 0.61. They observed a reduction in the charging time (a reduction of 18% for a mass flow rate of 6 L/min) due to the lower mass of the PCM in the storage system. An increase in the voidage led to a reduction in the interstitial fluid velocity and, consequently, a reduction in the capsule-water heat transfer coefficient. Thus, the reduction in the charging time was not proportional to the increase in the voidage. Fig. 15 shows the temperature evolution in the center of the bed for voidages of 0.49 and 0.61, where a reduction in the charging time is observed. This figure also shows a notably reduction in the phase change time in both cases of approximately 60 min for  $\varepsilon = 0.49$  and 30 min for  $\varepsilon = 0.61$ .

Saitoh and Hirose (1986) proposed the use of a heat pump system in parallel between a packed bed with a PCM heated by a conventional solar collector and the final systems for heating a building. In this way, the heating pump can compensate the supercooling problems observed when using salt hydrates as the PCM for the capsules of a packed bed. Fig. 16 shows how the PCM maintains the COP of the system at an approximately constant at value of four over two hours.

Mao (2016) reviewed the different geometrical parameters in the

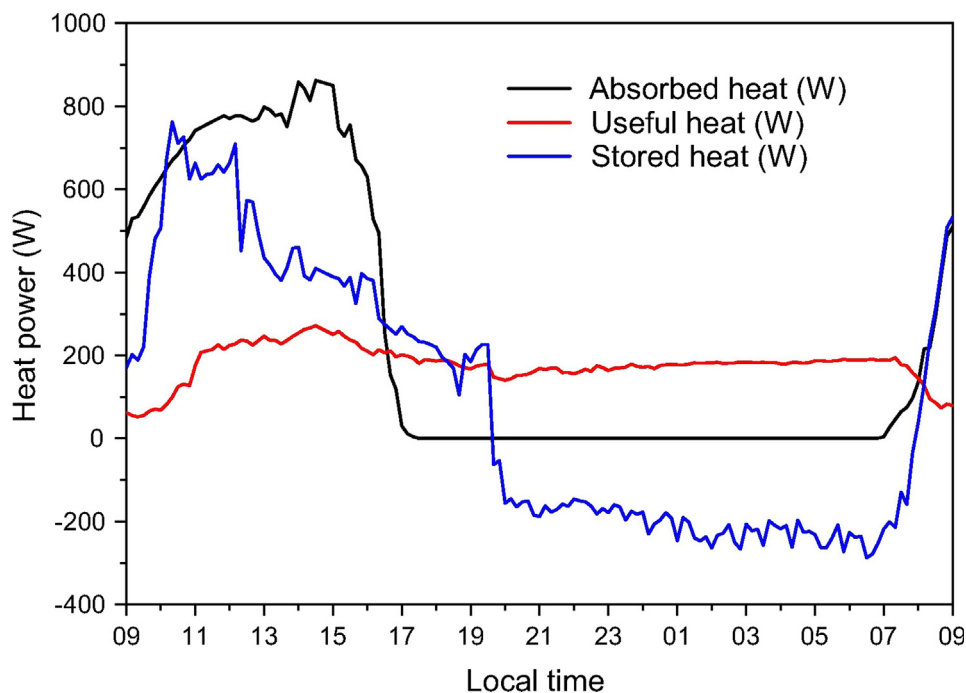


Fig. 14. Results obtained with the “SAHL-2 beds” system (Arfaoui et al., 2017) for the power absorbed (black line), net enthalpy flux carried out the air stream (red line) and stored power (blue line). (For interpretation of the references to color in this figure legend, the reader is referred to the web version of this article.)

TES that helps to improve the performance of the system. Mao (2016) concluded that, for packed beds with encapsulated PCMs, the geometrical parameters of the storage system can significantly affect the heat transfer rate. Several research works can be found in the literature that vary the geometrical parameters with the aim of reducing the charging times. The authors also highlighted that trends in packed beds are

towards TES containing encapsulated PCMs.

#### 2.2.2. High-temperature applications and experiments

For medium-temperature applications, phase change materials have been employed in packed bed storage units, one of the most promising being a solar thermal power plant powering an Organic Rankine Cycle

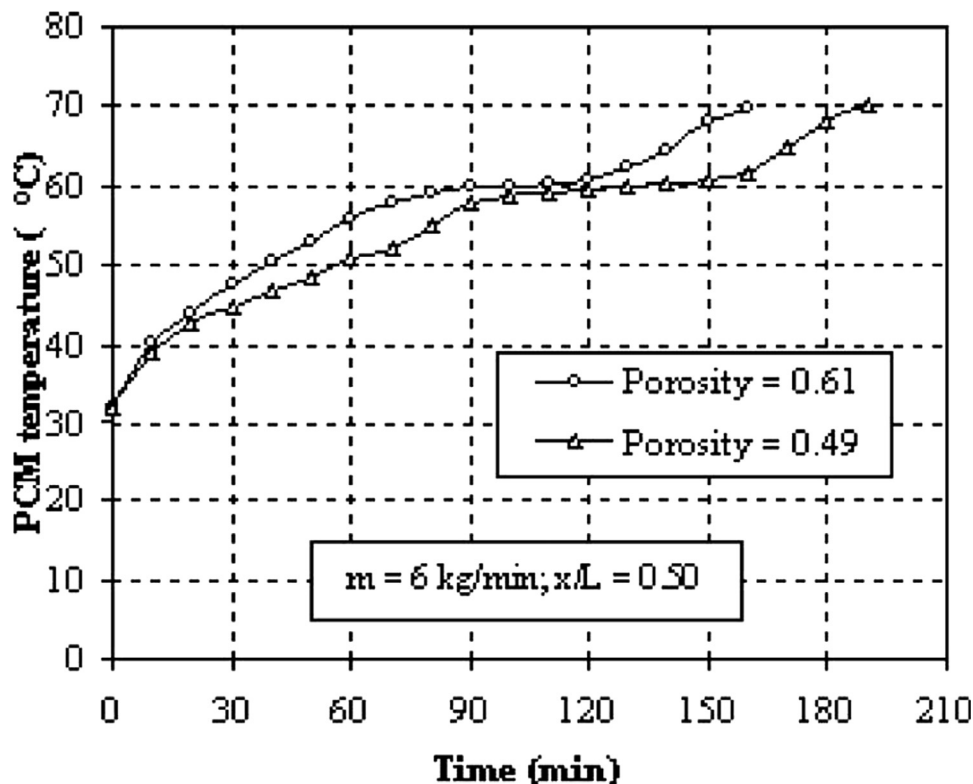


Fig. 15. Temperature evolution in the middle height of the packed bed used by Nallusamy and Velraj (2009) with water as the heat transfer fluid with a mass flow rate of 6 L/min and two different voidages.

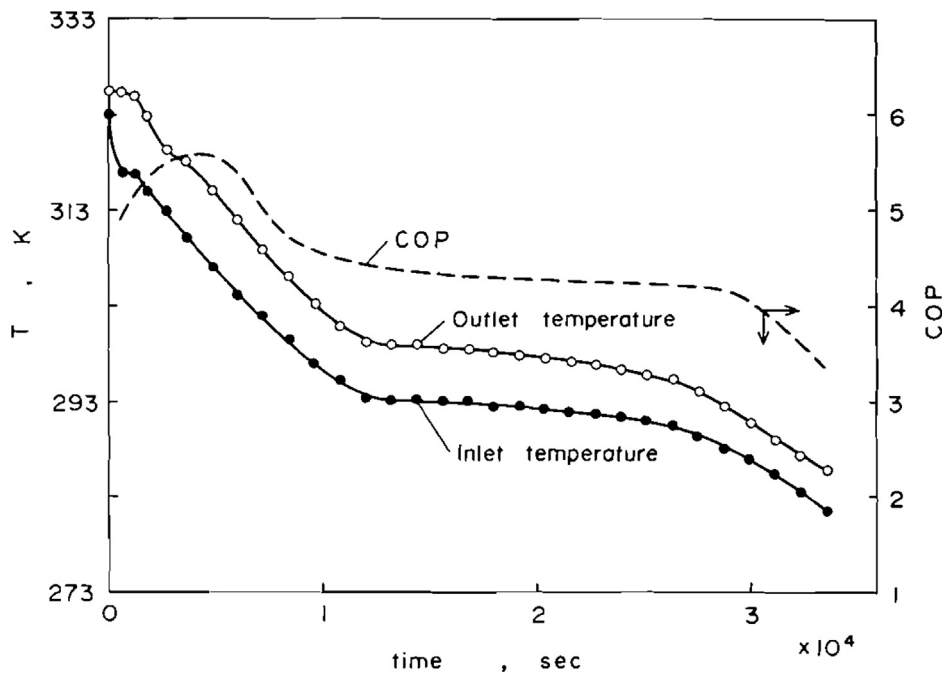


Fig. 16. Inlet and outlet temperatures of the water flowing through the PCM tank and COP of the system proposed by Saitoh and Hirose (1986).

(ORC) to be used in small- and medium-scale systems (from kilowatts to a few megawatts). Manfrida et al. (2016) simulated the operation of a solar power plant consisting of a solar field of parabolic through collectors, which fed both the evaporator of a basic ORC and two storage tanks filled with encapsulated spheres of a PCM installed in parallel. A dynamic simulation (over 1 week) of the system was conducted using TRNSYS, coupled with the transient model of the latent heat storage tank developed in EES. Erythritol ( $C_4H_{10}O_4$ ), which has a melting temperature of  $117^\circ\text{C}$ , was chosen as the PCM and was encapsulated in 4-cm-diameter spheres, and pressurized water was used as the HTF (15 bar). The simulation showed that, due to the heat storage system, the ORC plant could generate almost constant power over the period studied.

PCMs have also been investigated for application in the storage systems of CSP plants. However, a major drawback in using PCMs is their low thermal conductivity, which causes high thermal resistance to heat transfer during the charging and discharging period. Encapsulation of the PCM in small capsules, forming a packed bed, can overcome this limitation by increasing the surface heat transfer area between the PCM and the HTF. In molten salt storage tanks, dual-media thermocline tanks have been proposed to reduce the cost of the storage system, as part of the more costly molten salt is replaced by a low-cost particulate granular material. Moreover, only one tank is needed instead of the two tanks employed in commercial molten tank storage systems (one for hot and one for cold molten salt), as previously discussed in detail in Section 2.1.3.

A proposed design modification for reducing the tank size by increasing the energy density is the replacement of the internal filler rock with an encapsulated PCM (Flueckiger and Garimella, 2014). Smaller tanks are desired, as the tank height is constrained by the bearing capacity of the underlying soil, while a large tank diameter increases the potential for maldistribution of the fluid flow inside the porous bed. System-level simulations of a 100-MWe-power tower tank were conducted by Flueckiger and Garimella (2014) to evaluate the performance of a PCM to replace quartzite rock in a dual-media thermocline tank of Solar salt (60 wt.%  $\text{NaNO}_3$ , 40 wt.%  $\text{KNO}_3$ ), operating between  $300^\circ\text{C}$  and  $600^\circ\text{C}$ . To facilitate direct comparison, a hypothetical encapsulated PCM filler with a density, specific heat, and thermal conductivity equivalent to those of quartzite rock was considered. The model results

revealed that the use of a single PCM as the filler material did not provide a substantial increase in the plant's capacity factor, and in fact, at some of the melting temperatures tested, this ratio decreased. For low-melting-temperature filler materials, the tank stored more energy than a quartzite-filled tank, but at such low temperatures, this additional latent heat is not viable for steam generation, as the threshold temperature that qualifies as useful for steam generation is higher than the melting temperature. High melting temperatures can support steam generation, but only a portion of the filler material undergoes a phase change during charging, limiting the utilization of the latent heat. However, an alternative design, referred to as a cascade latent heat thermocline tank, consisting of a structure composed of three layers of PCM with different melting temperatures was proposed, which yielded a 9.7% increase in the annual power output relative to a quartzite-filled tank of the same dimensions. If the objective were to match the annual power plant output achieved with sensible heat material filler, the cascaded latent heat tank proposed should have a diameter 16% lower. However, the extra cost related with the PCM and the more sophisticated fabrication processes need to be taken into consideration to evaluate whether they can be effectively compensated by the increased plant revenue and the lower initial costs with the storage size reduction.

Wu et al. (2014) developed a transient one-dimensional dispersion-concentric model to simulate the cyclic operation of a molten salt packed bed TES system using spherical capsules. Two different cascaded systems of three (C3) and five layers (C5) of PCMs with different phase change temperatures were studied and compared with a system with a single PCM (non-cascaded system, NC) over the temperature range of  $290^\circ\text{C}$  to  $390^\circ\text{C}$  (see Fig. 17). They concluded that the system with non-cascaded PCM capsules may be inappropriate for use in TES systems utilizing a liquid as the HTF. In contrast, the cascaded system with five layers showed a shorter charging time, higher charging ratio (ratio of the amount of heat storage during the charging period to the total storable energy provided by the hot molten salt) and, at the same time, a low discharging time. Nevertheless, the authors noted that the discharging process should be optimized for a given application because it depends on the  $T_{\text{discharge, cut-off}}$  and the phase change temperature of the materials. The reported conclusions are explained by the fact that even if a prior investigation (Wu et al., 2016) recommended the selection of a material with a high phase change temperature, as it provides a longer

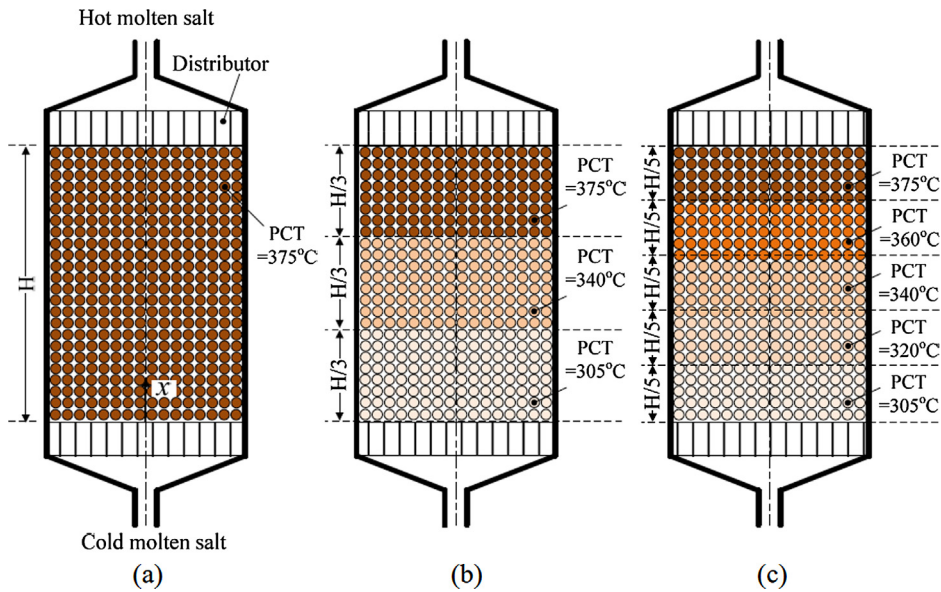


Fig. 17. Schematic of the three different systems compared in Wu et al. (2014): (a) single PCM, (b) cascaded with two different PCMs and (c) cascaded with five different PCMs.

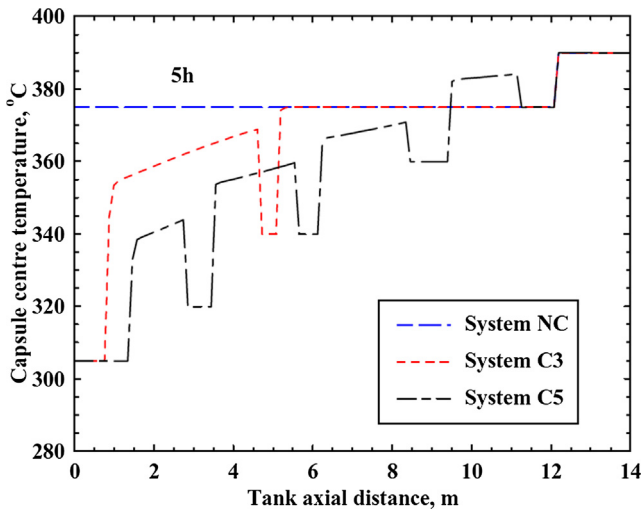


Fig. 18. Capsule center temperature along the tank height after 5 h of charging for the three different systems compared in Wu et al. (2014).

time with a high enough molten salt outlet temperature to support steam generation and higher discharging efficiency (ratio of the useful discharge energy to the total energy initially stored), this configuration does not utilize the latent heat inside the tank completely. This can be

seen in Fig. 18, which shows that after 5 h of charging the tank, most of the PCM capsules in system C5 were completely melted, while only the PCM capsules in the region between 12 and 14 m were completely melted in the NC system.

Alternatively, for cascaded PCM configurations, Galione et al. (2015) simulated the behavior of a multi-layered solid PCM packed bed, in which layers of a low-cost solid material (quartzite rock and sand) were combined with layers of PCMs with different phase change temperatures and molten salt as the heat transfer fluid, with an operation temperature in the range of 290–390 °C. In this design, a layer of PCM with a phase change temperature in the admissible temperature range for discharging ( $(T_{\text{discharge, cut-off}} - T_h)$ ) was placed at the top end of the tank, while a layer of PCM with a phase change temperature in the admissible temperature range for charging ( $(T_c - T_{\text{charge, cut-off}})$ ) was placed at the bottom end of the tank. Between them, one or more layers of solid material and eventually a layer of PCM with a transition temperature outside the admissible temperature ranges for charging and discharging were included. Fig. 19 gives a comparison of some of the different filler configurations. The three configurations shown in Fig. 19, present a layer of PCM on top of the tank with a melting temperature of 380 °C, which is slightly lower than the charging temperature (390 °C). Configurations C1 and F1 are able to provide stable outflow temperatures during the discharging process to be close to the charging temperature. However, this is not the case for configuration D1, since there is a thick layer of PCM in the middle zone, with a melting temperature of 340 °C, which acts as a thermal buffer

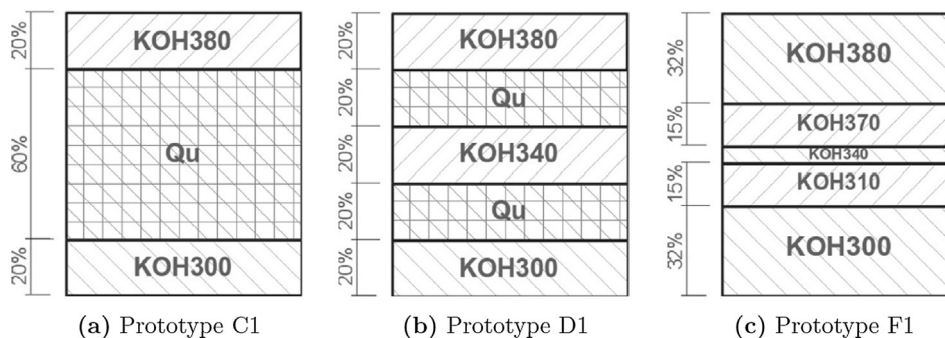


Fig. 19. Sketches of some of the different filler configurations compared in Galione et al. (2015). KOH refers to a fictitious PCM material with the same thermal properties as potassium hydroxide but different melting temperatures. Qu refers to a layer made of a mixture quartzite rock and sand.

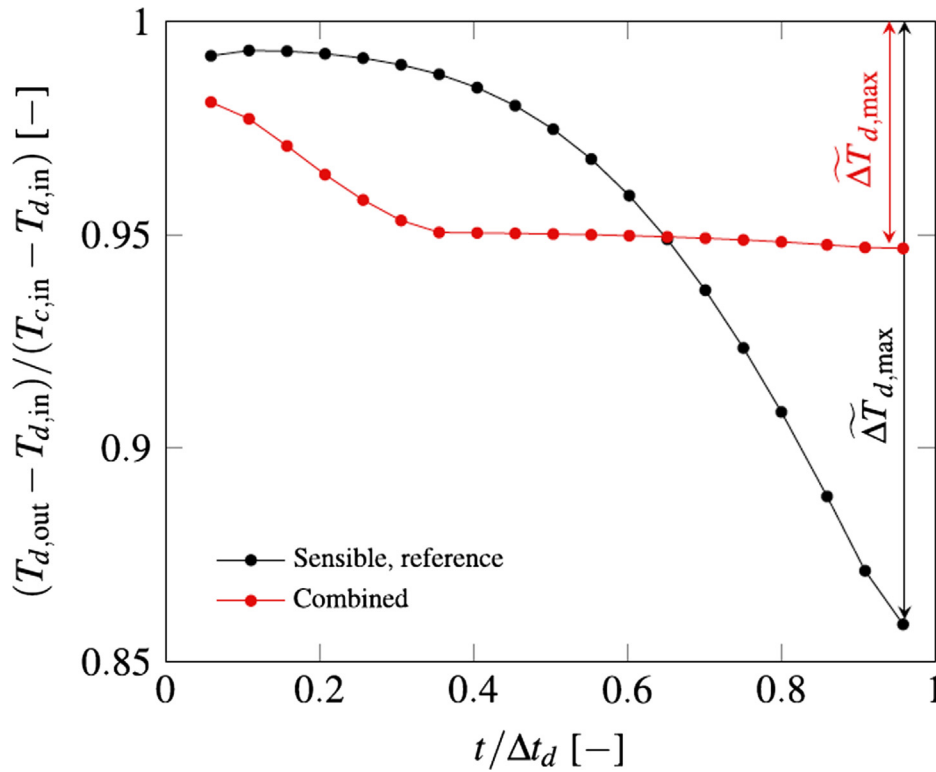


Fig. 20. Steady cycling outflow temperature during discharging for 23 MWh<sub>th</sub> sensible reference storage ( $H = 4$  m) and combined storage Geissbühler et al. (2016).

maintaining the temperature of the molten salt close to this melting point. Thus, the presence of the other PCM with a higher temperature (380 °C) at the exit of the tank is not enough to stabilize the outflow temperature. The same behavior is observed for the outlet temperature of the molten salt withdrawn from the bottom of the tank during the charging process. While configurations C1 and F1 are able to keep this temperature in the admissible range of 290–305 °C for a longer duration, configuration D1 exhibits a charging process that lasts one hour less, reached when the outlet temperature rises above the  $T_{\text{charge,cut-off}} = 305$  °C. The results of the simulations showed that although prototype F1 presented the highest energy storage and exergy flow (difference between the exergy exiting and entering the tank with the fluid), the ratio of stored energy to storage capacity was only 65%, with 61% of the PCM effectively changing phase. In contrast, a different concept, prototype C1, stored approximately 87% of the energy stored by prototype F1 but presented a higher ratio of stored energy to storage capacity (77%) and a similar exergy flow. Additionally, it employed only 40% of the mass of the PCM and 79% of the mass of the confined HTF of those in prototype F1 (which were replaced by a low-cost solid material), leading to a lower-cost storage system.

Liao et al. (2018) compared the thermal performance of a 100 MWh packed bed containing only rocks and with rocks and a layer of PCM on the top of the bed to maintain a more stable outflow temperature during the discharging process. As established by the previous authors, they remarked the importance of the proper selection of the cut-off temperatures for the charging or discharging processes because if they are not proper selected, the PCM can even reduce the storage capacity of the TES.

Zanganeh et al. (2015a) also combined sensible heat material and PCM in a packed bed with air as the HTF in the temperature range of 25–700 °C for CSP applications. A 42 kWh<sub>th</sub> lab-scale prototype 40 cm in diameter and 1.68 m in height was fabricated, containing a 9-cm-high layer of encapsulated phase change material (AlSi12) on top of a 127-cm-high packed bed of sedimentary rock with a mean diameter of approximately 3 cm. AlSi12, which melts in the range of 573–577 °C and

has a heat of fusion of 466 kJ/kg, was encapsulated in AISI316 tubes with a 16-mm inner diameter and 1-mm wall thickness. An experimental facility was used to validate a two-phase transient heat transfer model of the thermal storage cycle. The experimental results showed that although the outflow temperature during discharging initially drops faster for the tested prototype than for the same tank filled entirely by rocks, after approximately 70 min of discharging, the temperature of the “rocks only” setup dropped below that of the “rocks + PCM” setup. In this manner, the outflow air temperature was stabilized at around the melting temperature of AlSi12. According to the authors, the benefit of the propose prototype is that, regardless of if the downstream application is a steam or gas turbine, the temperature stabilization allows the turbine to operate at its design point. On the other hand, if the downstream application is a chemical process, stabilization may be crucial because it can ensure that the outflow temperature stays above the required reaction temperature. In another study, Geissbühler et al. (2016) conducted an efficiency and cost assessment of the described concept. The experimentally validated model was used to compare the performance of the combined sensible-latent heat storage design with a conventional sensible heat storage unit consisting of a packed bed of rocks. The systems were studied for application in two industrial-scale storage units: the industrial-scale packed bed storage in Ait Baha, Morocco, and the molten salt storage of the Andasol CSP plant. The sensible and combined storage configurations were compared in terms of the normalized maximum outflow temperature drop during discharging,

$$\widetilde{\Delta T}_{d,max} = \frac{T_{c,in} - T_{d,out,min}}{T_{c,in} - T_{d,in}}, \quad (5)$$

which is a parameter that should be minimized, as the temperature of the HTF entering the power block has a direct impact on the efficiency of the power block. Fig. 20 shows a comparison of the steady cycling outflow temperature during discharging for the sensible reference configuration and a combined storage tank (rocks with a layer of PCM on the top) both with the same height and volume. It can be observed

that after an initial decrease of the temperature, in which the PCM is cooled to its melting temperature, the combined storage can deliver heat maintaining almost constant the outlet temperature. This temperature drop can be reduced by two different methods. For the combined storage it can be reduced by increasing the amount of PCM on the top of the packed bed of rocks while it is kept constant the tank height, and hence reducing the amount of rocks accordingly. On the other hand, for the sensible heat storage configuration, the temperature drop can be reduced by increasing the height of the tank and therefore its volume. According to Yang and Garimella (2013) a shorter tank has a shorter heat-exchange zone, as at steady state this region occupies nearly the entire height of the storage. As a shorter heat exchange zone provides a smaller distance for the fluid to be completely heated or cooled, which results in a larger temperature difference between the filler and the fluid, greater heat transfer rates between the phases. The larger temperature difference results in a larger entropy change, leading to a more significant loss in the quality (i.e. temperature) of the available thermal energy, that is the stratification efficiency (Eq. (3)) would be lower. Sensible and combined storage units at steady cycling conditions and with the same charging and discharging times were compared, in terms of their exergy efficiency and specific material cost, as a function of the maximum temperature drop during discharging. It should be noted that the temperature drop is controlled by increasing the tank height in the sensible heat storage and therefore units with different height and volume are compared. In their study, Geissbühler et al. (2016) showed that the reduction in the maximum temperature drop during discharging upon increasing the height of the sensible bed resulted in a significant decline in exergy efficiency due to an increase in the thermal losses and pumping work resulting from the increased tank height. In contrast, the exergy efficiency of the combined storage is maintained above the limit of 95% of the exergy efficiency, independent of the maximum temperature drop during discharging. This exergy efficiency limit, together with the cost of the storage system being below 15 \$/kWh<sub>th</sub>, a maximum charge time of 6 h and minimum discharge period of 6 h, meets the target established by the U.S. Department of Energy's SunShot Initiative to make CSP cost competitive with other sources of power-generation technologies. Moreover, the material costs per net energy output of the combined storage option are lower than those of the sensible heat storage unit, because even if the PCM and encapsulation are costly, the required volume is very low, and this compensates for the increase in cost of the sensible storage unit resulting from the higher height needed to keep the output discharge temperature at a high level.

While low-temperature PCM encapsulation techniques are highly developed, the encapsulation of high-temperature PCMs for solar thermal plants requires other methods than the use of the polymeric shells usually employed at low temperatures. Gimenez-Gavarrell and Fereres (2017) summarized the shell materials used in the literature to encapsulate different types of high-temperature PCM (nitrates, chlorides and metals) and proposed borosilicate glass as an alternative shell material, which was compatible to both steam (HTF) and inorganic salts or metals (core material), with melting temperatures in the range of 300–400 °C, to be used for latent heat storage in direct steam generation (DSG) solar thermal plants. In a proof-of-concept study, spherical capsules 20 mm in diameter were fabricated and tested in an experimental rig. According to the authors, although the possibility of mass production and the fragility of the borosilicate shell capsules need to be further investigated, the tested capsules showed mechanical and thermal stability over 10–15 cycles. PCM capsules were also experimentally tested by Bellan et al. (2015) in a latent heat packed bed with air as the heat transfer fluid. In this case, spherical capsules approximately 3 cm in diameter of a molten salt PCM were encapsulated in a shell made of polymer using a non-vacuum encapsulation technique. The deformation experiments showed that the capsules did not collapse after 2200 thermal cycles.

### 2.2.3. Numerical modeling: description and results

Numerical modeling of packed beds with PCMs have been widely studied. Different authors have proposed different numerical models for predicting the thermal behavior of such beds. The majority of models published in the literature can be cataloged into two main groups: concentric dispersion models (Karthikeyan and Velraj, 2012; Oró et al., 2013; Karthikeyan et al., 2014; Bhagat and Saha, 2016) and continuous phase models (Beasley et al., 1989; Arkar and Medved, 2005; Rady, 2009a; Wu and Fang, 2011; Bellan et al., 2014; Izquierdo-Barrientos et al., 2016b). Different reviews have explained in detail the equations of both types of models (Ismail and Stuginsky, 1999; Xia et al., 2010; de Gracia and Cabeza, 2016). Concentric dispersion models typically solve the energy equation for the fluid phase flowing through the bed as well as the transient conduction equation within the capsules containing the PCM. Therefore, it is possible to determine the properties (typically, temperature and liquid fraction) of the PCM. In contrast, continuous phase models treat the phases (fluid and capsules or granules) as two interpenetrating media and two continuous phases. In this case, the temperature and liquid fraction of the PCM is obtained as a function of the axial position in the bed and time. Both models are physically correct, although depending on the latent energy storage system, the dimensions of the capsules containing the PCM and the heat transfer fluid, one model may be more accurate. One of the main parameters to consider when choosing the model, as mentioned previously for packed beds with sensible energy storage, is the Biot number, defined in Eq. (4).

Traditionally, for heat transfer problems, a practical limit of  $Bi < 0.1$  is set to render the thermal gradient inside the solid negligible. Therefore, packed beds composed of spheres or capsules several centimeters in diameter can reach high Biot numbers, and the concentric dispersion model may be more appropriate. Regarding the heat transfer fluid, when using air, the heat transfer coefficient  $h$  is typically one order of magnitude lower than that of water (Karthikeyan and Velraj, 2012) for the same mass flow rate, so with the same particle size, the Biot number with air is always smaller than that with water. For this reason, when using air and granulates a few millimeters in diameter, the two-phase continuous model reproduces the experimental data (Rady, 2009a; Izquierdo-Barrientos et al., 2016b). Karthikeyan and Velraj (2012) compared two different two-phase continuous models (regardless of the axial thermal conduction), and a concentric dispersion model solves the thermal gradient inside the particles. Fig. 21 shows a comparison of two continuous phase models (with and without conduction in the solid phase) and a concentric dispersion model, along with experimental results for two different air flow rates, 0.05 and 0.015 kg/s. The authors did not observe differences between model 1 (continuous phase model without conduction in the solid phase) and model 2 (with conduction). The experimental data were obtained for spheres 7 cm in diameter filled with paraffin max. For these experimental data, the Biot numbers were 7.5 and 4.7 for air flow rates of 0.05 and 0.015 kg/s, respectively. In both cases, the concentric dispersion model fit the experimental results better, though the differences between the models reduced as the Biot number decreased. Fig. 22 summarizes the numerical results obtained by Karthikeyan and Velraj (2012) when using air and water as the HTF and varying the sphere size (50, 70 and 100 mm) and the mass flow rate (0.05 and 0.015 kg/s). This figure compares the charging times at a bed height of  $X/L = 0.2$ . It is clearly observed that the differences between the models are smaller when using air as the HTF. The low thermal conductivity of air allows it to obtain lower Biot ( $Bi \lesssim 10$ ) numbers than water. When reducing the size of the spheres, the Biot number generally decreases, though not in the same proportion because the heat transfer coefficient increases (Karthikeyan and Velraj, 2012). In general, the lower the Biot number, smaller the difference between the models.

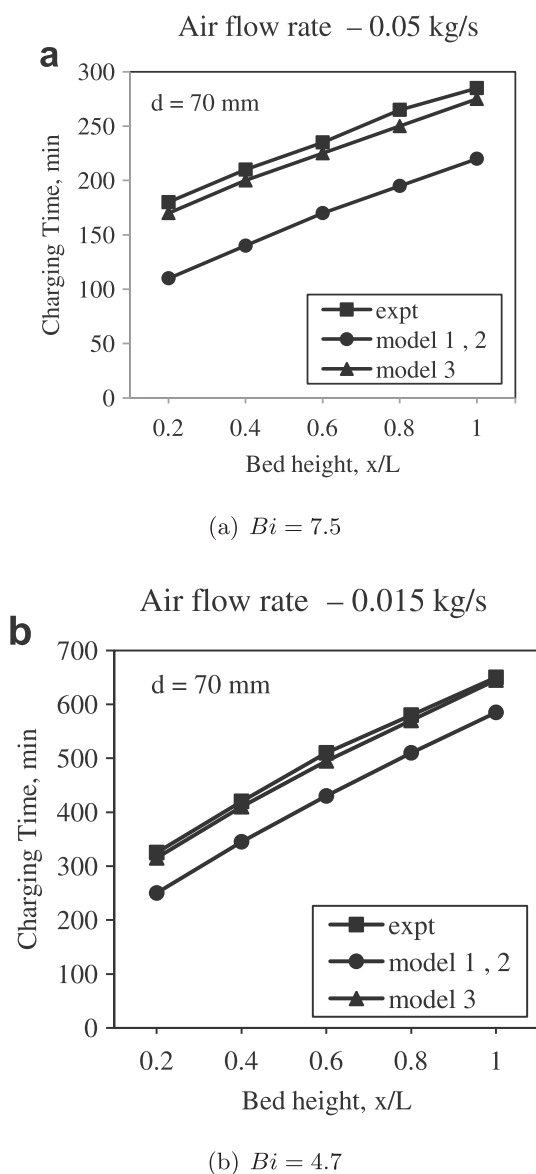


**Fig. 21.** Comparison of the continuous phase models without conduction in the solid phase (model 1) and with conduction (model 2) along with the concentric dispersion model (model 3) and the experimental data (Karthikeyan and Velraj, 2012). Experimental data were obtained using air as the heat transfer fluid and 70-mm-diameter spheres filled with paraffin wax as the PCM.

### 2.3. Thermochemical energy storage

In thermochemical energy storage, the energy is stored through a reversible reaction, which can be expressed in a general form as follows (Solé et al., 2015):



During the charging process, heat is supplied to the endothermic reaction to produce two new compounds, which can be stored, even at ambient temperature, without thermal losses to the surroundings. When the energy is to be discharged, the reaction is shifted to the left, and the two compounds B and C react in an exothermic reaction. Some authors discussed about the processes that should be called “Thermochemical Energy Storage” because they do not consider physical adsorption (a surface phenomenon in which one substance is adhered to the surface of an adsorbent without a change in the molecular structure of the compound) or physical absorption (when the molecules of one substance penetrate the volume of the adsorbent) to be a type of

thermochemical storage, as indicated in Fig. 23 (N’tsoukpoe et al., 2009). Some authors (Yu et al., 2013; Solé et al., 2015) have discussed the different processes and expressions used by other authors for the different processes shown in Fig. 23. In this section, we consider both processes, chemical and sorption processes, as we are only interested in particle technologies employed in reactors. We focus only on gas/solid reactions (for both low- and high-temperature applications) and not on gas/liquid or solid/liquid reactions (Linder, 2015; Yu et al., 2013).

#### 2.3.1. Low-temperature applications and experiments

For low-temperature applications ( $T \lesssim 150$  °C, temperatures suitable for solar collectors to obtain without concentration in buildings), sorption processes have been widely studied (Yu et al., 2013; Solé et al., 2015; Aydin et al., 2015) using zeolites, silica gel and salt hydrates as sorbents. When a packed or a fluidized bed is used with direct contact between the particles (sorbent) and the heat transfer fluid (typically air), in the charging process, hot and dry air is pumped through the bed of particles, and water is released, which is collected from the outlet of the bed as a stream of air and water at low temperature. During the discharge process, it is necessary to introduce a flow of air and water to the reactor, as water is retained in the sorbent during an exothermic process. The released energy increases the temperature of the air at the outlet of the reactor. The integration of the reactor with auxiliary systems can be in an open or a closed configuration, as shown in Fig. 24 (Solé et al., 2015; Krese et al., 2018). In an open system, the water produced during the charging process is released to the atmosphere. During the discharging process, atmospheric water is used to invert the process. In this open configuration, the atmospheric humidity plays an important role, and an additional humidifier may be necessary to increase the humidity to achieve a good discharging rate. In a closed configuration, water is condensed and stored in liquid form and is evaporated later during the discharging process. The closed configuration has the main advantage of permitting the control of the operating pressure in the reactor.

Johannes et al. (2015) constructed a prototype of low-temperature TCS with Na-X zeolites in a packed bed reactor. They distributed 80 kg of zeolites into two different packed beds of 40 kg each, and the beds could be combined in series or in parallel. They carried out different experiments with air flow rates of 120 and 180  $\text{m}^3/\text{h}$  and temperatures of 120 and 180 °C during the charging process. During the discharging process, the air temperature was fixed at 20 °C, and the relative humidity was varied between 50% and 70%. Fig. 25 shows the experimental results during charging (Fig. 25(a)) and discharging (Fig. 25(b)). The charging process is complete after approximately 5 h, when the temperatures at the bottom and at the top of the packed bed remain constant and equal to 110 °C. The temperature difference between the inlet temperature of the air and the steady state after 5 h is related to thermal losses to the surroundings. During the discharging process, the air temperature is increased up to 57 °C and maintained at this temperature over approximately 4 h. After approximately 7 h, the bed is fully discharged. The authors obtained the COP values, defined as the ratio between the heat gained and the sum of the electric consumption of the fan and the humidifier, which varied between 1.7 and 6.8 depending on the operating conditions, along with recovery efficiency values (ratio between the released and the stored energy) of 50% in most cases.

In a different work, Zondag et al. (2008) experimentally studied a packed bed of reduced dimensions (diameter of 1 cm) with the solid salts  $\text{MgSO}_4$  and  $\text{CaCl}_2$  and zeolites. Fig. 26 shows the experimental data obtained during the charging process with the salt  $\text{CaCl}_2$ . The bed was initially at 50 °C and a stream of steam was introduced in the bed at 10 °C. The exothermic process led to an increase in the bed temperature of approximately 10 °C. The salt temperature is higher at the top of the bed than at the bottom. Zondag et al. (2008) observed that in a packed bed reactor, the heat and mass transfer rates are low, which led to longer charging and discharging times. As a possible solution, they

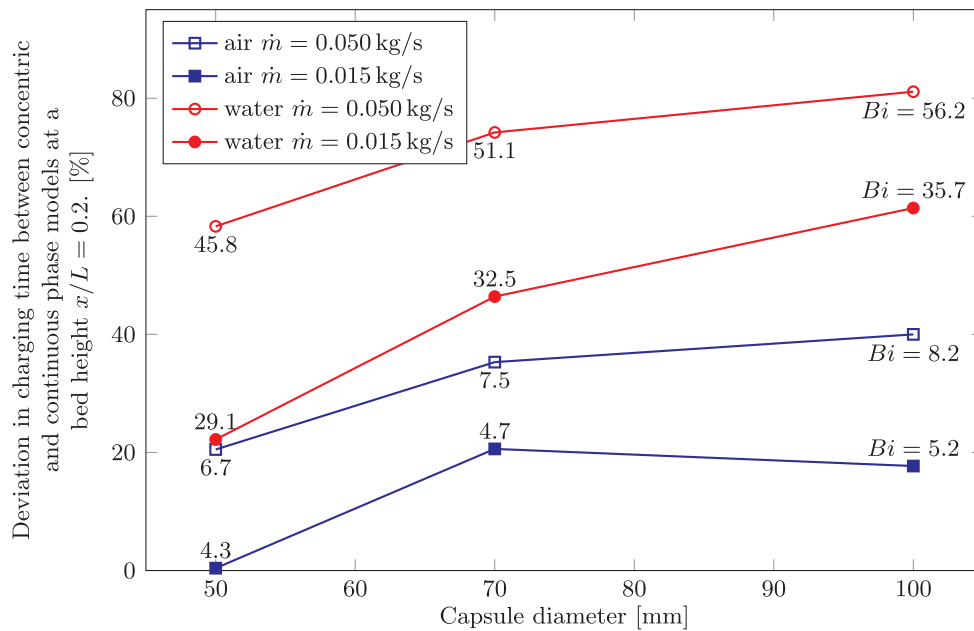


Fig. 22. Deviations in the charging times obtained at a bed height of  $x/L = 0.2$  for the concentric and the continuous phase model obtained by Karthikeyan and Velraj (2012). Data were obtained for different diameters and mass flow rates using air and water as heat transfer fluids. The Biot number is also indicated in the figure.

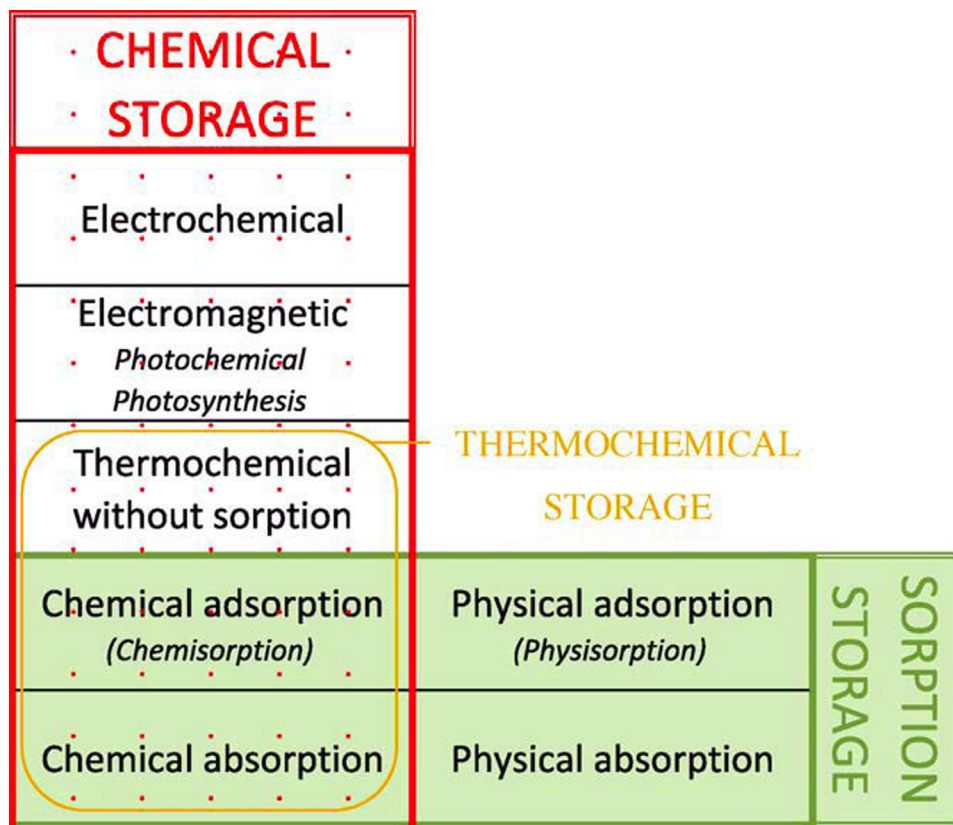


Fig. 23. Classification of the different chemical and sorption storage processes according to N'tsoukpoe et al. (2009).

proposed to stir the reactor and remove the inert gas. Fig. 27 compares the charging process of the packed bed with zeolites and the same bed but stirred. It is clearly observed that the agitation process improves the heat and mass transfer rates to produce higher temperatures.

The ECN (Energy Center Netherlands) developed a seasonal energy storage system based on a packed bed with  $MgCl_2 \cdot 6H_2O$  as the thermochemical storage material (Ferchaud et al., 2012). They constructed

a 20-L prototype. Showing that the  $MgCl_2 \cdot 6H_2O$  could be dehydrated at temperatures below  $130\text{ }^\circ\text{C}$ , while subsequent hydration process could be generate sufficiently high temperatures to provide tap water heating at  $60\text{ }^\circ\text{C}$ .

Krese et al. (2018) reviewed thermochemical energy storage systems for building applications and concluded that the most promising technology is that based on physical sorption with water vapor as

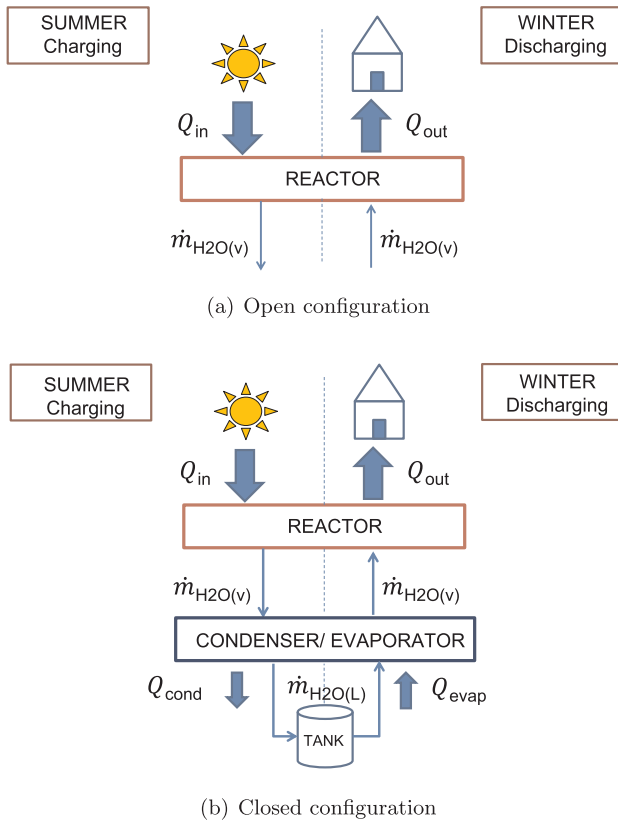


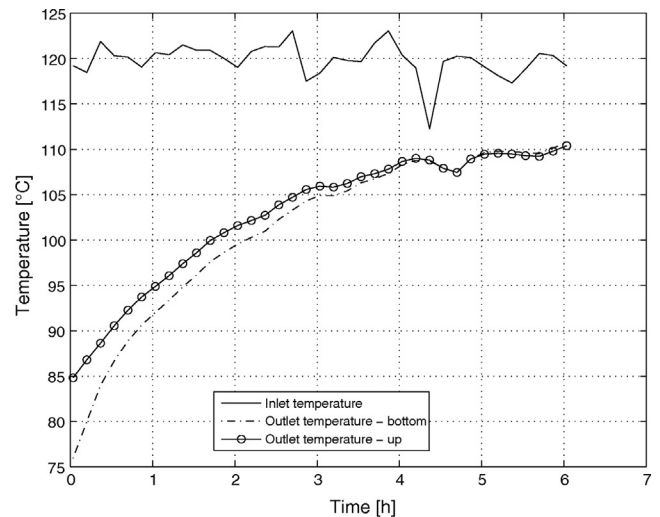
Fig. 24. Open (a) and closed (b) configurations for the integration of a sorption reactor system (Solé et al., 2015).

sorbate. The authors also remarked that, the prototypes tested so far did not perform as successful as expected, exhibiting a lower thermal storage capacity due to the low heat and mass transfer rates in the packed bed reactors.

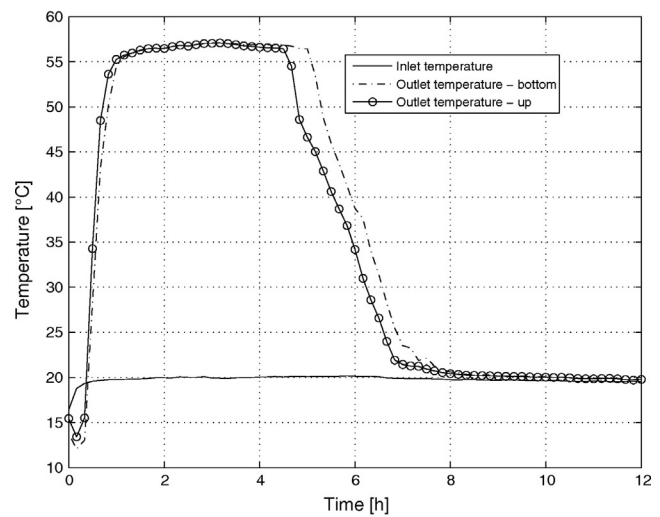
### 2.3.2. High-temperature applications and experiments

High-temperature thermochemical energy storage aims to increase the maximum temperature in CSP over the actual limit imposed by molten salts (approximately 565 °C) to enhance the efficiency of the power cycle (Pardo et al., 2014b; Prieto et al., 2016; André et al., 2016; Pan and Zhao, 2017). Pan and Zhao (2017) compared the different reactors employed for high-temperature TES and noted that packed beds have been extensively studied experimentally by different researchers, although their intrinsic drawbacks (low heat and mass transfer rates) limit their applicability. They proposed other reactor types, including continuous reactors (such as fluidized beds and rotary kilns), where the motion of the particles improve the heat and mass transfer rates, and direct-type reactors, which avoid air gaps among particles in the packed beds, which can lead to low thermal conductivity. They concluded that more investigation is needed for continuous and direct-type reactors due to their high potential for large-scale and seasonal energy storage. Pan and Zhao (2017) also analyzed different reactions and recommended different reactors for each reaction. Table 6 summarizes the recommendations for packed and fluidized bed reactors. For the four reactions studied by the authors the fluidized bed was preferred due to their higher heat and mass transfer rates compared with packed beds, what favours the kinetic of the thermochemical reactions. Only in metal/metal hydride reactions fluidized beds are not recommended due to safety reasons, because the hydrogen produced during the reactions is highly explosive.

The first studies on high-temperature TES in packed beds were carried out during the early 1980s. The pioneering works of Kanzawa and Arai (1981) and Fujii et al. (1985) proposed different systems with



(a) Charging process



(b) Discharging process

Fig. 25. Experimental results obtained by Johannes et al. (2015) during the charging process (a) and discharging process (b). In both cases, the air mass flow rate was 180 m<sup>3</sup>/h, and the relative humidity of the air in the discharging process was 70%.

extended surfaces to improve the heat transfer rate in a packed bed reactor filled with particles of calcium oxide, which were hydrated to obtain calcium hydroxide, according to the following reaction:



These initial works noted the main drawbacks of packed beds reactors, i.e., their low thermal conductivity and heat transfer rate, and proposed solutions to overcome these problems.

More recently, Schaube et al. (2013) and Yan and Zhao (2016) experimentally studied the same reaction (Eq. (7)) in packed beds. Schaube et al. (2013) studied a packed bed with a height of 158 mm and a diameter of 54.5 mm that was filled with 60 g of Ca(OH)<sub>2</sub> particles with a mean particle diameter of  $d_p = 5.26 \mu\text{m}$ . These small-sized particles are Geldart C particles (see Fig. 2). The interparticle forces in this type of particle are strong, and the authors observed agglomeration during the tests; the mean particle size grew to 11.1  $\mu\text{m}$  and 17.6  $\mu\text{m}$  after 25 cycles. This notably reduced the diffusion process in the particles, which indicates that such small particles are not favorable for this process. Yan and Zhao (2016) studied a larger reactor with a volume of 1 L and introduced 400 g of sample in the bed. The authors did

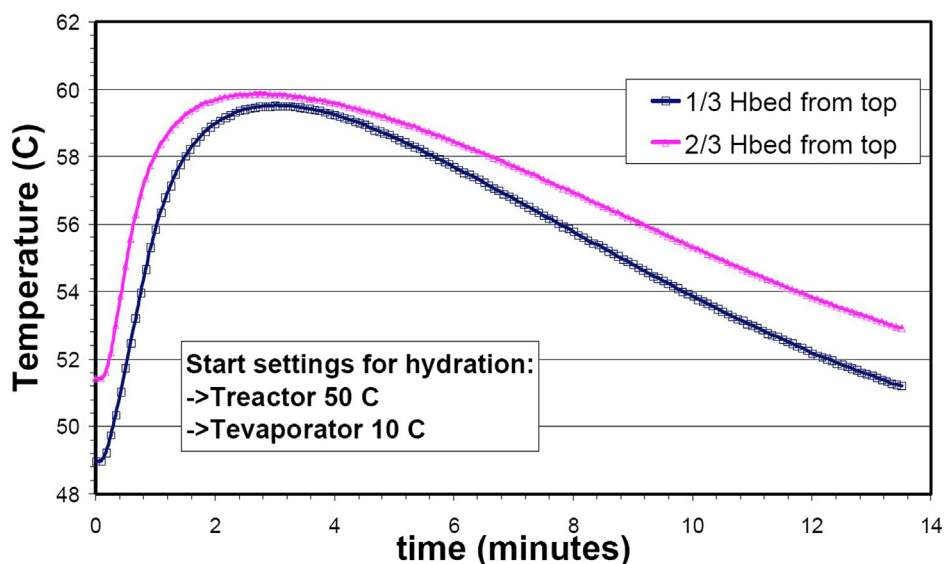


Fig. 26. Experimental results in a packed bed with a 1-cm diameter obtained by Zondag et al. (2008) during the discharging process using CaCl<sub>2</sub>. The initial temperature of the reactor was 50 °C and the steam was introduced in the reactor at 10 °C.

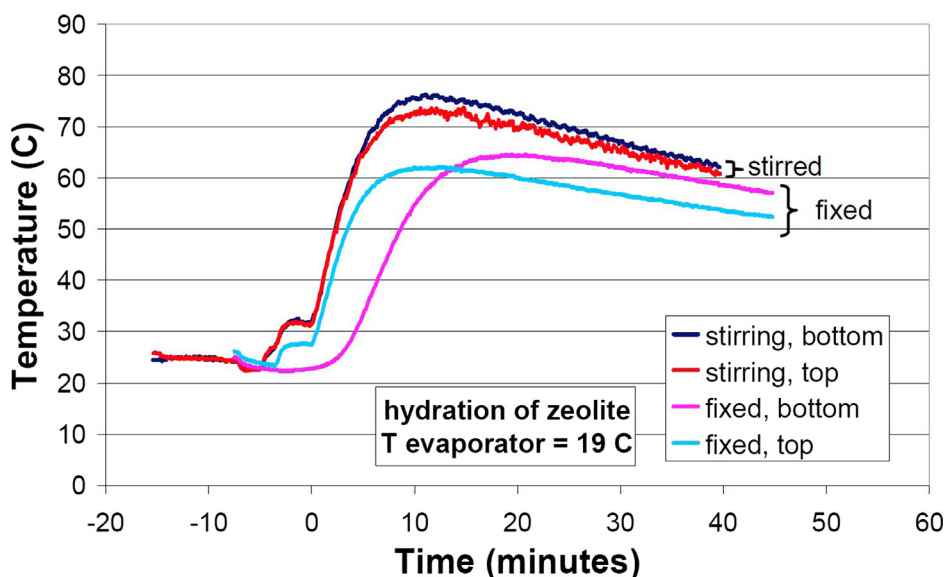


Fig. 27. Comparison of the charging process in a packed bed filled with zeolites, where the bed was in the steady state or stirred (Zondag et al., 2008).

Table 6

Popular reactors for different high-temperature reactions (Pan and Zhao, 2017). “Favorite” indicates that the reactor is recommended, “Acceptable” indicates that the reactor can be used with some intrinsic drawbacks, and “Unavailable” indicates that the reactor is not suitable.

	Packed beds	Fluidized beds
Oxide/hydroxide	Favorite	Favorite
Metal/metal hydride	Favorite	Unavailable
Oxide/carbonate	Acceptable	Favorite
Redox reaction	Acceptable	Favorite

not indicate the particle size. They measured temperatures at different positions in the bed, as indicated in Fig. 28(a), where thermocouples A and B are located inside the reactor and thermocouple C in located on the outer wall. Position D indicates the water vapor inlet in the reactor. Fig. 28(b) shows the experimental results obtained during the charging process. The temperature measured by thermocouple B,  $T_B$ , was always higher than that measured by thermocouple A,  $T_A$ , because the reactor

was heated by electrical resistance from the outer wall. The difference between the temperatures is caused by the low thermal conductivity of the bed. The same figure shows the outlet temperature in the bed and  $\alpha_{de}$ , which is the percentage of mass in the bed that reacted.

Wokon et al. (2017) carried out experiments in a tube 54.3 mm in diameter, with a packed bed of granular manganese-iron oxide. The redox reaction in the reactor is



They introduced approximately 500 g of material in the packed bed with an initial mean particle size of 2.13 mm. After various cycles, the particles were eroded, and the mean particle size was reduced to 1.74 mm. Fig. 29 shows the temperatures along the bed height and the O<sub>2</sub> concentration during the full charging-discharging cycle. The bed was at 940 °C at the beginning of the experiment, and the temperature of the inlet air was increased up to 1040 °C. After 150 min the discharging process began, reducing the air temperature at a rate of 5 K/min. Wokon et al. (2017) concluded that the charging time is reduced when the air flow rate and/or the air inlet temperature are augmented.

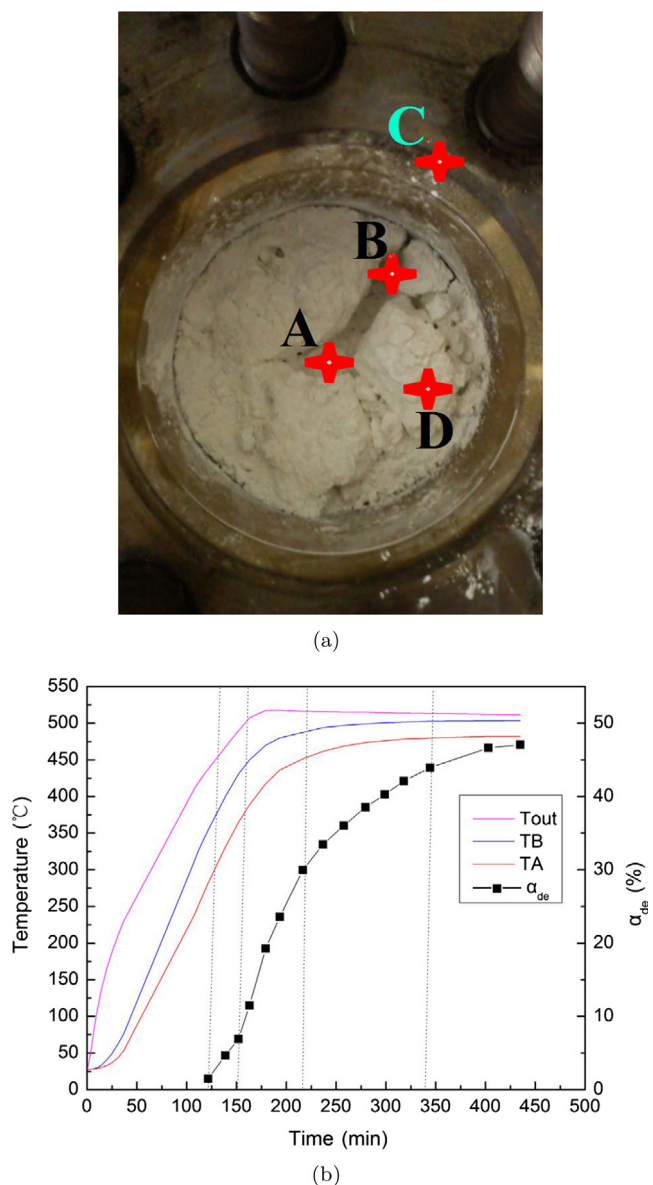


Fig. 28. (a) Location of the thermocouples in the reactor used by Yan and Zhao (2016) and (b) experimental results obtained during a charging process.

Ströhle et al. (2017) proposed a novel heat storage system combining a sensible packed bed energy storage unit and a thermochemical storage unit on the top of the bed to maintain more stable the outlet temperatures of the HTF during the discharging period. In a conventional packed bed with sensible energy storage, the outlet temperature decreases with time, which can lead to a significant decrease in the efficiency of the power block. The configuration proposed by Ströhle et al. (2017) permits to maintain very stable the outlet temperatures of the HTF for prolonged periods of the discharging stage. In the thermochemical section, the gas and the solid are placed inside tubes, which are physically separated from the HTF, allowing the reaction pressure to be adjusted to the operating conditions. They used the thermochemical reaction of manganese oxide:



Ströhle et al. (2017) carried out numerical simulations of the proposed system following the model proposed by the same authors (Ströhle et al., 2014). Ströhle et al. (2017) studied a storage tank with 1 m<sup>2</sup> of cross section area and a total height of 4 m. They compared the performance of this tank filled with sensible energy storage material with

two different alternatives: CS1 (which consisted in a storage of 3.5 m in height of sensible and 0.5 m of thermochemical energy storage material) and CS2 (3.25 m in height of sensible and 0.75 m of thermochemical energy storage material). Fig. 30 shows the HTF outlet temperature of both thermochemical configurations compared with the 4 m in height sensible heat material packed bed under the same experimental conditions. In both cases the outlet temperature remained nearly constant during 12 h, whereas a progressive reduction was observed for the sensible packed bed.

Álvarez de Miguel (2017) experimentally compared the redox reaction of manganese oxide pellets (commercial Mn<sub>3</sub>O<sub>4</sub>LH material) under packed and fluidized bed conditions. The pellets were between 2 and 3.6 mm in size, which makes them type D particles according to Geldart's classification (Geldart, 1973). Fig. 31(a) shows the experimental measurements of the temperature evolution in the packed bed, with an air flow rate of 20 N m<sup>3</sup>/h over 25 cycles. In the upper-right zone of the graph, the reduction process occurs, and the oxidation process occurs in the lower-left region, where the temperature is at a minimum. The lines that do not follow the general trend represent the first cycles, which are affected by the initial conditions in the bed. Álvarez de Miguel (2017) studied the pellet properties before and after the cycling process and observed two different materials after the cycling process: a black material located at the top of the bed, which did not suffer high temperatures, and a brown-red material at the bottom of the bed, which was heated to high temperatures. The main difference was observed in the mean pellet size, which was reduced from 2.9 mm to 2.7 mm and 2.6 mm for the pellets located at the top and bottom of the bed, respectively. The hardness of the pellet notably increased from an initial value of 33–45 N for the black material at the top of the bed and to 77 N for the brown-red material at the bottom. No relevant differences were observed in the pellet density. Fig. 31(b) shows the experimental results obtained with a pellet of manganese oxide doped with 5% iron. In this case, the pellet density increased from an initial value of 1700–2200 kg/m<sup>3</sup>. The temperature range of the doped material slightly increased compared to that of the regular material. Additionally, the repeatability of the cycles is better when using the doped material.

### 3. Fluidized beds

#### 3.1. Low-temperature sensible energy storage

The application of fluidized beds to sensible heat storage has been experimentally investigated, and it has been shown that a fluidized bed behaves similar to a well-mixed tank with negligible variations in the temperature along the bed (Elsayed et al., 1988; El-Refaee et al., 1988; Megahed et al., 1988; Izquierdo-Barrientos et al., 2013; Izquierdo-Barrientos et al., 2015a; Mahfoudi et al., 2015). For this reason, when the bed is coupled with a solar collector, packed beds are preferred because stratification permits an increase in the thermal efficiency of the solar collection system, as was explained in Section 2.1.

##### 3.1.1. Applications and experiments

Elsayed et al. (1988) experimentally tested sand particles ( $d_p = 0.4$  mm, Geldart B) in a cylindrical bed with different inlet air temperature ramps: constant supply temperature and temperatures increasing linearly or exponentially. They observed that the storage efficiency is always higher with a constant supply temperature. 90% of the maximum energy is reached after  $\tau = 12$  ( $\tau$  being a non-dimensional time) with a constant air temperature at the inlet of the fluidized bed, whereas  $\tau = 24$  is needed when the supply air temperature is increased linearly or exponentially. El-Refaee et al. (1988) developed a numerical model that satisfactory corresponded with the experimental results of Elsayed et al. (1988). Megahed et al. (1988) used the numerical model of El-Refaee et al. (1988) to study the performance of a fluidized bed coupled with a solar concentrator. Their results showed that there is a

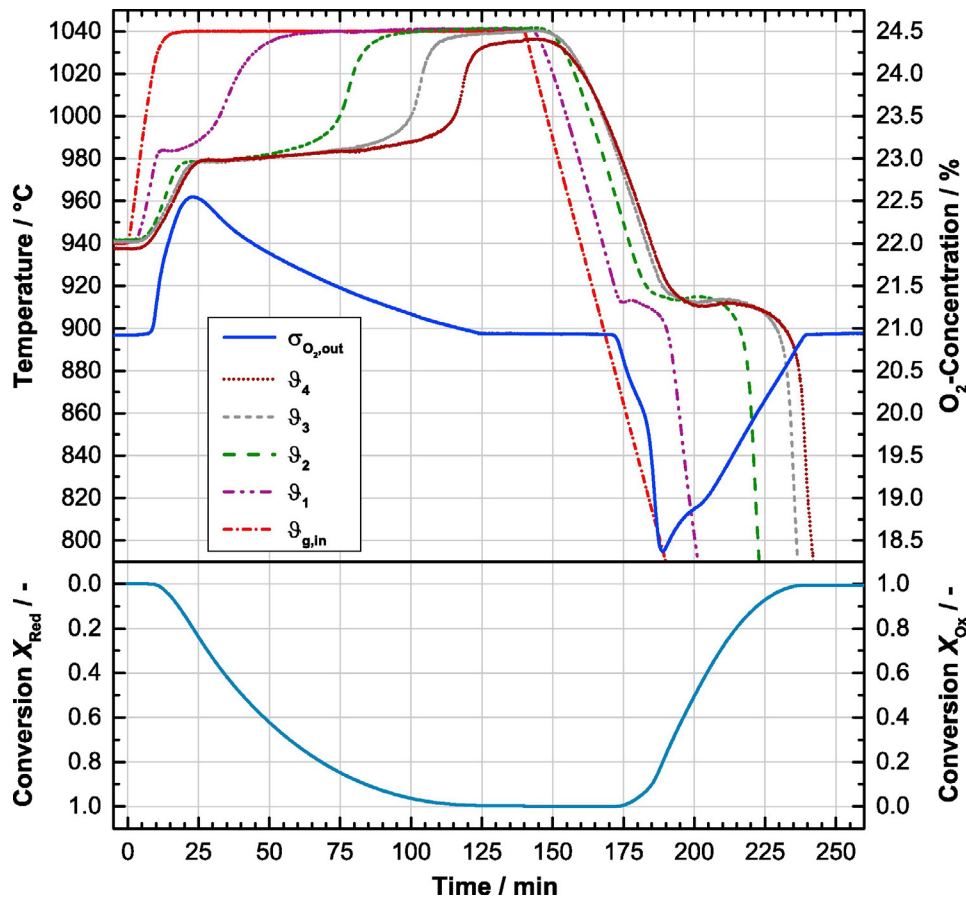


Fig. 29. Experimental results of the full charging-discharging process in a lab-scale packed bed through the redox reaction of manganese-iron oxide. In the discharging process, the air inlet temperature is reduced at a rate of 5 K/min (Wokon et al., 2017).

ratio between the area of the bed and the area of the concentrator that maximizes the efficiency of the system.

The more recent works by Izquierdo-Barrientos et al. (2013, 2015a) compared the performance of a fluidized bed with a sensible material (Geldart B sand particles) and one with the granular PCM from Rubitherm described in Section 2.2.1, but with a low particle size more suitable for use in a fluidized bed (Izquierdo-Barrientos et al., 2016d). Rady (2009a,b) and Izquierdo-Barrientos et al. (2013, 2016b), in their studies for packed beds with PCM, used granular PCMs with particle sizes between 1 and 3 mm, whereas Izquierdo-Barrientos et al. (2013, 2015a) used the same material but with a particle size between 0.2 and 0.6 mm, which belongs to Geldart B particles (Izquierdo-Barrientos et al., 2016d). The experimental results presented by Izquierdo-Barrientos et al. (2013, 2015a) corroborate the well-mixed behavior of the fluidized bed with sand.

When the particles are fluidized, the heat transfer coefficient between the fluidized particles and any internal surface notably increases due the continuous motion of the particles in comparison with a packed bed. Izquierdo-Barrientos et al. (2015b) experimentally measured values in the range 100–200 W/(m<sup>2</sup> K) for sand particles in a packed bed, whereas the same particles fluidized reached values up to approximately 900 W/(m<sup>2</sup> K) for a superficial air velocity 1.6 times over minimum fluidization conditions. This fact opens the possibility of introducing an internal heat exchanger in the fluidized bed to recover the energy from the solids continuously, avoiding the need to work discontinuously. Izquierdo-Barrientos et al. (2016a) studied different heat exchanger geometries (helical coils) immersed in a fluidized bed and observed that when the coils are separated, the contact between the fluidized particles and the heat transfer surface is improved, increasing the heat transfer coefficient. Izquierdo-Barrientos et al. (2015b, 2016c)

measured the heat transfer coefficient in a fluidized bed with sand (see Fig. 32(a)) and observed a heat transfer coefficient between 500 and 900 W/(m<sup>2</sup> K) for fluidization velocities up to 1.6  $u_{mf}$ . Mahfoudi et al. (2015) numerically studied with Fluent the potential of a fluidized bed to be used as energy storage system. They concluded the chaotic behavior of the bubbles in the bed allowed a high heat transfer coefficient between the gas and the fluidized solids.

### 3.2. High-temperature sensible energy storage

CSP plants typically use HTFs such as thermal oils or molten salts, whose main inconvenience is their operating limit temperature: 400 °C and 560 °C, respectively. Thus, there is considerable interest in the search for new HTFs that permits elevation of the maximum temperature to improve the cycle efficiency. In this context, the use of solid particles is becoming in a true alternative to conventional HTFs because they can reach temperatures up to 1000 °C without degradation, well above the limit of 560 °C of the current CSP system obtained with molten salts as HTFs (Ho, 2016; Calderón et al., 2018).

The use of particles in CSP has been previously studied by different researchers. For example, Hrubby (1986) and Greif and Crowe (1987) were the pioneers in the development of downstream particle receivers.

Fig. 33 summarizes the different receiver designs proposed by Ho (2016), who classified them in two main categories, depending on whether the solar radiation is supplied directly or not on the particles. Direct particle heating receivers irradiate the particles directly as they fall through a receiver, while indirect particle heating receivers utilize tubes or other enclosures to convey heat to the particles. Alternative direct particle receiver designs include free-falling, obstructed flow, centrifugal and fluidized beds. The main advantage of all these designs,

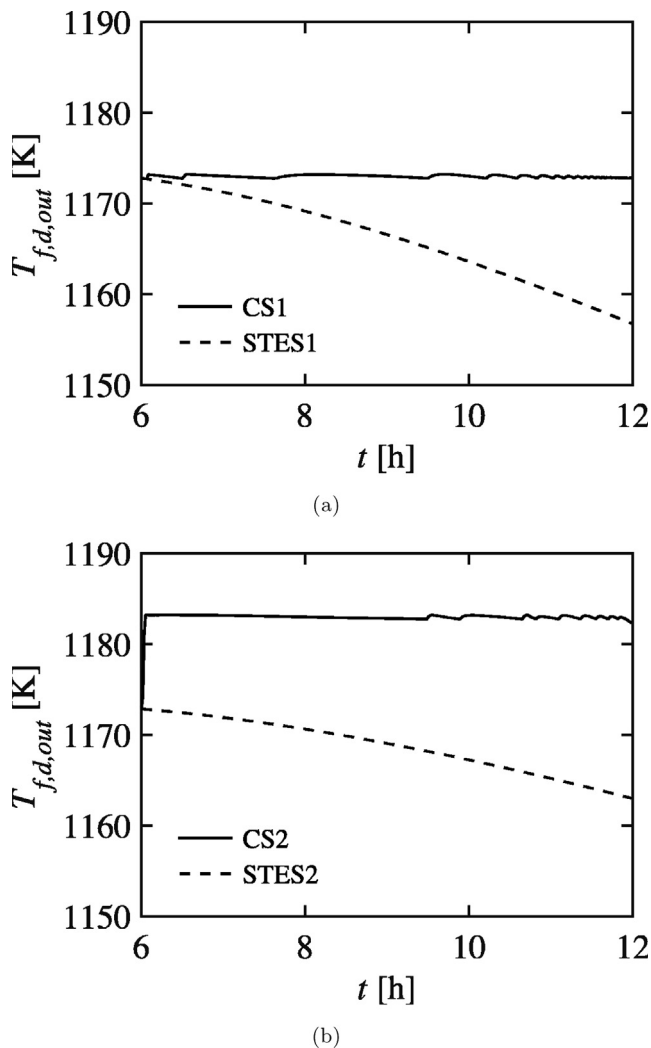


Fig. 30. Numerical results of the charging process obtained by Ströhle et al. (2017) in a reactor with a diameter of 1 m and height of 4 m. In (a), the temperature profile over time along the bed height is shown, and (b) shows the details of the thermochemical section at the top of the reactor, including the temperatures of the tubes and the HTF.

thanks to direct heating of the working fluid, is that the energetic losses through an intermediate heat exchanger are reduced in a power cycle; furthermore, the flux and the temperature limitations associated with a tubular central receiver (high stresses resulting from the containment of high-temperature, high-pressure fluids) are mitigated. However, indirect particle designs (gravity-driven particle flow through enclosures, flow in tubes with or without fluidization) have the ability to store the particles for energy production during non-solar hours.

Matsubara et al. (2014) distinguished between two different schematics of CSP reflector systems: a conventional tower system (Fig. 34(a)) and beam-down reflector system (Fig. 34(b)). Both schemes can be used to directly radiate the particles in a fluidized bed, although the beam-down reflector is preferred because it avoids the high pumping cost of moving the particles up. Flamant (1982) proposed a novel fluidized-bed receiver to be located on the top of the tower, similar to a conventional tower system, although this design was not developed. Most of the research using fluidized beds with direct radiation on particles used beam-down systems (Flamant, 1982; Flamant and Olalde, 1983; Matsubara et al., 2014; Tregambi et al., 2016; Salatino et al., 2016). Table 7 summarizes the different particles used by different researchers who used a fluidized bed with direct radiation on particles.

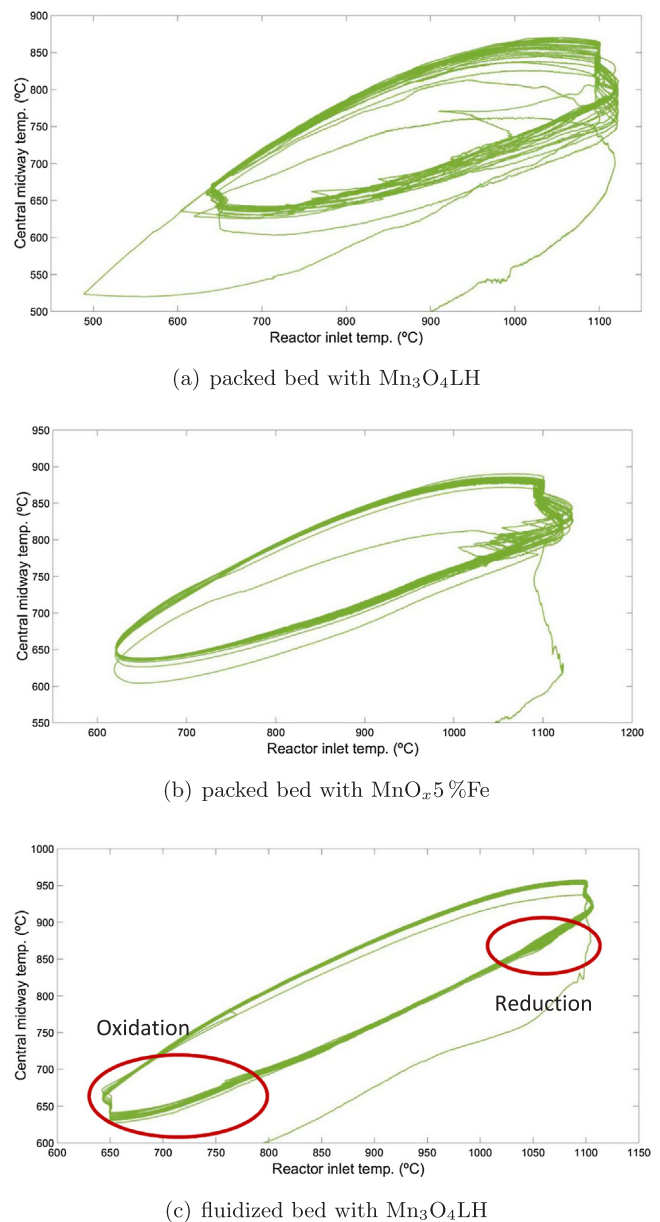


Fig. 31. Temperature in the middle of the reactor versus the air inlet temperature over 25 consecutive cycles with (a) a packed bed containing  $\text{Mn}_3\text{O}_4\text{LH}$  particles, (b) a packed bed containing doped particles  $\text{MnO}_x.5\%\text{Fe}$  and (c) a fluidized bed containing  $\text{Mn}_3\text{O}_4\text{LH}$  particles.

### 3.2.1. Direct particle radiation

According to Flamant and Olalde (1983) the fluidization process has several advantages, such as high absorptance, uniform temperature distribution and high heat transfer coefficients (insomuch as the particles are in continuous movement). The author compared packed and fluidized bed receivers through a high-temperature solar receiver bed (temperature level of air ranges 700–1500 K, depending on the concentrated solar flux, which ranges 250–2200  $\text{kW}/\text{m}^2$ ). Using the experimental results of Flamant and Olalde (1983), Figs. 35 and 36 compare the temperature profiles and the efficiencies obtained for both beds.

Fig. 35 shows the temperature profile for a packed and fluidized bed as a function of axial distance for each receiver. The fluidized bed exhibits a large plateau indicating a stable temperature (close to 1000 K) in approximately 80% of the bed height. In the fixed bed, higher temperatures (over 1300 K) are reached on the top of the bed, where the solar radiation impinges, which results in higher IR emission losses,

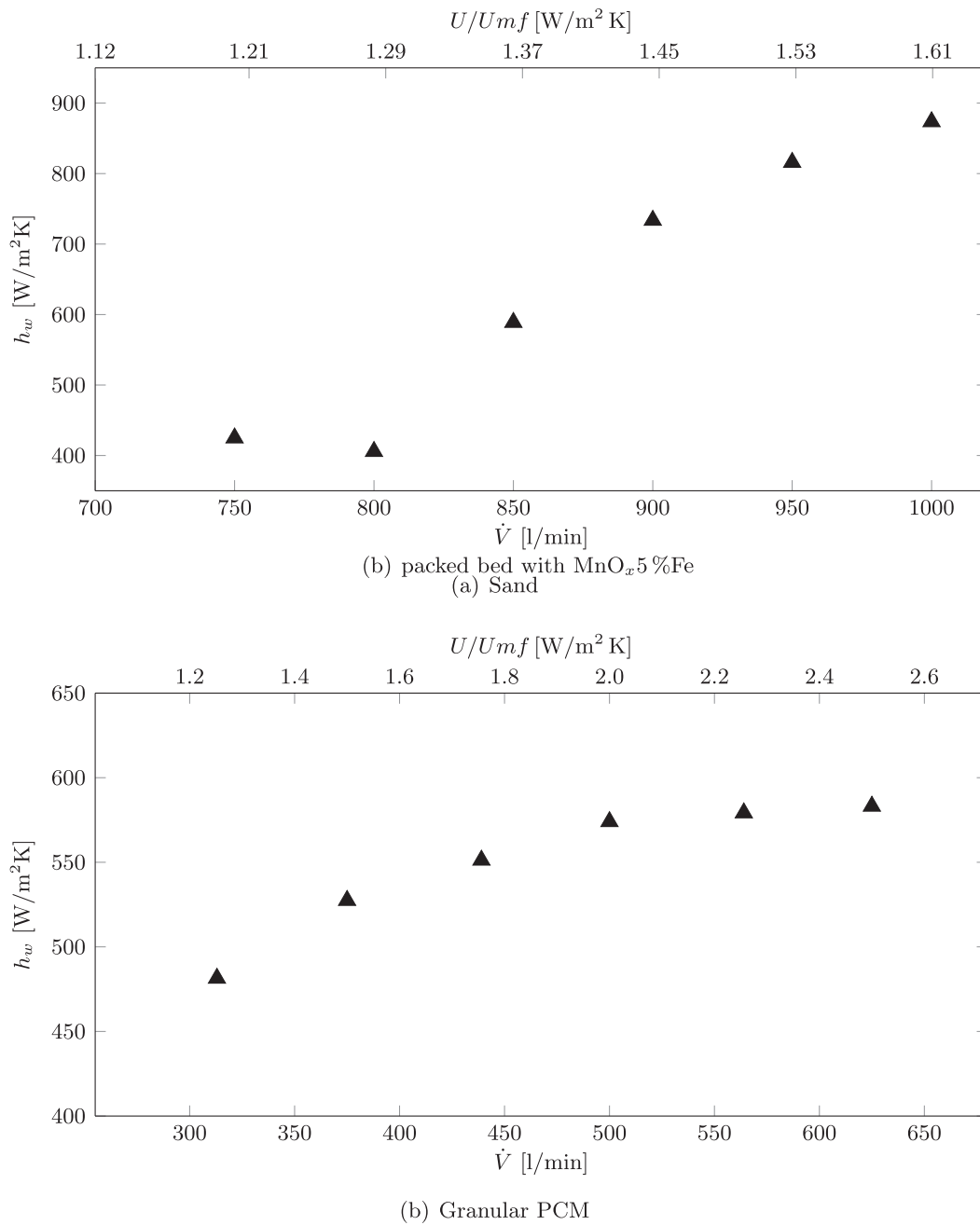


Fig. 32. Experimental heat transfer coefficient in a fluidized bed of (a) sand and (b) granular PCM (Izquierdo-Barrientos et al., 2015b).

which are 3.8 times greater than for the fluidized bed.

Fig. 36 shows the thermal efficiency vs. mass flow for two different materials: SiC and ZrO<sub>2</sub> for packed and fluidized beds. Thermal

efficiency was defined by Flamant and Olalde (1983) as the ratio between the thermal power given by the particles to the gas stream divided by the incident power on the bed. The thermal efficiency

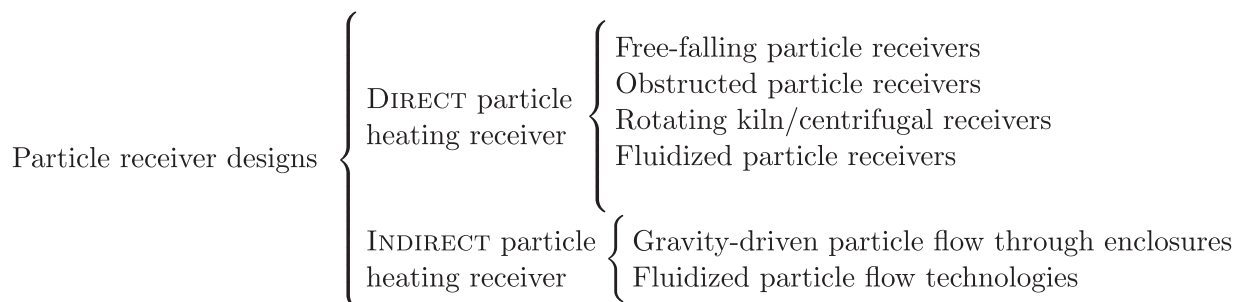


Fig. 33. Scheme of classification of different particle receiver design. Ho (2016).

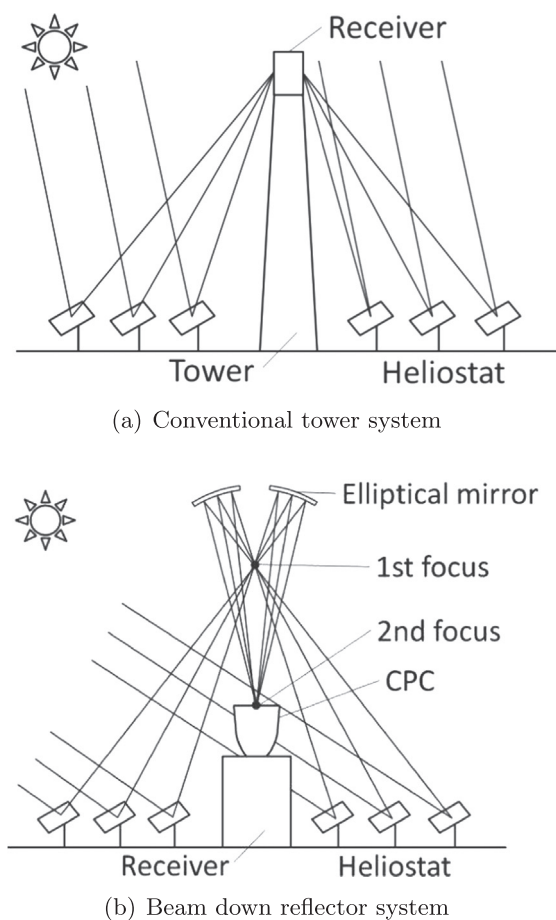


Fig. 34. Different configurations of a CSP reflector system, depending on the location of the receiver Matsubara et al. (2014).

increases with the gas flow rate. Although it is not plotted in Fig. 36, the range of outlet gas temperature is 800–1550 K for packed and 650–1150 K for fluidized beds. In view of these results, Flamant and Olalde (1983) proposed a linear relationship between the outlet gas temperature and the thermal efficiency of the system. For the same flow rate, higher thermal efficiencies are obtained when working with SiC instead of  $ZrO_2$  and with fluidized beds instead of fixed beds.

Furthermore, one conclusion of this work involves the combined efficiency, defined as the ratio between the net power of a thermal cycle and the incident power on the bed. They did not study any specific

cycle. Instead, the authors assumed a modified Carnot efficiency for the cycle efficiency. The maximum value of the combined efficiency for packed bed was 0.27, and it reached the range of 750–950 K for the SiC and 0.18 in the range of 1100–1300 K for  $ZrO_2$ . For fluidized beds, higher efficiencies were obtained: the maximum combined efficiencies were 0.40 and 0.24 with SiC and  $ZrO_2$  in the range 700–900 K and 800–1000 K, respectively.

Table 8 shows the energy balance in the packed and fluidized beds studied by Flamant and Olalde (1983) for different bed materials. The main conclusion is that fluidized beds obtain higher fractions of the energy transferred to the air than packed beds, mainly due to the high values of reflected solar radiation and energy losses by IR emission in packed beds, which can reach values up to 70%. The high values of infrared losses in packed beds are directly related to the high temperatures on the bed surface, as represented in Fig. 35.

In a previous work, Flamant (1982) proposed a theoretical model to describe the heat transfer phenomena and determine the temperature profile, total emissivity, flux density distribution, and effective mean penetration distance from measurements in high-temperature solar fluidized beds. His results correlated well at incipient fluidizing conditions for beds of silicon carbide and chamotte (both materials with high values of absorption and emissivity) but were imprecise for beds of zirconia and silica sand.

Tregambi et al. (2016) experimentally studied the behavior of a laboratory-scale fluidized bed radiated with a 4 kW short-arc Xe lamp. The authors characterized the solar flux density of the bed surface and measured the bed surface temperature with an IR camera. They studied the effect of bursting bubbles on the bed surface using SiC particles with a mean particle size of 127  $\mu\text{m}$  (Geldart B particles) with a minimum fluidization velocity of 0.018 m/s at ambient temperature. Fig. 37 shows the probability density functions of the bed surface temperature under freely bubbling conditions with increasing gas flow rates. Tregambi et al. (2016) observed how increasing the air flow rate made the distribution of the bed surface temperature narrower due to the higher mixing rate and larger particle diffusion in the fluidized bed.

Recently, Salatino et al. (2016) proposed some prerequisites for fluidized beds and thus achieved an effective CSP application. These standard requirements are focused on minimization of parasitic energy losses associated with the establishment of the fluidized state, large surface-to-bed heat transfer coefficients and very large thermal diffusivity. The minimization of parasitic energy losses and the maximization of surface-to-bed heat transfer can be solved using fine bed solids (groups of Geldart A or B powders) and operating at gas superficial velocities just beyond incipient fluidization. To achieve high thermal diffusivities, which permit minimizing the large thermal gradients in a bed with a concentrated energy input, Salatino et al. (2016) proposed

Table 7  
Particles used by different researchers for fluidized bed with direct radiation on particles.

Material	Geldart	Diameter	Density	Emissivity	Absorbance	Other	Reference
Silicon carbide (SiC)	A–B (*)	$\leq 0.25$ mm	–	$1 \pm 0.05$	$0.95 \pm 0.05$	Temperature range: 900–1500 K	Flamant (1982)
Chamotte	A–B (*)	$\leq 0.25$ mm	–	$0.8 \pm 0.03$	$0.75 \pm 0.05$	Temperature range: 1000–1300 K	Flamant (1982)
Zirconia	A–B (*)	$\leq 0.25$ mm	–	$0.3 \pm 0.05$	$0.50 \pm 0.05$	Temperature range: 1300–1500 K	Flamant (1982)
Silica sand	A–B (*)	$\leq 0.25$ mm	–	$0.72 \pm 0.03$	$0.50 \pm 0.05$	Temperature range: 1000–1350 K	Flamant (1982)
Silicon carbide (SiC)	D	$\leq 0.72$ mm	$3 \times 10^3$ kg/m <sup>3</sup>	1	0.9	Maximum temperature 1920 K	Flamant and Olalde (1983)
Zirconia	D	$\leq 0.60$ mm	$5.2 \times 10^3$ kg/m <sup>3</sup>	0.5	0.5	Maximum temperature 2700 K	Flamant and Olalde (1983)
Ceramic particles (NiFe <sub>2</sub> O <sub>4</sub> /mZrO <sub>2</sub> )	–	0.21–0.71 mm	–	–	–	Maximum temperature 1700 K Spouted bed	Matsubara et al. (2014)
Silicon carbide	B	$\leq 0.127$ mm	3210 kg/m <sup>3</sup>	–	–	–	Tregambi et al. (2016)

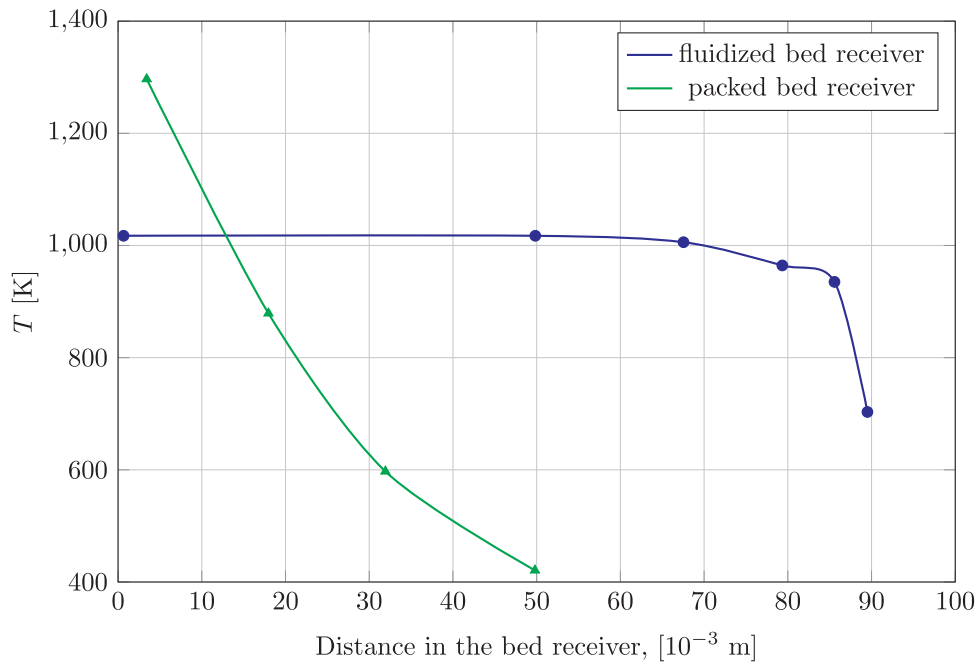


Fig. 35. Experimental temperature profile as a function of axial distance in the fluidized and packed bed receiver Flamant and Olalde (1983). Both experiments were performed on SiC with a gas mass flow rate of 0.27 kg/m<sup>2</sup> s.

two different alternatives to traditional fluidized beds: uneven and unsteady (pulsed) fluidized beds.

Figs. 38 and 39 show the differences between even and uneven fluidization. Fig. 38 is a qualitative scheme that compares the gross solids flow patterns that are likely establish in the case of even (A) and uneven (B) fluidization. In uneven fluidization, a fraction  $f$  of the bed cross-section is fluidized at a gas superficial velocity exceeding the minimum fluidization velocity ( $U_{mf}$ ), where  $(1-f)$  is the fractional cross-section of the bed that is kept at incipient fluidization. Fig. 39 amplifies the qualitative features displayed in the previous figure and presents snapshots from 2D CFD computations of the flow structures of the fluidized beds of Geldart group B particles ( $d_p = 2.5 \times 10^{-4}$  m;  $\rho = 2560$  kg/m<sup>3</sup>) operating with each mechanism of fluidization (even

Table 8

Experimental heat balance of both receivers. Terms are representative of a fraction of incident solar power. Flamant and Olalde (1983).<sup>\*</sup> And transmission in fluidized bed.

	Packed bed		Fluidized bed	
	ZrO <sub>2</sub>	SiC	ZrO <sub>2</sub>	SiC
Fraction lost by reflexion <sup>*</sup>	50%	10%	55%	19%
Fraction lost by conduction-convection	5%	5%	5–10 %	5–20%
Fraction lost by IR emission	15–25%	45–55%	1–6%	10–25%
Fraction transferred to the gas	20–30%	30–40%	30–40%	40–70%

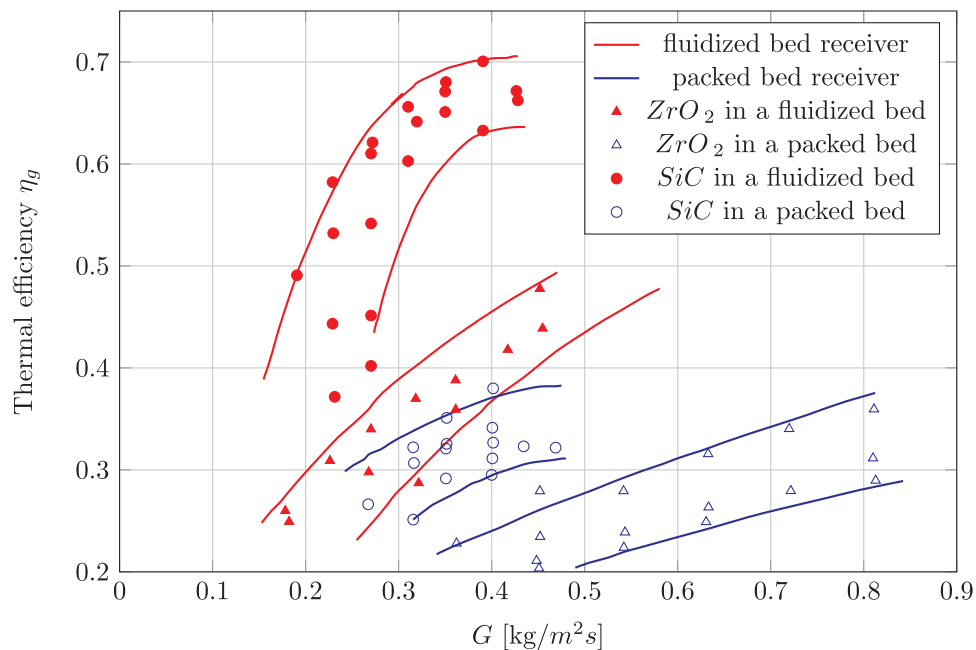


Fig. 36. Thermal efficiency vs mass flow rate in the fluidized and packed bed receivers. Flamant and Olalde (1983).

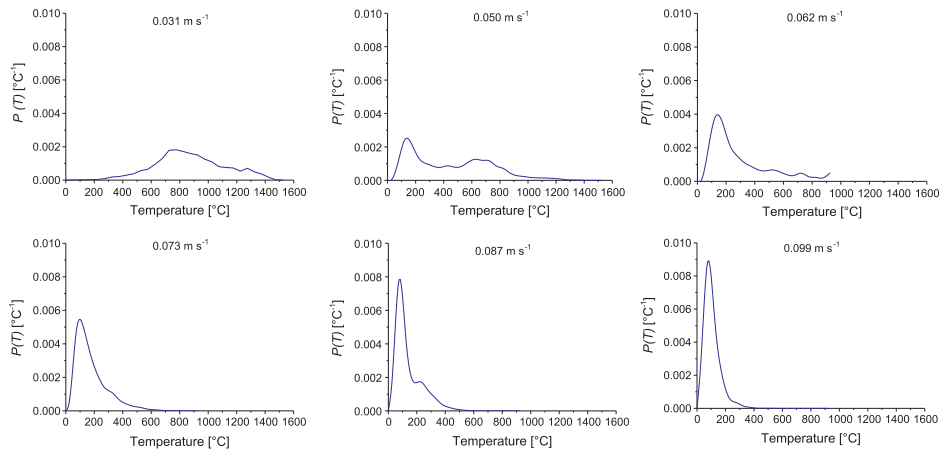


Fig. 37. Probability density functions of the bed surface under freely bubbling conditions for different air flow rates. Data obtained by Tregambi et al. (2016).

and uneven fluidization). Salatino et al. (2016) estimated that uneven fluidization can improve the solid diffusivity by one order of magnitude, augmenting the effective bed solid diffusivity from  $O(10^{-2})$  m<sup>2</sup>/s up to  $O(10^{-1})$  m<sup>2</sup>/s.

In addition, according to Salatino et al. (2016) unsteady fluidization (pulsed) has two other main advantages: (a) the thermal properties can be continuous modulated, and (b) a pulsed bed can operate with similar effective thermal properties with superficial velocities, on a time-average basis, lower than the minimum required to fluidize the bed.

One of the main parameters to define in any fluidized system is the gas flow rate, which has to be higher than the minimum needed for fluidization. In general, as the gas velocity increases, a greater agitation occurs and therefore the mixing of the particles is favored, reaching high and homogeneous temperatures in most parts of the bed. Such temperature uniformity was observed by Flamant (1982) (Fig. 40) and by Matsubara et al. (2014) (Fig. 41). Fig. 40 shows the axial temperature profiles in a bubbling fluidized bed for different excess gas velocities over the minimum fluidization. The results clearly indicate how increasing the gas velocity increases the uniformity of the temperature and reduces the average temperature in the well-mixed region. For the highest gas velocity tested by Flamant (1982), which 1.7 times over minimum fluidization velocity, almost 80% of the bed height is fully mixed with an average temperature close to 1000 K. Only at the bottom of the bed, which can be influenced by the jets coming from the distributor (Rees et al., 2006), is the temperature lower.

Matsubara et al. (2014) experimentally studied a spouted bed with a draft tube, which organizes the particle motion in the bed. They measured the temperature distribution in the bed, maintaining a ratio between the gas velocity in the core and in the annulus of the bed

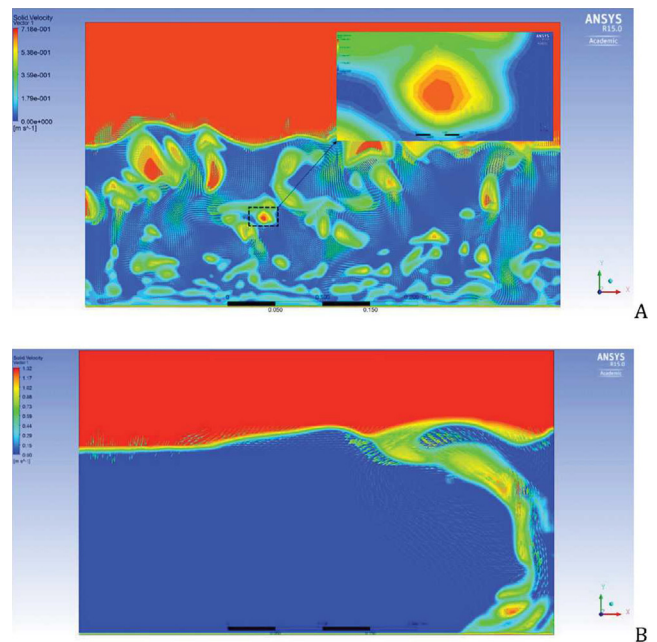


Fig. 39. Solid flow patterns in dense gas fluidized beds from 2D CFD computations: (A) even fluidization ( $U = U_{mf}$ -in the inset: details of the flow patterns around a rising bubble) and (B) uneven fluidization ( $f = 1/5$ ;  $U/f = 6U_{mf}$ ;  $U/(1-f) = 1.5U_{mf}$ ) (Salatino et al., 2016).

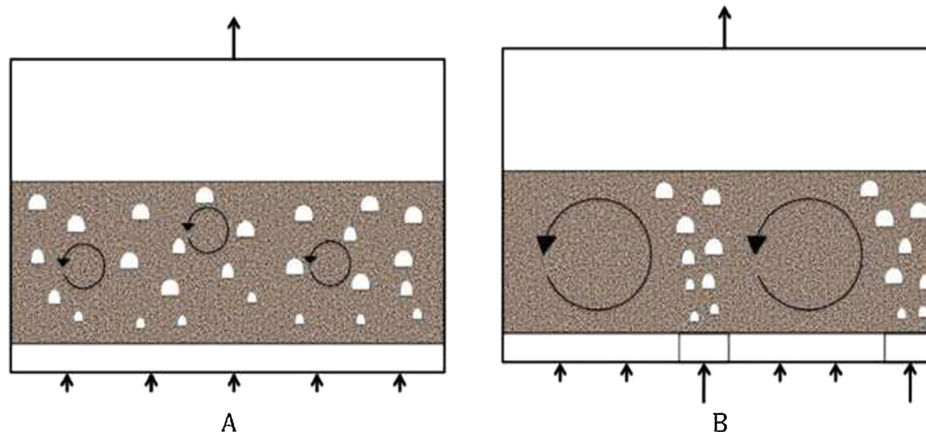


Fig. 38. Qualitative outline of the solid flow patterns in dense gas fluidized beds: (A) even fluidization and (B) uneven fluidization. (Salatino et al., 2016).

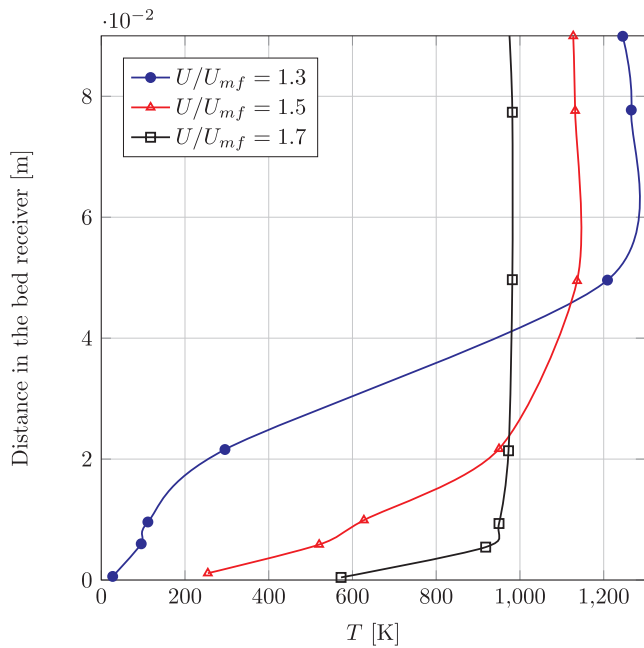


Fig. 40. Experimental axial temperature distribution in the fluidized bed vs. number of fluidization: silicon carbide,  $d = 0.25 \cdot 10^{-3}$  m;  $\phi_1 = 20 \cdot 10^{-4}$  W/m<sup>2</sup> (Flamant, 1982).

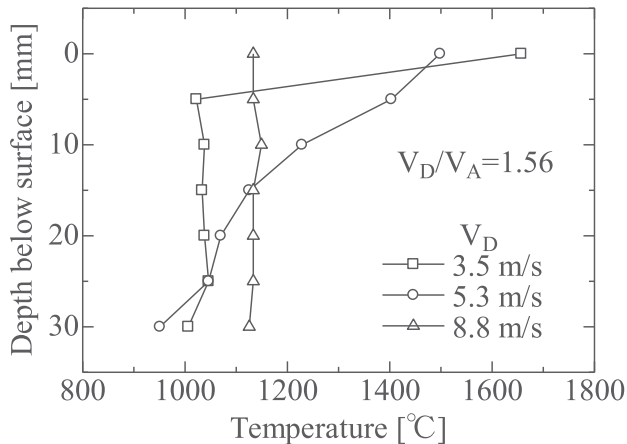


Fig. 41. Temperature distribution in the fluidized bed receiver proposed by Matsubara et al. (2014).

$v_D/v_A = 1.56$  (see Fig. 41). Their results also show that when the air flow rate is increased, the bed of particles is better mixed, and the temperature is more homogenous along the bed height.

One of the main disadvantages of the use of a fluidized bed located on the ground is the high temperature that the secondary reflector has to support. Even if constructed with a highly reflective material, the ratio between the area of the heliostat field and the area of the secondary reflector could be very high. To overcome this difficulty, Gómez-Hernández et al. (2017) proposed a novel ground solar receptor, which is shown schematically in Fig. 42. With a linear Fresnel system, it is possible to increase progressively and linearly the temperature of the solids that are displaced horizontally due to the action of the fluidization process. The particles are fluidized by the air action and move horizontally. Their study showed that in moving 0.1 kg/s of sand particles (Geldart B classification) with a total length of 30 m, the temperature can reach 900 °C, assuming a solar radiation of 100 kW/m<sup>2</sup>.

In direct-particle receivers systems there is an important lack of information about the properties of the materials to be used during the fluidization process at very high temperatures, one of the most

promising being desert sand, due to its very low cost and optimum site for the CSP location. Diago et al. (2018) fully characterized these particles for high-temperature TES. For some samples they observed that at certain temperatures, the particles agglomerated, in a similar manner that Izquierdo-Barrientos et al. (2016d) observed for granular PCMs. Although Diago et al. (2018) indicated that the agglomeration was soft, it can provoke the defluidization of the bed. Further research is required in this field.

### 3.2.2. Indirect particle radiation

Recently, other authors proposed transporting fluidized particles inside a tube (indirect receiver) radiated by a sun oven (Flamant et al., 2013; Benoit et al., 2015; García-Triñanes et al., 2016; Zhang et al., 2016; Gomez-Garcia et al., 2017; Zhang et al., 2017; García-Triñanes et al., 2018). Fig. 43 shows how the solar absorber tube is suspended on a horizontal metallic frame, thus allowing its thermal expansion through two end-fitted compensators. The bottom of the tube is colder than the top (red-hot) because of the cold particle feed. The particles get hotter while passing through the irradiated cavity. Benoit et al. (2015) were able to maintain a solid temperature of 750 °C with tube temperature under its maximum operation limit. They increased the particle temperature 200 °C in a length of 50 cm of irradiated tube. In this type of indirect radiation system, it is very important to have high heat transfer coefficients for the particle suspension in order to reduce the temperature and the thermal stress on the tube. The data obtained by Zhang et al. (2017) show, under their experimental conditions (Geldat A particles, SiC, with a mean particle size of 64 μm and solid flux under 100 kg/(s m<sup>2</sup>)), the heat transfer coefficient increases approximately linearly with the flux of solid moving in the tube. Fig. 44(a) shows how the heat flux transferred to the particles in the bed increases linearly with the particle flow for both single- and multi-tube systems. Fig. 44(b) shows the increase in the heat transfer coefficient with the solid flux for different tube diameters. Zhang et al. (2017) did not observe high differences in this coefficient by changing the diameter, although the use of fins in the tube notably increased (by a multiple of two) the heat transfer coefficient. García-Triñanes et al. (2018), under the same experimental conditions of Zhang et al. (2017), measured the particle motion within the tube together with the heat transfer coefficient. They concluded that the motion of particles on the inner surface of the wall tube is the dominant factor that controls the overall heat transfer coefficient at the tube.

### 3.2.3. Integration in a power block

Gomez-Garcia et al. (2017) and Zhang et al. (2017) proposed different alternatives to integrate a solar indirect particle receiver with the power block. Gomez-Garcia et al. (2017) proposed a series of fluidized-bed heat exchangers to evaporate water and carry out a simple Rankine cycle of 50 MW with one reheater. As an alternative, Zhang et al. (2017) proposed a combined cycle. The authors claimed to obtain 1.3 MW<sub>el</sub> with an overall efficiency of 47% with a LCOE below 100 euros/MWh.

## 3.3. Latent energy storage with PCMs

### 3.3.1. Applications and experiments

Very few works have explored the use of granular PCM in fluidized beds units to store energy for solar applications. Izquierdo-Barrientos et al. (2013) conducted experiments where a tank filled with a granular phase changing composite (Rubitherm-GR50) was charged with a hot air stream up to 65 °C. This PCM was a commercial product that consisted of a natural porous mineral matrix and a PCM (paraffin wax in this case) that was bounded to the matrix, ensuring that, when in the liquid form, it did not leak out of the granulate. The result is that the bound PCM is always a solid in its macroscopic form. Material with a mean particle size of 0.5 mm was chosen in one of the configurations experimentally studied, where the bed was operated in the bubbling fluidization regime. The material tested (with a transition temperature

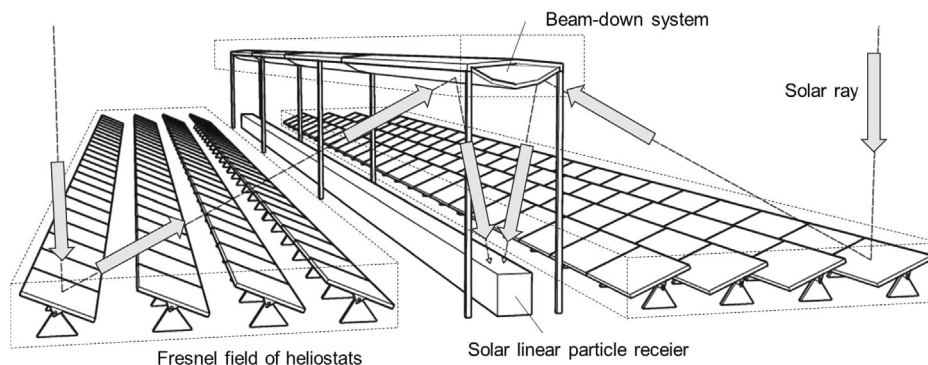


Fig. 42. General scheme of the linear-ground fluidized-bed receiver proposed by Gómez-Hernández et al. (2017).



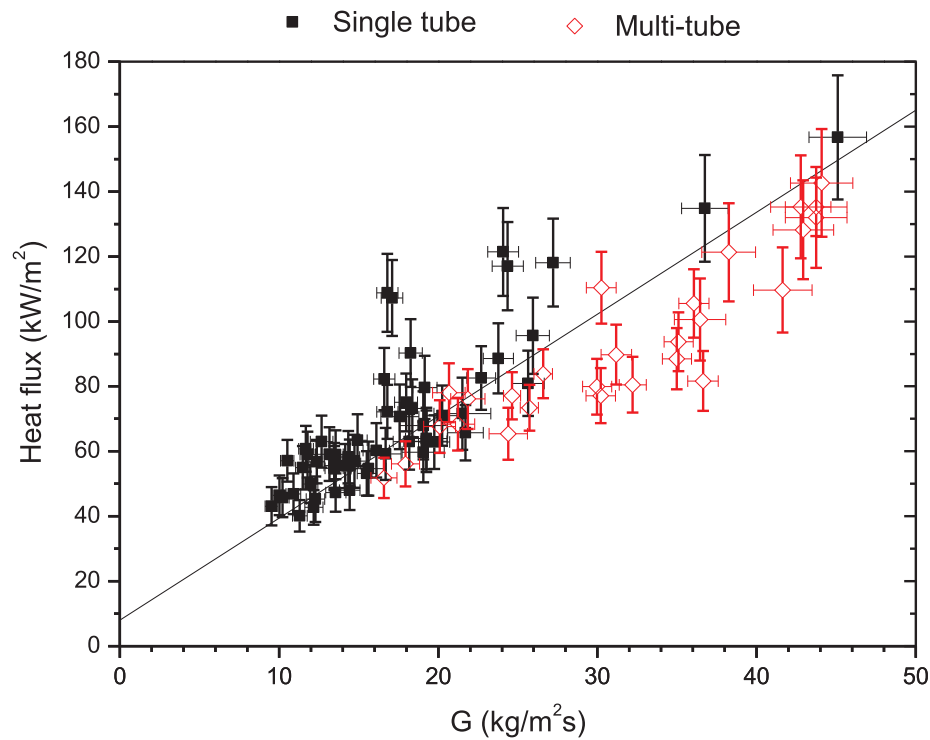
Fig. 43. Photograph of the sun-heated absorber tube in the solar receiver during cooling. (Benoit et al., 2015).

of 50 °C) was properly fluidized when the paraffin was in the liquid state and endured 75 h of continuous operation and 15 melting-solidification cycles, maintaining its fusion and solidification enthalpy unaltered (Izquierdo-Barrientos et al., 2016d). In a subsequent work, Izquierdo-Barrientos et al. (2016a) experimentally showed a comparative study where a bed of the same change material charged with hot air was discharged with a water stream that circulated inside a coil immersed in the bed. The performance of the fluidized bed of granular PCM was compared to that of well-known storage methods such as fluidized beds with sand and packed beds with sand or PCM. Higher heat transfer coefficients and heat exchanger effectiveness were measured for the fluidized bed compared with the packed bed and for the PCM compared with the sand. These results demonstrated the benefits of maintaining the bed fluidized when it is discharged using a heat exchanger immersed in it. Izquierdo-Barrientos et al. (2015b) measured the heat transfer coefficient in a fluidized bed with sand and PCM, and both results are compared in Fig. 32. For the PCM case, the heat transfer coefficient was between 500 and 600 W/(m<sup>2</sup> K) for fluidization velocities up to  $2.5u_{mf}$ . Izquierdo-Barrientos et al. (2015b) observed an important increase in the heat transfer coefficient with granular PCM when it changed its phase. Fig. 45 shows a heating-cooling experiment in a fluidized bed with a granular PCM. The figure shows the bed and the air temperature together with the heat transfer coefficient measured with a heat transfer probe. When the bed temperature was over 50 °C, the phase change temperature of the material and the heat transfer coefficient was around 350 W/(m<sup>2</sup> K). In contrast, during the discharge of the bed when the temperature dropped below 50 °C, the heat transfer

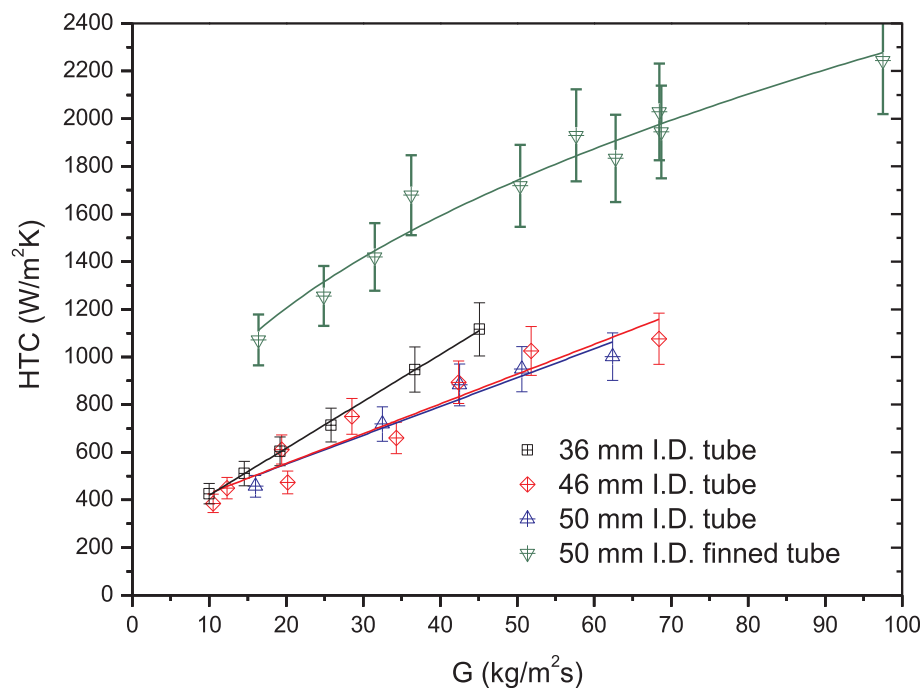
coefficient increased up to 850 W/(m<sup>2</sup> K) due to the energy released during the liquid-solid transition of the granular material.

Fluidization has also proven to be beneficial when applied in thermal energy storage systems that employ a liquid instead of air as fluidizing agent. Sozen et al. (1988) performed thermal cycling experiments of hollow polypropylene spheres 25 mm in diameter that encapsulated a fluid mixture consisting of 96% by weight Glauber's salt and 4% borax. The spheres were fluidized in a cylindrical column. Additional experiments were performed under fixed bed conditions in the same column with the same capsules simply by decreasing the superficial water velocity in the column below the minimum fluidization velocity. Fluidization reduced the segregation within Glauber's salt capsules, achieving charging efficiencies of nearly 60% over 96 cycles. Under fixed bed conditions, the heat storage capacity of the same capsules dropped to approximately 38%. Beemkumar et al. (2017) compared the performance of fixed and fluidized beds using spheres (100 mm diameter) filled with D-mannitol as PCM and Therminol-66 as heat transfer fluid. They studied different encapsulations for the PCM: copper, aluminum and brass. The fluidized bed with aluminum encapsulation system obtained the lower cost per kW of energy stored. The authors also concluded that fluidization improves the energy transfer in comparison with fixed beds, but they indicated that the pressure drop could be higher.

Another application of heat storage in a fluidized bed of PCM was studied by Belmonte et al. (2016), who conducted TRNSYS simulations of the heating system of a single-family house consisting of a solar air heater integrated with a fluidized bed energy storage unit that contained the same granular PCM employed by Izquierdo-Barrientos et al. (2016d). Fig. 46 shows the schematic of the system simulated. During the loading process, hot air was blown through the solar collectors to transfer heat energy to the storage unit, melting the PCM. The unloading process occurred during non-sunny hours, supplying hot air to the heated zones of the building to either partially or fully meet the heating demands. The simulations revealed that, compared with conventional storage system technologies, such as water tanks used in liquid-based system or pebble bed storage units typically used in air-based systems, the fluidized bed system exhibited the capacity to provide higher solar fractions with relatively low tank sizes. The advantages of the described system summarized by the authors are as follows: (1) the low heat capacity of the air requires smaller amounts of solar radiation to operate the system; (2) unlike liquid solar heating systems, solar air heating systems do not require heat exchangers to heat an intermediate HTF; (3) the high heat transfer coefficients of the fluidized bed system provides efficient charging and discharging of the fluidized bed storage system; and (4) because the building is heated by an all-air heating system, in which thermal energy is directly carried by duct work to the conditioned spaces, avoiding the need of an intermediate heat exchanger, the temperature level required at the air collector outlet is lower, increasing the collector efficiency.



(a) Heat flux



(b) Heat transfer coefficient

Fig. 44. (a) Heat flux transferred to the particles for a single and a multi-tube particle solar receiver and (b) heat transfer coefficient for different single tube diameters. Experimental data reported by Zhang et al. (2017).

### 3.4. Thermochemical energy storage

To the author's knowledge, there is no relevant research on the use of fluidized bed technology for thermochemical energy storage in the low-temperature range (below 150 °C). Thus, this section is focused on

high-temperature thermochemical conversion with fluidized beds for CSP applications.

#### 3.4.1. Applications and experiments

Flamant et al. (1980) was one of the first works on this topic. They

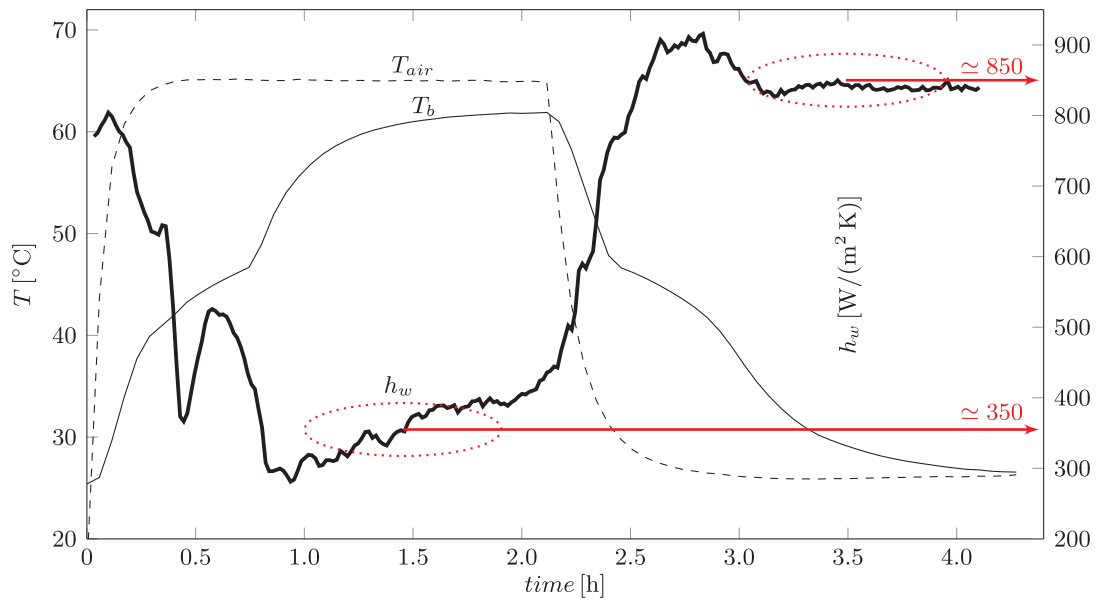


Fig. 45. Evolution of the heat transfer coefficient in a fluidized bed with a granular PCM (Izquierdo-Barrientos et al., 2015b).  $T_{air}$  is the air inlet temperature and  $T_b$  the bed temperature.

compared the performance of both a fluidized bed and a rotary kiln as a high-temperature thermochemical reactor for CSP applications with the reversible reaction of decarbonation of calcite at 900 °C:



Fig. 47 shows the experimental data obtained by Flamant et al. (1980) in a small-scale fluidized bed with an inner diameter of  $d_{bed} = 3.6$  cm and 10 g of calcite. The particle size was 200–315  $\mu\text{m}$ , and the gas velocity was two times the minimum fluidization velocity. Curves A and B show the temperature inside the bed and on the bed surface, respectively. The bed temperature increases rapidly and remains flat for approximately 300 s when the reversible reaction (Eq. (10)) occurs. Compared with a rotary kiln, the fluidized bed reaches higher efficiencies of the thermal conversion and of the decarbonation of the  $CaCO_3$ : 40% and 20%, respectively, for the fluidized bed, whereas the maximum values obtained with the rotary kiln were 30% and 15%, respectively. In addition, the conversion for decarbonation reaches 100% in the fluidized bed, remaining at 60% for the rotary kiln. The main disadvantage of the fluidized bed noted by Flamant et al. (1980) was the low absorptivity of the system, which can reach values of approximately 0.5. To overcome this drawback and maintain the

advantage of the fluidization process, the authors proposed the reactor shown in Fig. 48, which consists of an annular fluidized bed with an internal cavity of high absorptivity.

More recently, Pardo et al. (2014a) experimentally studied the  $Ca(OH)_2/CaO$  reversible reaction (Eq. (7)) in a fluidized bed reactor. They explained that the main difficulty in directly fluidizing the commercial particles of calcium hydroxide was their small particle size, which is typically close to 1–15  $\mu\text{m}$  and belong to Geldart C particles (Geldart, 1973). When they tried to directly fluidize these particles, they observed gas channeling and fissures in the bed of particles, as shown in Fig. 49. They proposed to mix alumina particles, with a mean particle size of 171.7  $\mu\text{m}$  (Geldart A particles), with the Geldart C calcium hydroxide particles, with a mass proportion of 70 %w  $Al_2O_3$ /30 %w  $Ca(OH)_2$ . Pardo et al. (2014a) experimentally observed that the temperature in the bed was uniform, which is indicative of a proper fluidization of the mixture of particles.

Pardo et al. (2014a) also analyzed the stability of the fluidization process and the thermochemical conversion during various cycles, as shown in Fig. 50. The discontinuities observed after 17, 32 and 44 cycles occurred because the bed was opened to remove particles

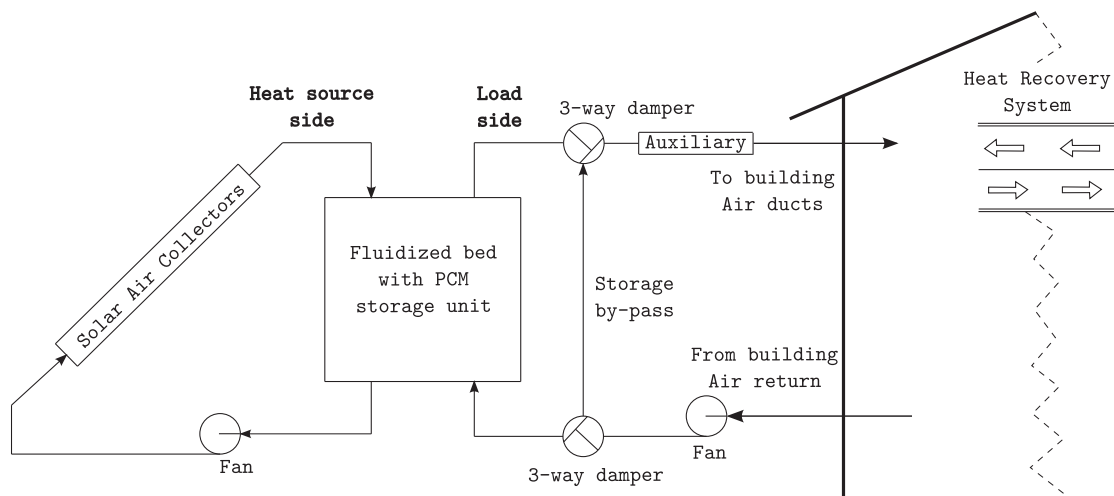


Fig. 46. Schematic of the solar heating system simulated by Belmonte et al. (2016).

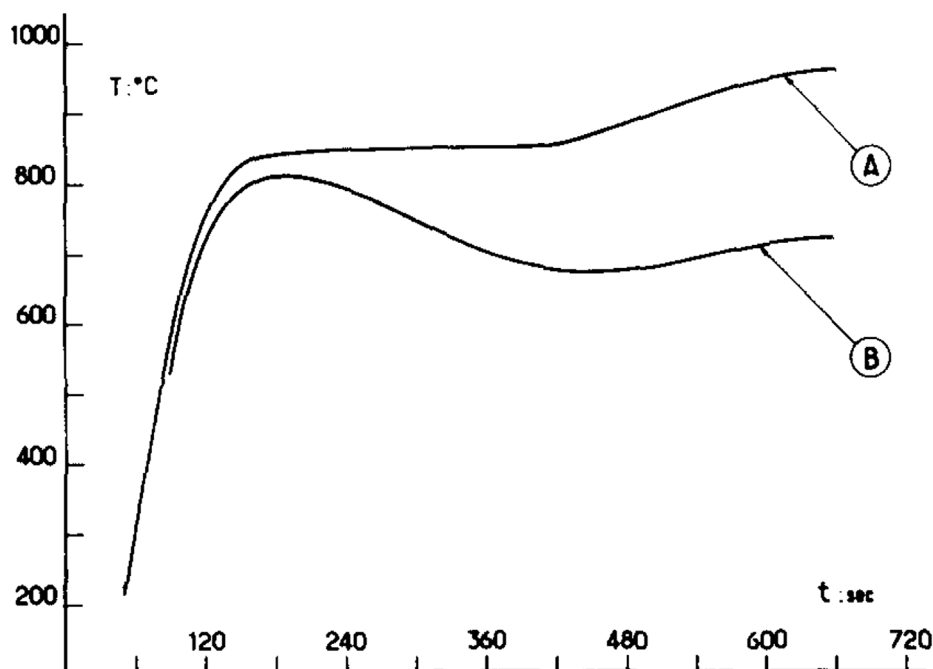


Fig. 47. Temperature evolution versus time obtained by Flamant et al. (1980) in a fluidized bed with 10 g of calcite. Curve A represents the temperature within the bed and curve B the temperature of the free bed surface.

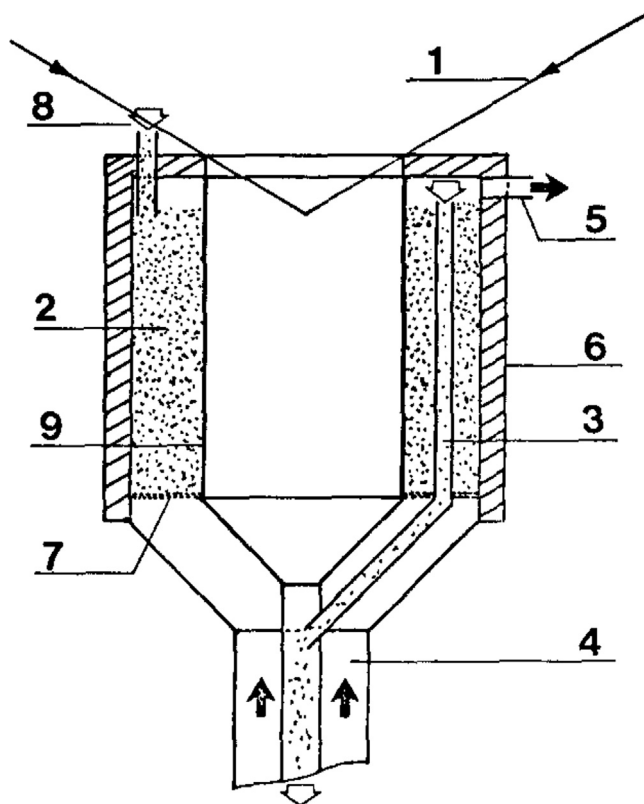


Fig. 48. Scheme of the annular-fluidized bed thermochemical reactor proposed by Flamant et al. (1980).

accumulated at the top larger section of the bed and return them into the main reaction zone. This issue could be solved with the use of a cyclone.

Criado et al. (2017) modified the experimental facility employed by Pardo et al. (2014a) to operate at conditions relevant for large-scale systems. They also studied the thermochemical  $\text{Ca}(\text{OH})_2/\text{CaO}$  reaction

experimentally in a fluidized bed of larger dimensions (0.105 m diameter and 0.9 m height). In addition, the particle size employed by Criado et al. (2017) was sieved in the range of 200–400  $\mu\text{m}$ , which belongs to group B particle according to the Geldart classification (Geldart, 1973). They used between 1.5 and 3.0 kg in each experiment, and the power supplied to the bed with electrical resistances located around the bed was approximately 3–4  $\text{kW}_{\text{th}}$ . Fig. 51 shows the temperature measured at different axial and radial positions in the fluidized bed used by Criado et al. (2017) in a complete cycle with 1.8 kg of material in the fluidized bed. The temperatures measured are independent of the position within the bed, which indicates a good mixing and fluidization quality. The temperature  $T_{B6}$  differs from the other temperatures because this temperature is over the bed surface. Criado et al. (2017) also proposed a K-L model (where the letters refers to Kunii and Levenspiel (1991)), which was satisfactorily validated with their experimental results. The K-L model of a fluidized bed reactor assumes that the temperature in the dense phase is uniform whereas the temperature of the gas that crosses the bed in the form of bubbles varies along the height of the bed. Kunii and Levenspiel (1991) explained in detail this model.

In a different work, Rougé et al. (2017) modified the experimental facility employed by Criado et al. (2017) to include an internal heat exchanger in the fluidized bed to maintain a steady temperature in the reactor supplying or removing energy during the dehydration or hydration process. The reactor operates under realistic conditions during various hours, and the steady state measurements were compared with a proposed K-L model. The particles employed were type B according to the Geldart classification (Geldart, 1973), with a sieve diameter in the range of 200–800  $\mu\text{m}$ . Fig. 52 shows the comparison of the experimental data, in terms of  $\text{H}_2\text{O}$  production during the hydration process. In this experiment, a molar fraction of  $\text{H}_2\text{O}$  of 0.5 was used in the mixture air/ $\text{H}_2\text{O}$  introduced to fluidize the bed, with a superficial velocity of 0.6 m/s. The model properly predicts the experimental results.

Criado et al. (2014) proposed the scheme shown in Fig. 53 for a large-scale  $\text{CaO}/\text{Ca}(\text{OH})_2$  thermochemical energy storage with fluidized beds. They proposed the use of a circulating fluidized bed instead of a bubbling one due to its capacity to handle large circulation rates of solids. The proposed system has two storage silos for  $\text{CaO}$  and  $\text{Ca}(\text{OH})_2$ .

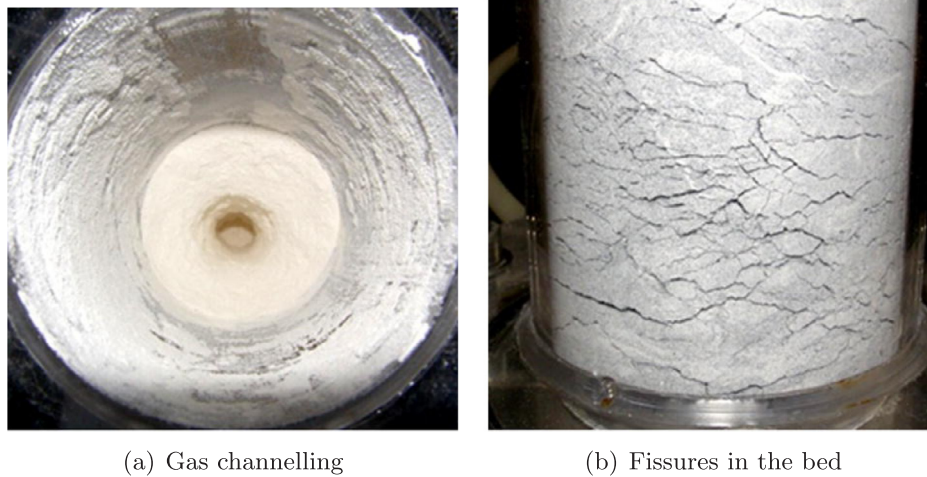


Fig. 49. Experimental observation of Pardo et al. (2014a) when they tried to directly fluidize  $\text{Ca}(\text{OH})_2$  with a mean particle size of  $3.8 \mu\text{m}$ .

An intermediate heat exchanger recovers sensible energy from the solids leaving the reactor to produce steam. They analyzed a system of  $100 \text{ MW}_{\text{th}}$ , and the results indicate that the operation could be technically viable.

Álvarez de Miguel (2017) compared the performance of manganese oxide pellets in packed and fluidized beds. Fig. 31 compares both experimental results. The repeatability of the cycles during the fluidization test (Fig. 31(c)) was notably better than in the packed bed case (Fig. 31(a)) with the same pellets. The larger size of the pellets (2–3.6 mm) requires the use of very high flow rates of  $45 \text{ N m}^3/\text{h}$ , with a minimum fluidization velocity approximately  $2.25 \text{ m/s}$ . Also in the fluidized bed, the variation of the pellet properties is more relevant: the mean pellet size is reduced from 2.9 mm to 2.3 mm after 25 cycles. The density and the hardness increase from  $2150 \text{ kg/m}^3$  to  $3000 \text{ kg/m}^3$  and from 33 N to 120 N, respectively.

Flegkas et al. (2018) proposed a numerical model for the  $\text{MgO}-\text{Mg}(\text{OH})$  reaction in a fluidized bed, taking into account the kinetic of the reaction. They observed that the particles must have sufficient residence time in the fluidized bed to complete the reactions. This fact provokes that the energy recovery should be at a temperature level lower than the equilibrium temperature.

#### 3.4.2. Integration in a power block

Regarding the integration of a TCS system in a packed or fluidized bed with the power block of a CSP plant, Ströhle et al. (2016) performed an interesting study comparing the performance of a packed and a fluidized bed integrated with a power block. They studied two different configurations: with the TCS system in parallel (Fig. 54) or in serial (Fig. 55) with the power block. The authors studied the reaction:

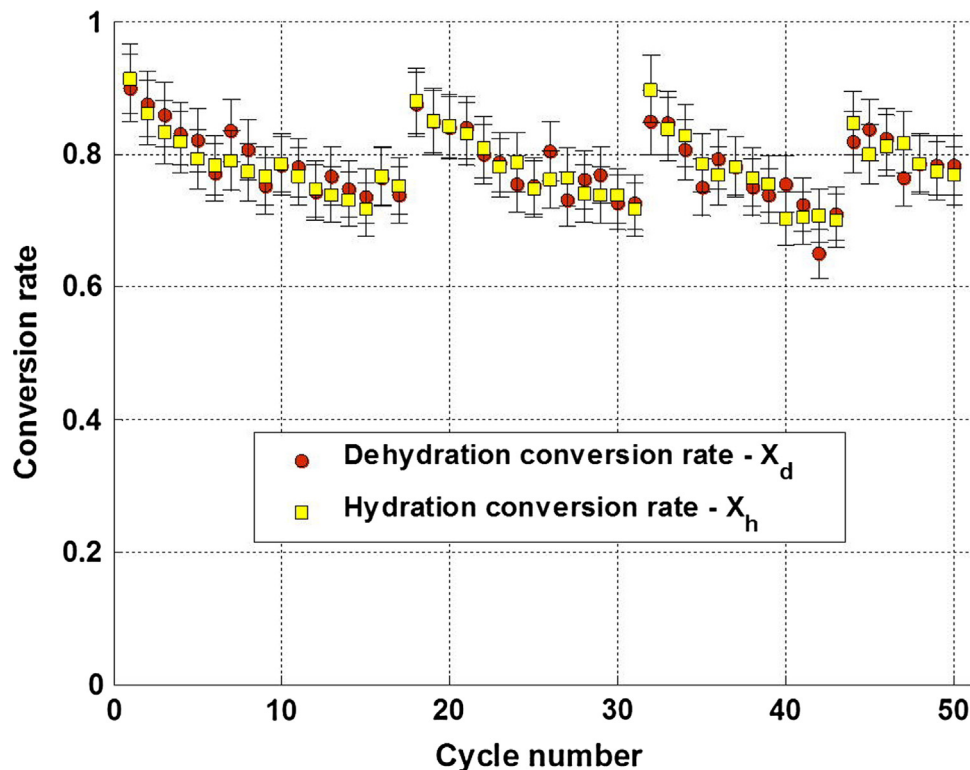


Fig. 50. Cycling study carried out by Pardo et al. (2014a).

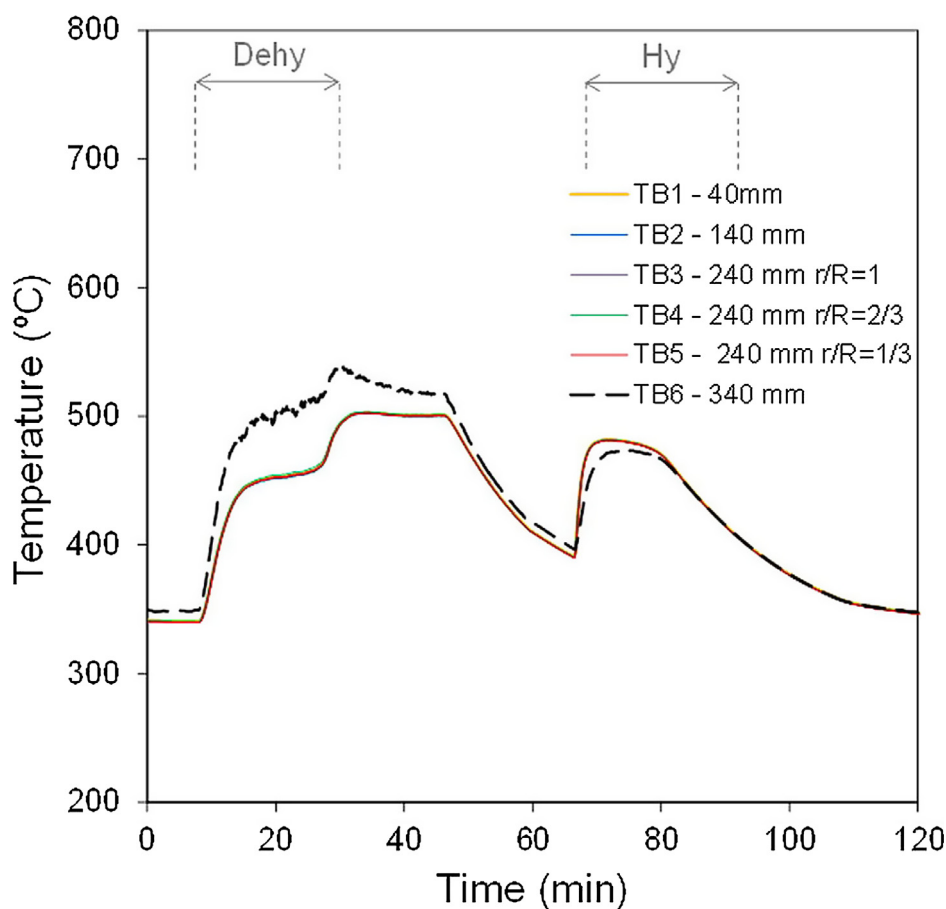


Fig. 51. Temperatures measured in the bed during a full charging-discharging cycle in a fluidized bed with 1.8 kg of  $\text{CaO}/(\text{Ca}(\text{OH})_2)$  (Criado et al., 2017).

in a packed bed of 1.5 m high and particles type D according with Geldart classification ( $d_p = 5$  mm) and in a fluidized bed of 0.4 m height with Geldart A particles ( $d_p = 100$   $\mu\text{m}$ ). They concluded that parallel configuration is not recommended with a fluidized bed TCS because  $T_{f,c,out}$  is set by the temperature of the thermochemical reaction during the charging process, and this temperature is generally much higher than the temperature of the HTF leaving the power block ( $T_{f,c,out} \gg T_{PB,out}$ ), which result in high exergy losses. In contrast, in a serial configuration, the high temperature of the HTF leaving the TCS during the charging process can be directly supplied to the power block. For a packed bed, the parallel configuration is preferred because the chosen operating condition allowed  $T_{f,c,out} \approx T_{f,d,in} = T_{PB,out}$  resulting in low exergy losses from the two HTF streams.

Ströhle et al. (2016) also showed that the thermochemical conversion in the fluidized bed reactor is superior than in the packed bed, because in the packed bed only 14% of the total material in the bed reacted. As a consequence in the packed bed configuration only 9% of the energy stored was thermochemical, and the rest 91% was in sensible form. In the fluidized bed, 95% of the material reacted and 37% of the energy was stored in sensible form and 63% in thermochemical form. In view of these results Ströhle et al. (2016) suggest the possibility of filling the packed bed on the top with inert material, which is cheaper and store the energy in sensible form. Ströhle et al. (2016) also remarked that the sensible energy stored in a TCS is not negligible and should be taken into account. Under their conditions the total amount of energy stored in the packed bed was 11% higher than the fluidized bed, although in sensible (not thermochemical) form.

#### 4. Discussion

In view of the different studies reviewed, it is clear that both particle

technologies: packed and fluidized beds have been extensively used in different applications for thermal energy storage. Packed beds, due to their simplicity and easier operation in comparison with fluidized beds, have been more used in actual applications, specially for low temperature applications and not large powers. For example, packed beds have the important advantage of the thermal stratification when used with a conventional SAH, because the HTF is returned to the SAH from the bottom of the bed, where the temperature is lower, increasing the efficiency of the solar collector and increasing the overall efficiency of the solar facility. In fluidized beds, the temperature is homogenous in the bed, and consequently the efficiency of the SAH during operation is reduced. In contrast, the use of fluidized beds permits to reduce the charging/discharging times because the particle size employed is smaller, increasing the heat transfer surface and the heat transfer coefficients are also higher compared with packed beds. Nevertheless, the charging times in packed beds, although are lower, are highly enough for charging during the day and discharging during the night or non-sunny periods in low temperature applications, so fluidized beds are not competitive for low-temperature sensible energy storage applications. In addition, the packed beds present the advantage of its higher exergy content due to the stratification in the bed. Some studies tried to maximize this exergy content in a packed bed maintaining, during longer periods of time, the outflow temperature as high as possible. In this way, different works probed that the segmentation of the bed tends to increase the exergy content in the bed (Crandall and Thacher, 2004; White et al., 2016; McTigue and White, 2016). Other researchers explored the possibility of modifying the geometrical parameters of the bed (Zanganeh et al., 2012; Mao, 2016) or the use of PCMs combined with sensible heat materials (Flueckiger and Garimella, 2014; Galione et al., 2015; Geissbühler et al., 2016).

The use of granular PCMs with fluidized beds for low temperature

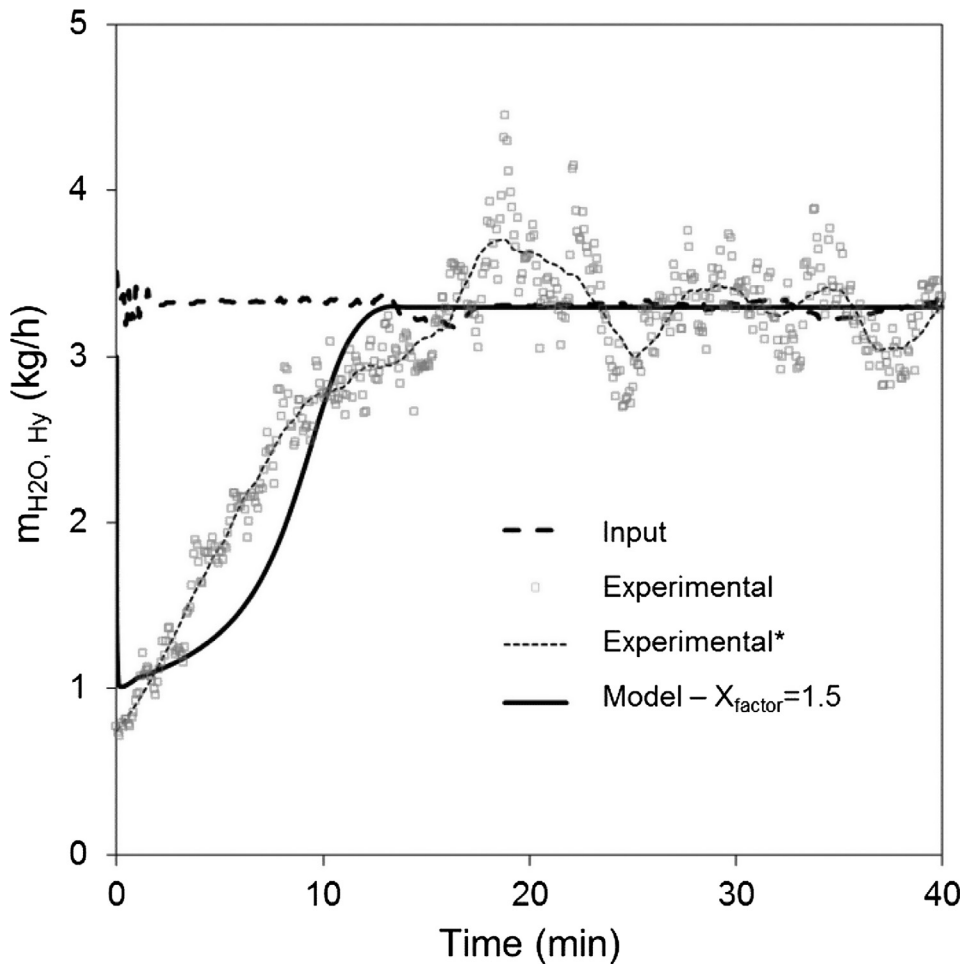


Fig. 52. Comparison of the experimental data obtained by Rougé et al. (2017) with their model. The smooth curve of the experimental data represented with a dotted line was obtained with a Savitzky-Golay smooth 4th degree filter. The  $X_{factor} = 1.5$  indicates the interchange between the bubble and the emulsion phase in the K-L model.

applications (Izquierdo-Barrientos et al., 2013), opens the possibility of maintaining the temperature level in the bed at the desired temperature. If the storage system is properly designed, the particles in the bed can reach a maximum temperature established by the PCM. In this case, there is no differences in the solar facility efficiency because the temperature in the bed is imposed by the PCM, not by the stratification or

the mixing in the bed. This technology, although has been preliminary tested in lab-scale facilities (Izquierdo-Barrientos et al., 2013) is not commercially available. It is necessary to test and produce in large quantities, with a reasonable price, granular PCMs with a particle size suitable to be used in fluidized beds ( $0.1 \text{ mm} \lesssim d_p \lesssim 1 \text{ mm}$ ) and with a high resistance due to the high abrasion process under fluidization

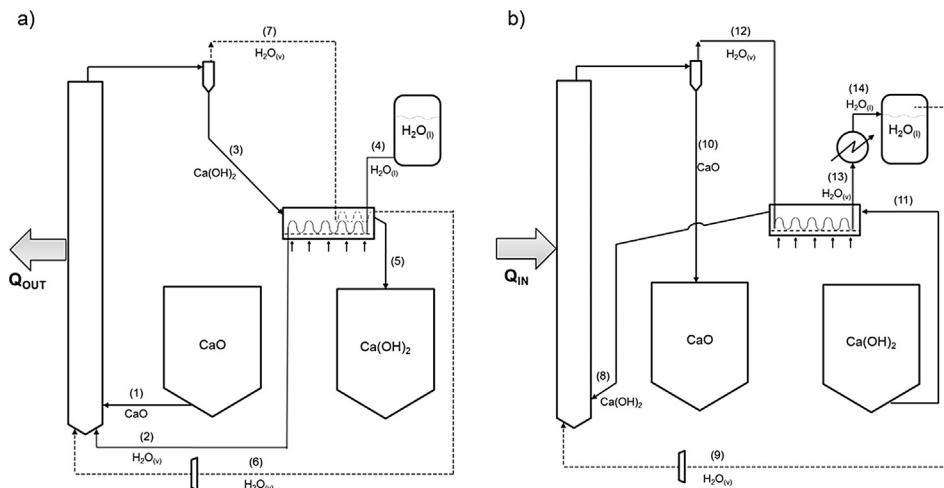


Fig. 53. Scheme of the CaO/Ca(OH)<sub>2</sub> thermochemical energy storage system with a circulating fluidized bed during (a) discharge (hydration) process and (b) discharge (dehydration) process.

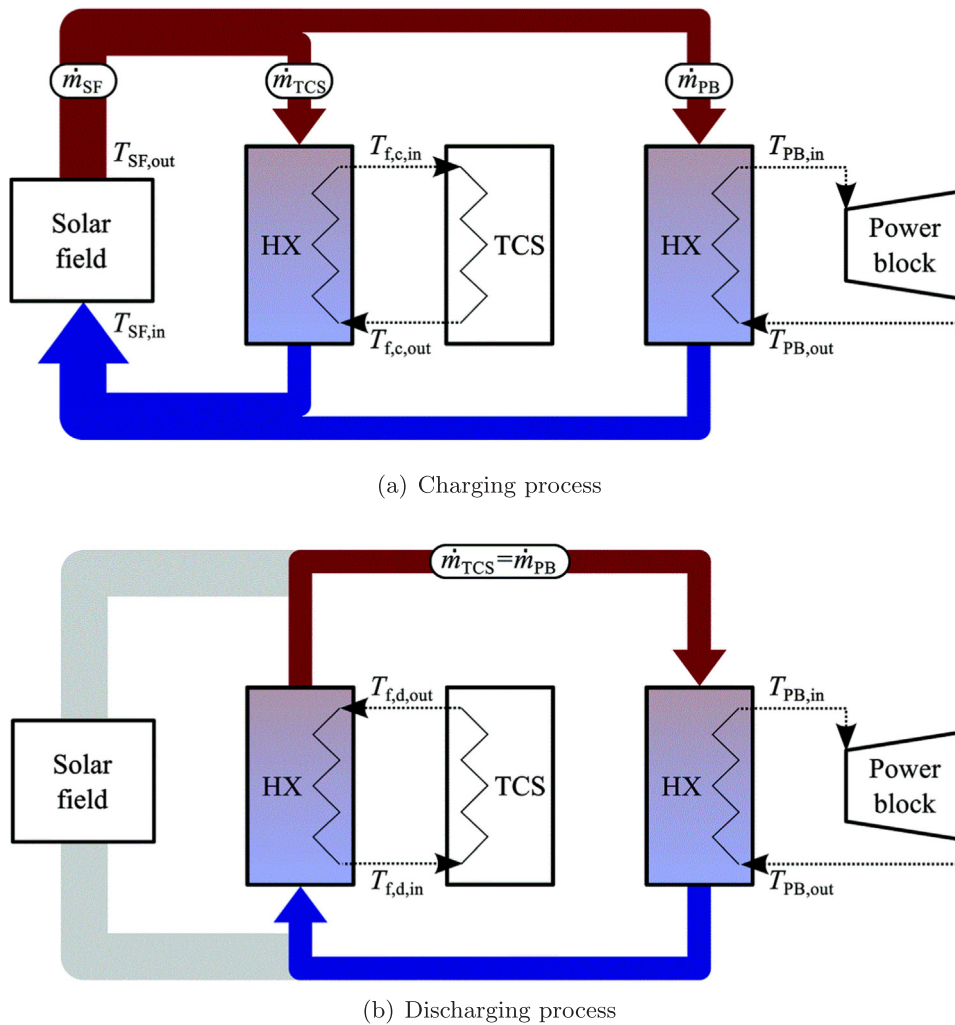


Fig. 54. Scheme of a TCS system in parallel configuration (Ströhle et al., 2016).

conditions (Izquierdo-Barrientos et al., 2016d).

For high temperature applications in CSP, thermocline tanks has been showed to be competitive in comparison with the two-tanks system with molten salts, due to the reduction in costs (Pacheco et al., 2002). There are also different studies that integrate different PCM increasing the energy density of the tank, which have been proved to be energy efficient, although there is no economic studies that assures to make profitable the higher cost of the material. Also, more studies in large scale facilities and during longer periods of time are necessary to contrast the performance of the PCM.

The natural trend to increase the efficiency of actual CSP is to increase the temperature at which the energy is stored. Actual CSP plants are limited to 565 °C or 400 °C when using molten salts or thermal oil, in central receiver or parabolic trough collectors, respectively. Nowadays there is a notable interest in the use of solid particles, storing the energy in sensible form, reaching temperatures up to 1000 °C (Ho, 2016; Calderón et al., 2018). In this research line, the high heat transfer coefficient and elevated mixing rates of fluidized beds, in comparison with packed beds, makes them suitable for this application (Flamant, 1982; Flamant and Olalde, 1983; Matsubara et al., 2014; Tregambi et al., 2016; Salatino et al., 2016). Salatino et al. (2016) properly explained that working with a fluidized bed of Geldart A or B particles and gas velocities just beyond the minimum fluidization velocity, permits to operate with elevated surface-to-bed heat transfer rates and maintain the energy parasitic losses low. In addition, he proposed the use of uneven and pulsed fluidization to improve the effective solid diffusivity

in the fluidized bed, that permits to rapidly distribute the concentrated solar energy on the top of the bed (beam-down reflector) to all the particles. It is clear that fluidized bed is the proper technology for a CSP with a beam-down reflector. The main difficulty to implement this technology in the near future, is not related with the fluidization technology, is the high temperature that the secondary reflector has to support in large scale CSP with various megawatts.

A different alternative, to store the solar energy in particles is to transport the fluidized particles in a tube, and radiate the external surface of the tube (Flamant et al., 2013; Benoit et al., 2015; García-Triñanes et al., 2016; Zhang et al., 2016; Gomez-Garcia et al., 2017; Zhang et al., 2017; García-Triñanes et al., 2018). This technology has been proved experimentally in a solar furnace with solar energy concentrated in the tube between 213 and 393 kW/m<sup>2</sup> (Benoit et al., 2015). This indirect radiation technology has two main drawbacks compared with a central solar receiver with molten salts: the low heat transfer coefficients and mass flow rate of particles transported. Benoit et al. (2015) measured heat transfer coefficients between the internal surface of the tube and the particles in the range 600–800 W/(m<sup>2</sup> K), whereas with molten salts flowing with a velocity of 1.8 m/s inside tubes with an internal diameter of 4 cm (similar to the one used by Benoit et al. (2015) with particles) the heat transfer coefficient is around 6 kW/(m<sup>2</sup> K) (Rodríguez-Sánchez et al., 2014). Chen et al. (2016), also using molten salts, measured heat transfer coefficients between 3 and 8 kW/(m<sup>2</sup> K) with fluid velocities between 1 and 5 m/s in a 2 cm i.d. tube. As a conclusion, the heat transfer coefficients in molten salts are

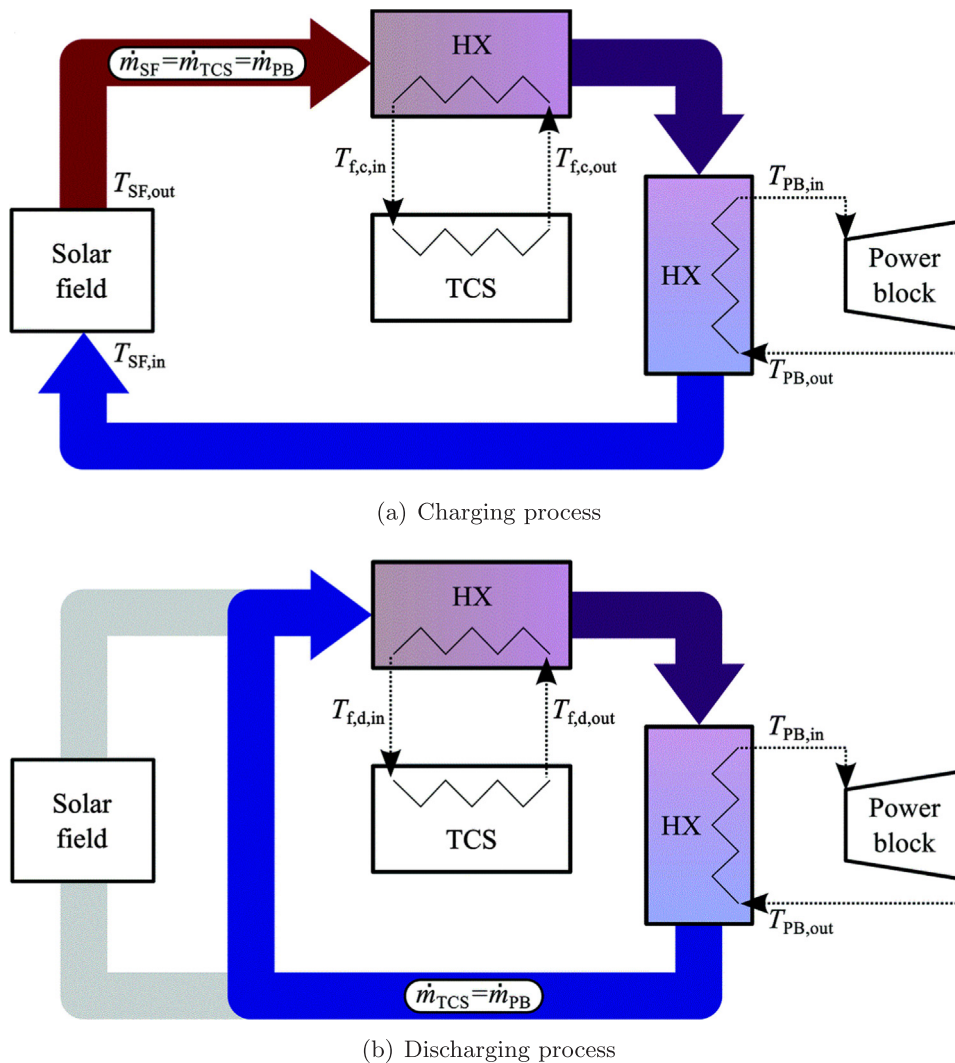


Fig. 55. Scheme of a TCS system in serial configuration (Ströhle et al., 2016).

one order of magnitude higher than with fluidized particles. In addition Benoit et al. (2015) used a superficial mass-flow rate of  $50 \text{ kg}/(\text{s m}^2)$ , whereas in a conventional solar central receiver with molten salts this value is around  $3 \times 10^3 \text{ kg}/(\text{s m}^2)$  (Rodríguez-Sánchez et al., 2014), various orders of magnitude higher. In summary, the low heat transfer coefficients and mass flow rates when using particles in a tube, provokes a low capacity of the particles to transport energy. As a consequence, in a large scale CSP plant with indirect solar radiation, the tube has to support very high temperatures and can suffer thermal stress (Rodríguez-Sánchez et al., 2014; Marugán-Cruz et al., 2016).

In either direct or indirect radiation system, it is also necessary more research on the behaviour of the material employed in the fluidized bed during operation and during various cycles at high temperatures. It is necessary to test the possible variations in the particles properties (Diago et al., 2018) (such as density, for example) that could affect the fluidization process. Also the abrasion or agglomeration processes should be studied in deep prior to test this technology in the near future in large scale power plants. Nowadays there is lack in the literature about this topic.

In thermochemical energy storage, it seems clear that fluidized bed technology, due to their high heat and mass transfer coefficients and mixing rates, compared with a packed bed, is the appropriated particle technology. For sorption processes of low temperature applications, the few experimental works published in the literature (Johannes et al., 2015; Zondag et al., 2008; Ferchaud et al., 2012), used packed bed

technology. Some authors remarked that the main limitation when using a packed bed is its low heat and mass transfer rates, which limits the kinetic of the thermochemical reaction (Aydin et al., 2015; Zondag et al., 2008; Solé et al., 2015). In this context, fluidized technology can help to improve this packed bed limitations. In this point, it is necessary to have materials with a particle size and density appropriated to be fluidized (see Figs. 2 and 3).

For high-temperature thermochemical energy storage, the same problems observed in sorption processes have been detected when using a packed bed: low heat and mass transfer rates. First works during the 80s tried to overcome this problem with use of extended surfaces in the packed bed reactor (Kanzawa and Arai, 1981; Fujii et al., 1985). Schaubé et al. (2013) experimentally study a packed bed for thermochemical energy storage with particles if very small size ( $d_p = 5.26 \mu\text{m}$ , Geldart C particles). This so small particles, although present a very high heat transfer surface per unit of bed volume, are not suitable to be used in neither a packed or a fluidized bed. In Geldart C particles, interparticles forces are very high and provokes agglomeration and channeling in the bed. As a consequence there is no good contact between the gas percolating the bed and the particles. Pardo et al. (2014a) mixed Geldart C particles with Geldart A particles of higher diameter to be able to fluidize them. This solution, has the disadvantage that the thermochemical energy storage capacity is reduced, because the inert material introduced to improve the fluidization quality only store energy in sensible form. Criado et al. (2017) used Geldart B particles, with

**Table 9**  
Summary of the main highlights for packed and fluidized beds for different thermal energy storage forms and temperatures.

	Packed beds	Fluidized beds
Sensible low temperature	Mature and optimal technology. The stratification in the bed increases the efficiency of the SAH.	More complicated technology and it does not offer important improvements over packed beds.
Sensible high temperature	Thermocline tanks can be used in CSP plants as an alternative to two-tanks of HTF.	This particle technology is suitable to store the solar radiation directly (with a beam-down receiver) or indirectly, with the particles fluidized inside a tube. It is necessary more studies and research with larger powers and materials suitable to be used in high-temperature fluidization conditions.
Latent low temperature	Experimentally studied in tanks for DHW applications, where the PCM permits to maintain the temperature level in tank at the desired temperature, reducing the exergy loss.	Some experimental studies at lab-scale have proved the possibility of using this technology, but there is necessary more research on new PCMs suitable to be used in fluidized beds.
Latent high T	There are some experiments combining PCMs with different transition temperatures in cascade or in different layers in the bed. It is necessary more research in large scale applications and also on PCMs for high temperature applications and their encapsulation.	There is no studies in this field.
Thermochemical low T	Different experimental studies, most of them in lab-scale facilities. Most of the studies highlight the same problems: low heat and mass transfer rates in packed beds, which reduces the kinetic of the thermochemical reactions and provokes very large storage volumes and charging/discharging times.	There is no studies of TCS systems in fluidized beds for low temperature sorption processes, although it could be a promising technology due to their higher heat and mass transfer rates compared to packed beds. There are some preliminar studies in lab-scale facilities, with satisfactory results. More research is needed in higher sizes facilities and with different materials.
Thermochemical high T		

a particle size in the range 200–400  $\mu\text{m}$  and were properly fluidized without agglomeration process. So, fluidized bed technology is appropriated for high temperature thermochemical energy storage, but it is necessary to have particles belonging to group A or B, according to Geldart classification to assure a good fluidization process with high heat and mass transfer rates.

Finally, Table 9 summarized the main aspects observed in the review for the different thermal energy storage forms studied in this review: sensible, latent and thermochemical for packed and fluidized beds.

## 5. Conclusions

This review has showed that packed beds are a simple and efficient particle technology for storing thermal energy at low temperature sensible form, as it has the advantage of the thermal stratification in the bed, which increases the solar collectors efficiency. Packed beds have been also used with success for high temperature applications, such as dual-media thermocline tanks for CSP plants. New geometries, segmentation of the bed and the combination of sensible energy storage tanks with PCMs in the recent years are the new and promising research lines to improve the performance of packed beds, aiming at maintaining high and nearly constant the outflow temperature. In contrast, fluidized beds are more appropriated for CSP plants with direct radiation on particles. The high mixing rates of fluidized beds permit to rapidly distribute a concentrated energy on the top of the bed when a beam-down CSP plant is used. The high heat and mass transfer rates of fluidized beds, compared to packed beds, makes them the preferred technology for thermochemical storage. Nevertheless, in both cases it is necessary more efforts in finding new materials with the suitable particle size and density for fluidized beds (particles type A or B according Geldart classification). In addition, greater knowledge of the behaviour of these materials during various charging/discharging cycles and during longer working periods in large scale facilities is necessary for the proper design, sizing and operation of thermal storage units.

## 6. Notation

$Bi$	Biot number [–]
$c_p$	specific heat of the particle [J/kg K]
$d_p$	particle size [m]
$d_p^*$	non-dimensional particle size defined by Eq. (1) [–]
$h$	convective heat transfer coefficient [W/(m <sup>2</sup> K)]

$k_p$	thermal conductivity of the particles [W/(m K)]
$Re$	Reynolds number [–]
$T$	temperature [K]
$u_{mf}$	superficial velocity at minimum fluidization conditions [m/s]
$u_s$	superficial velocity [m/s]
$u_s^*$	non-dimensional superficial velocity defined by Eq. (2) [–]
$\dot{V}$	volumetric flow rate [m <sup>3</sup> /s]

### 6.1. Abbreviations

CSP	Concentrating Solar Power
DHW	Domestic Hot Water
DSG	Direct Steam Generation
FCC	Fluid Catalytic Cracking
HTF	Heat Transfer Fluid
HVAC	Heating, Ventilating and Air Conditioning
ORC	Organic Rankine Cycle
PCM	Phase Change Material
PCT	Phase Change Temperature
SAH	Solar Air Heater
TES	Thermal Energy Storage

### 6.2. Greek symbols

$\varepsilon$	voidage [–]
$\mu_g$	gas viscosity [Pa s]
$\rho_g$	gas density [kg/m <sup>3</sup> ]
$\rho_p$	particle density [kg/m <sup>3</sup> ]
$\psi$	sphericity [–]

## Acknowledgments

The work is partially funded by the Spanish government (ENE2016-78908-R).

## References

- Abu-Hamdeh, N.H., 2003. Simulation study of solar air heater. *Solar Energy* 74 (4), 309–317.
- Achenbach, E., 1995. Heat and flow characteristics of packed beds. *Exp. Therm. Fluid Sci.* 10 (1), 17–27.
- Agrawal, P., Gautam, A., Kunwar, A., Kumar, M., Chamoli, S., 2018. Performance assessment of heat transfer and friction characteristics of a packed bed heat storage system embedded with internal grooved cylinders. *Solar Energy* 161, 148–158.
- Ahmed Ghoneim, A.A., 1989. Efficient Collection and Storage of Solar Energy, Ph.D.

- thesis. Faculty of Engineering. University of Alexandria.
- Alkilani, M.M., Sopian, K., Alghoul, M.A., Sohif, M., Ruslan, M.H., 2011. Review of solar air collectors with thermal storage units. *Renew. Sustain. Energy Rev.* 15 (3), 1476–1490.
- Álvarez de Miguel, S., 2017. Analysis of Redox Reactions in a Fluidized/Fixed Bed Reactor for Thermochemical Energy Storage in Solar Thermal Power Plants, Ph.D. thesis. Escuela Técnica Superior de Ingeniería y Diseño Industrial, Universidad Politécnica de Madrid.
- Anderson, R., Bates, L., Johnson, E., Morris, J.F., 2015. Packed bed thermal energy storage: a simplified experimentally validated model. *J. Energy Stor.* 4, 14–23.
- Anderson, R., Shiri, S., Bindra, H., Morris, J.F., 2014. Experimental results and modeling of energy storage and recovery in a packed bed of alumina particles. *Appl. Energy* 119, 521–529.
- André, L., Abanades, S., Flamant, G., 2016. Screening of thermochemical systems based on solid-gas reversible reactions for high temperature solar thermal energy storage. *Renew. Sustain. Energy Rev.* 64, 703–715.
- Anzelius, A., 1926. Heating by means of percolating media. *J. Mech. Des.* 6, 291–294.
- Arfaoui, N., Bouadila, S., Guizani, A., 2017. A highly efficient solution of off-sunshine solar air heating using two packed beds of latent storage energy. *Solar Energy* 155, 1243–1253.
- Arkar, C., Medved, S., 2005. Influence of accuracy of thermal property data of a phase change material on the result of a numerical model of a packed bed latent heat storage with spheres. *Thermochim. Acta* 438 (1), 192–201.
- Atalay, H., Coban, M.T., Kincay, O., 2017. Modeling of the drying process of apple slices: application with a solar dryer and the thermal energy storage system. *Energy* 134, 382–391.
- Aydin, D., Casey, S.P., Riffat, S., 2015. The latest advancements on thermochemical heat storage systems. *Renew. Sustain. Energy Rev.* 41, 356–367.
- Bayon, R., Rojas, E., 2013. Simulation of thermochemical storage for solar thermal power plants: from dimensionless results to prototypes and real-size tanks. *Int. J. Heat Mass Transfer* 60, 713–721.
- Beasley, D.E., Ramanarayanan, C., Torab, H., 1989. Thermal response of a packed bed of spheres containing a phase-change material. *Int. J. Energy Res.* 13 (3), 253–265.
- Beemkumar, N., Karthikeyan, A., Shiva Keshava Reddy, K., Rajesh, K., Anderson, A., 2017. Thermal analysis of fluidized bed and fixed bed latent heat thermal storage system. In: *Materials Science and Engineering Conference Series*, vol. 197. p. 012033.
- Bellan, S., Alam, T.E., González Aguilar, J., Romero, M., Rahman, M.M., Goswami, D.Y., Stefanakos, E.K., 2015. Numerical and experimental studies on heat transfer characteristics of thermal energy storage system packed with molten salt PCM capsules. *Appl. Therm. Eng.* 90, 970–979.
- Bellan, S., Gonzalez-Aguilar, J., Romero, M., Rahman, M.M., Goswami, D.Y., Stefanakos, E.K., Couling, D., 2014. Numerical analysis of charging and discharging performance of a thermal energy storage system with encapsulated phase change material. *Appl. Therm. Eng.* 71 (1), 481–500.
- Belmonte, J.F., Izquierdo-Barrientos, M.A., Molina, A.E., Almendros-Ibáñez, J.A., 2016. Air-based solar systems for building heating with pcm fluidized bed energy storage. *Energy Build.* 130, 150–165.
- Benoit, H., López, I.P., Gauthier, D., Sans, J.-L., Flamant, G., 2015. On-sun demonstration of a 750 °C heat transfer fluid for concentrating solar systems: dense particle suspension in tube. *Solar Energy* 118, 622–633.
- Bhagat, K., Saha, S.K., 2016. Numerical analysis of latent heat thermal energy storage using encapsulated phase change material for solar thermal power plant. *Renew. Energy* 95, 323–336.
- Bruch, A., Fourmigué, J., Couturier, R., 2014. Experimental and numerical investigation of a pilot-scale thermal oil packed bed thermal storage system for CSP power plant. *Solar Energy* 105, 116–125.
- Cabeza, L.F., Martorell, I., Miró, L., Fernández, A.I., Barreneche, C., 2015. Introduction to thermal energy storage (tes) systems. In: Cabeza, L.F. (Ed.), *Advances in Thermal Energy Storage Systems: Methods and Applications*. Woodhead Publishing, pp. 1–28.
- Calderón, A., Palacios, A., Barreneche, C., Segarra, M., Prieto, C., Rodríguez-Sánchez, A., Fernández, A.I., 2018. High temperature systems using solid particles as TES and HTF material: a review. *Appl. Energy* 213, 100–111.
- Chen, Y., Wang, Y., Zhang, J., Yuan, X., Tian, J., Tang, Z., Zhu, H., Fu, Y., Wang, N., 2016. Convective heat transfer characteristics in the turbulent region of molten salt in concentric tube. *Appl. Therm. Eng.* 98, 213–219.
- Choudhury, C., Chauhan, P., Garg, H., 1995. Economic design of a rock bed storage device for storing solar thermal energy. *Solar Energy* 55 (1), 29–37.
- Crandall, D., Thacher, E., 2004. Segmented thermal storage. *Solar Energy* 77 (4), 435–440.
- Criado, Y., Alonso, M., Abanades, J., Anxionnaz-Minvielle, Z., 2014. Conceptual process design of a cao/ca (oh) 2 thermochemical energy storage system using fluidized bed reactors. *Appl. Therm. Eng.* 73 (1), 1087–1094.
- Criado, Y.A., Huille, A., Rougé, S., Abanades, J.C., 2017. Experimental investigation and model validation of a cao/ca (oh) 2 fluidized bed reactor for thermochemical energy storage applications. *Chem. Eng. J.* 313, 1194–1205.
- de Gracia, A., Cabeza, L.F., 2016. Numerical simulation of a PCM packed bed system: a review. *Renew. Sustain. Energy Rev.* 69, 1055–1063.
- Diago, M., Iniesta, A.C., Soum-Glaude, A., Calvet, N., 2018. Characterization of desert sand to be used as a high-temperature thermal energy storage medium in particle solar receiver technology. *Appl. Energy* 216, 402–413.
- Dincer, I., Rosen, M., 2011. *Thermal Energy Storage: Systems and Applications*. Wiley.
- Dixon, A.G., Cresswell, D.L., 1979. Theoretical prediction of effective heat transfer parameters in packed beds. *AIChE J.* 25 (4), 663–676.
- Duffie, J., Beckman, W., 2013. *Solar Engineering of Thermal Processes*, fourth edition. Wiley-Interscience Publication, Wiley.
- Duomarco, J.L., 2015. Figure of merit for solar domestic hot water systems. *Solar Energy* 111, 151–156.
- El-Refaee, M.M., Elsayed, M.M., Megahed, I.E., 1988. Parametric study on fluidized bed thermal storage. *Heat Mass Transfer* 23 (1), 55–60.
- Elsari, M., Hughes, R., 2002. Axial effective thermal conductivities of packed beds. *Appl. Therm. Eng.* 22 (18), 1969–1980.
- Elsayed, M.M., Megahed, I.E., El-Refaee, M.M., 1988. Experimental testing of fluidized bed thermal storage. *Solar Wind Technol.* 5, 15–25.
- Epstein, N., 2003. Chapter 26. Liquid-solids fluidization. In: Yang, W.-C. (Ed.), *Handbook of Fluidization and Fluid-Particle Systems*. Marcel Dekker Inc.
- Epstein, N., Grace, J.R., 2011. *Spouted and Spout-Fluid Beds: Fundamentals and Applications*. Cambridge University Press.
- Ergun, S., 1952. Fluid flow through packed columns. *Chem. Eng. Prog.* 48, 89–94.
- Esakkimuthu, S., Hassabou, A.H., Palaniappan, C., Spinnler, M., Blumenberg, J., Velraj, R., 2013. Experimental investigation on phase change material based thermal storage system for solar air heating applications. *Solar Energy* 88, 144–153.
- Esence, T., Bruch, A., Molina, S., Stutz, B., Fourmigué, J.-F., 2017. A review on experience feedback and numerical modeling of packed-bed thermal energy storage systems. *Solar Energy* 153, 628–654.
- Faas, S.E., Thorne, L., Fuchs, E., Gilbersten, N., 1986. 10 MWe Solar Thermal Central Receiver Pilot Plant: Thermal Storage Subsystem Evaluation, June, Final Report. Tech. rep., Sandia National Laboratories.
- Ferchaud, C., Zondag, H., Rubino, A., de Boer, R., 2012. Seasonal sorption heat storage—research on thermochemical materials and storage performance. In: *Proceedings of Heat Powered Cycles Conference*, 10–12 September 2012, Alkmaar, Netherland.
- Fernandez-Torrijos, M., Sobrino, C., Almendros-Ibáñez, J.A., 2017. Simplified model of a dual-media molten-salt thermochemical tank with a multiple layer wall. *Solar Energy* 151, 146–161.
- Flamant, G., 1982. Theoretical and experimental study of radiant heat transfer in a solar fluidized-bed receiver. *AIChE J.* 28 (4), 529–535.
- Flamant, G., Gauthier, D., Benoit, H., Sans, J.-L., Garcia, R., Boissière, B., Ansart, R., Hemati, M., 2013. Dense suspension of solid particles as a new heat transfer fluid for concentrated solar thermal plants: on-sun proof of concept. *Chem. Eng. Sci.* 102, 567–576.
- Flamant, G., Hernandez, D., Bonet, C., Traverse, J.-P., 1980. Experimental aspects of the thermochemical conversion of solar energy; decarbonation of cao3. *Solar Energy* 24 (4), 385–395.
- Flamant, G., Olalde, G., 1983. High temperature solar gas heating comparison between packed and fluidized bed receivers - i. *Solar energy* 31 (5), 463–471.
- Flegkas, S., Birkelbach, F., Winter, F., Freiburger, N., Werner, A., 2018. Fluidized bed reactors for solid-gas thermochemical energy storage concepts-modelling and process limitations. *Energy* 143, 615–623.
- Flueckiger, S., Garimella, S., 2014. Latent heat augmentation of thermochemical energy storage for concentrating solar power – a system-level assessment. *Appl. Energy* 116, 278–287.
- Flueckiger, S., Yang, Z., Garimella, S.V., 2011. An integrated thermal and mechanical investigation of molten-salt thermochemical energy storage. *Appl. Energy* 88, 2098–2105.
- Flueckiger, S.M., Garimella, S.V., 2012. Second-law analysis of molten-salt thermal energy storage in thermochemicals. *Solar Energy* 86, 1621–1631.
- Flueckiger, S.M., Iverson, B.D., Garimella, S.V., Pacheco, J.E., 2014. System-level simulation of a solar power tower plant with thermochemical thermal energy storage. *Appl. Energy* 113, 86–96.
- Fohr, J.-P., Figueiredo, A., 1987. Agricultural solar air collectors: design and performances. *Solar Energy* 38 (5), 311–321.
- Fricker, H.W., 2004. Regenerative thermal storage in atmospheric air system solar power plants. *Energy* 29, 871–881.
- Fujii, I., Tsuchiya, K., Higano, M., Yamada, J., 1985. Studies of an energy storage system by use of the reversible chemical reaction:  $\text{CaO} + \text{H}_2\text{O} \rightleftharpoons \text{Ca}(\text{OH})_2$ . *Solar Energy* 34 (4–5), 367–377.
- Furnas, C.C., 1930. Heat transfer from a gas stream to a bed of broken solids—III, 2. *Ind. Eng. Chem.* 22 (7), 721–731.
- Galione, P., Pérez Segarra, C., Rodríguez, I., Rigola, R., 2015. Multi-layered solid-PCM thermochemical thermal storage concept for CSP plants. numerical analysis and perspectives. *Appl. Energy* 142, 337–351.
- García-Trinián, P., Seville, J., Ansart, R., Benoit, H., Leadbeater, T., Parker, D., 2018. Particle motion and heat transfer in an upward-flowing dense particle suspension: Application in solar receivers. *Chem. Eng. Sci.* 177, 313–322.
- García-Trinián, P., Seville, J., Boissière, B., Ansart, R., Leadbeater, T., Parker, D., 2016. Hydrodynamics and particle motion in upward flowing dense particle suspensions: application in solar receivers. *Chem. Eng. Sci.* 146, 346–356.
- Geissbühler, L., Kolman, M., Zanganeh, G., Haselbacher, A., Steinfeld, A., 2016. Analysis of industrial-scale high-temperature combined sensible/latent thermal energy storage. *Appl. Therm. Eng.* 101, 657–668.
- Geldart, D., 1973. Types of gas fluidization. *Powder Technol.* 7 (5), 285–292.
- Gil, A., Medrano, M., Martorell, I., Lázaro, A., Dolado, P., Zalba, B., Cabeza, L.F., 2010. State of the art on high temperature thermal energy storage for power generation. Part 1 - concepts, materials and modellization. *Renew. Sustain. Energy Rev.* 14 (1), 31–55.
- Gimenez-Gavarrell, P., Ferrer, S., 2017. Glass encapsulated phase change materials for high temperature thermal energy storage. *Renew. Energy* 107, 497–507.
- Gomez-García, F., Gauthier, D., Flamant, G., 2017. Design and performance of a multi-stage fluidised bed heat exchanger for particle-receiver solar power plants with storage. *Appl. Energy* 190, 510–523.
- Gómez-Hernández, J., Laporte, M., Villa-Briongos, J., Santana, D., 2017. Ground solar receptor. X Congreso Internacional de Ingeniería Termodinámica, 28–30 de June. Lleida, Spain.

- Grace, J.R., 1986. Contacting modes and behaviour classification of gas-solid and other two-phase suspensions. *Can. J. Chem. Eng.* 64 (3), 353–363.
- Greif, R., Crowe, C., 1987. Gas-particle flow within a high temperature solar cavity receiver including radiation heat transfer. *J. Solar Energy Eng.* 109 (2), 134–142.
- Gupta, S., Chaube, R., Upadhyay, S., 1974. Fluid-particle heat transfer in fixed and fluidized beds. *Chem. Eng. Sci.* 29 (3), 839–843.
- Hanchen, M., Bruckner, S., Steinfeld, A., 2011. High-temperature thermal storage using a packed bed of rocks - heat transfer analysis and experimental validation. *Appl. Therm. Eng.* 31, 1798–1806.
- Helwa, N., Abdel Rehim, Z., 1997. Experimental study of the performance of solar dryers with pebble beds. *Energy Sour.* 19 (6), 579–591.
- Ho, C.K., 2016. A review of high-temperature particle receivers for concentrating solar power. *Appl. Therm. Eng.* 109, 958–969.
- Ho, C.K., 2017. Advances in central receivers for concentrating solar applications. *Solar Energy* 152, 38–56.
- Hruby, J., 1986. *Technical Feasibility Study of a Solid Particle Solar Central Receiver for High Temperature Applications*, Tech. rep. Sandia National Labs., Livermore, CA, USA.
- Hughes, P.J., Klein, S.A., Close, D.J., 1976. Packed bed thermal storage models for solar air heating and cooling systems. *J. Heat Transfer* 98 Ser C (2), 336–338.
- Ismail, K.A.R., Stuginsky Jr., R., 1999. A parametric study on possible fixed bed models for PCM and sensible heat storage. *Appl. Therm. Eng.* 19 (7), 757–788.
- Izquierdo-Barrientos, M.A., Fernández-Torrijos, M., Almendros-Ibáñez, J.A., Sobrino, C., 2016a. Experimental study of fixed and fluidized beds of PCM with an internal heat exchanger. *Appl. Therm. Eng.* 106, 1042–1051.
- Izquierdo-Barrientos, M.A., Sobrino, C., Almendros-Ibáñez, J.A., 2013. Thermal energy storage in a fluidized bed of PCM. *Chem. Eng. J.* 230, 573–583.
- Izquierdo-Barrientos, M.A., Sobrino, C., Almendros-Ibáñez, J.A., 2015a. Energy storage with PCM in fluidized beds: modeling and experiments. *Chem. Eng. J.* 264, 497–505.
- Izquierdo-Barrientos, M.A., Sobrino, C., Almendros-Ibáñez, J.A., 2015b. Experimental heat transfer coefficients between a surface and fixed and fluidized beds with PCM. *Appl. Therm. Eng.* 78, 373–379.
- Izquierdo-Barrientos, M.A., Sobrino, C., Almendros-Ibáñez, J.A., 2016b. Modeling and experiments of energy storage in a packed bed with PCM. *Int. J. Multiph. Flow* 86, 1–9.
- Izquierdo-Barrientos, M.A., Sobrino, C., Almendros-Ibáñez, J.A., 2016c. Modeling the heat transfer coefficient between a surface and fixed and fluidized beds with phase change material. *J. Heat Transfer* 138 (7), 072001.
- Izquierdo-Barrientos, M.A., Sobrino, C., Almendros-Ibáñez, J.A., Barreneche, C., Ellis, N., Cabeza, L.F., 2016d. Characterization of granular phase change materials for thermal energy storage applications in fluidized beds. *Appl. Energy* 181, 310–321.
- Jain, D., 2005. Modeling the performance of greenhouse with packed bed thermal storage on crop drying application. *J. Food Eng.* 71 (2), 170–178.
- Jalalzadeh-Azar, A., Steele, W., Adebijoyi, G., 1996. Heat transfer in a high-temperature packed bed thermal energy storage system - roles of radiation and intraparticle conduction. *J. Energy Resour. Technol.* 118 (1), 50–57.
- Jefferson, C.P., 1972. Prediction of breakthrough curves in packed beds: I. Applicability of single parameter models. *AIChE J.* 18 (2), 409–416.
- Johannes, K., Kuznik, F., Hubert, J.-L., Durier, F., Obrecht, C., 2015. Design and characterisation of a high powered energy dense zeolite thermal energy storage system for buildings. *Appl. Energy* 159, 80–86.
- Kanzawa, A., Arai, Y., 1981. Thermal energy storage by the chemical reaction augmentation of heat transfer and thermal decomposition in the  $\text{CaO}/\text{Ca}(\text{OH})_2$  powder. *Solar Energy* 27 (4), 289–294.
- Karaki, S., Armstrong, P., Bechtel, T.N., 1977. *Evaluation of a Residential Solar Air Heating and Nocturnal Cooling System*. Solar Energy Applications Laboratory, Colorado State University.
- Karthikeyan, S., Solomon, G.R., Kumaresan, V., Velraj, R., 2014. Parametric studies on packed bed storage unit filled with PCM encapsulated spherical containers for low temperature solar air heating applications. *Energy Convers. Manage.* 78, 74–80.
- Karthikeyan, S., Velraj, R., 2012. Numerical investigation of packed bed storage unit filled with pcm encapsulated spherical containers—a comparison between various mathematical models. *Int. J. Therm. Sci.* 60, 153–160.
- Kearney, D., Herrmann, U., Nava, P., Kelly, B., Mahoney, R., Pacheco, J., Cable, R., Potrovitza, N., Blake, D., Price, H., 2003. Assessment of a molten salt heat transfer fluid in a parabolic trough solar field. *J. Solar Energy Eng.* 125 (2), 170–176.
- Kearny, D., Herrmann, U., Nava, P., Kelly, B., Mahoney, R., Pacheco, J., Cable, R., Potrovitza, N., Blake, D., Price, H., 2003. Assessment of a molten salt heat transfer fluid in a parabolic trough solar field. *J. Solar Energy Eng.* 125 (2), 170–176.
- Klein, S., Beckman, W., Mitchell, J., 2017. TRNSYS 18. a TRAnsiEnt SYstem Simulation program. Solar Energy Laboratory, Univ of Wisconsin-Madison.
- Kolb, G.J., 2011. Evaluation of annual performance of 2-tanks and thermocline thermal storage systems for trough plants. *J. Solar Energy Eng.* 133, 031023.
- Kolb, G.J., Hassani, V., 2006. Performance analysis of thermocline energy storage proposed for the 1 mw saguaro solar trough plant. In: *Proceedings of ISEC 2006*. ASME International Solar Energy Conference, July. Denver, CO, p. 99005.
- Krese, G., Butala, V., Strith, U., et al., 2018. Thermochemical seasonal solar energy storage for heating and cooling of buildings. *Energy Build.* 164, 239–253.
- Krupiczka, R., 1967. Analysis of thermal conductivity in granular materials. *Int. Chem. Eng.* 7 (1), 122–144.
- Kuhn, J.K., Vonfuchs, G., Zob, A., 1980. *Developing and Upgrading of Solar System Thermal Energy Storage Simulation Models*. NASA STI/Recon Technical Report N 81.
- Kunii, D., Levenspiel, O., 1991. *Fluidization Engineering*. Butterworth-Heinemann.
- Liao, Z., Zhao, G., Xu, C., Yang, C., Jin, Y., Ju, X., Du, X., 2018. Efficiency analyses of high temperature thermal energy storage systems of rocks only and rock-pcm capsule combination. *Solar Energy* 162, 153–164.
- Linder, M., 2015. Using thermochemical reactions in thermal energy storage systems. In: Cabeza, L.F. (Ed.), *Advances in Thermal Energy Storage Systems. Methods and Applications*. Woodhead Publishing Series in Energy, vol. 66 Elsevier.
- Maaliou, O., McCoy, B., 1985. Optimization of thermal energy storage in packed columns. *Solar Energy* 34 (1), 35–41.
- Mahfoudi, N., El Ganaoui, M., Moumni, A., 2015. Heat storage potential of the fluidized bed technology: hydrodynamics and thermal analysis. In: *International Conference on Materials and Energy*, 19–22 of May. Tetouan, Morocco.
- Manfrida, G., Secchi, R., Stańczyk, 2016. Modelling and simulation of phase change material latent heat storages applied to a solar-powered organic rankine cycle. *Appl. Energy* 179, 378–388.
- Mao, Q., 2016. Recent developments in geometrical configurations of thermal energy storage for concentrating solar power plant. *Renew. Sustain. Energy Rev.* 59, 320–327.
- Marugán-Cruz, C., Flores, O., Santana, D., García-Villalba, M., 2016. Heat transfer and thermal stresses in a circular tube with a non-uniform heat flux. *Int. J. Heat Mass Transfer* 96, 256–266.
- Matsubara, K., Kazuma, Y., Sakurai, A., Suzuki, S., Soon-Jae, L., Kodama, T., Gokon, N., Seok, C.H., Yoshida, K., 2014. High-temperature fluidized receiver for concentrated solar radiation by a beam-down reflector system. *Energy Proc.* 49, 447–456.
- McTigue, J.D., White, A.J., 2016. Segmented packed beds for improved thermal energy storage performance. *IET Renew. Power Gener.* 10 (10), 1498–1505.
- Megahed, I.E., Elsayed, M.M., El-Refae, M.M., 1988. Fluidized bed-solar concentrator thermal storage system performance. *Heat Mass Transfer* 23 (4), 187–194.
- Meier, A., Winkler, C., Wullemin, D., 1991. Experiment for modeling high temperature rock bed storage. *Solar Energy Mater.* 24, 255–264.
- Milián, Y.E., Gutiérrez, A., Grágeda, M., Ushak, S., 2017. A review on encapsulation techniques for inorganic phase change materials and the influence on their thermo-physical properties. *Renew. Sustain. Energy Rev.* 73, 983–999.
- Mumma, S., Marvin, W., 1976. A method of simulating the performance of a pebble bed thermal energy storage and recovery system. In: *American Society of Mechanical Engineers and American Institute of Chemical Engineers, Heat Transfer Conference*, August 9–11. ASME, St. Louis, Mo. (6 p.).
- Nallusamy, N., Sampath, S., Velraj, R., 2007. Experimental investigation on a combined sensible and latent heat storage system integrated with constant/varying (solar) heat sources. *Renew. Energy* 32, 1206–1227.
- Nallusamy, N., Velraj, R., 2009. Numerical and experimental investigation on a combined sensible and latent heat storage unit integrated with solar water heating system. *J. Solar Energy Eng.* 131, 041002.
- Navarro, L., Barreneche, C., Castell, A., Redpath, D.A., Griffiths, P.W., Cabeza, L.F., 2017. High density polyethylene spheres with PCM for domestic hot water applications: water tank and laboratory scale study. *J. Energy Stor.* 13, 262–267.
- Nsofor, E.C., Adebijoyi, George, A., 2001. Measurements of the gas-particle convective heat transfer coefficient in a packed bed for high-temperature energy storage. *Exp. Therm. Fluid Sci.* 24, 1–9.
- N'tsoukpoe, K.E., Liu, H., Le Pierrès, N., Luo, L., 2009. A review on long-term sorption solar energy storage. *Renew. Sustain. Energy Rev.* 13 (9), 2385–2396.
- Nunes, V., Queirós, C., Lourenço, M., Santos, F., de Castro, C.N., 2016. Molten salts as engineering fluids—a review: part i. molten alkali nitrates. *Appl. Energy* 183, 603–611.
- Oró, E., Chiu, J., Martin, V., Cabeza, L.F., 2013. Comparative study of different numerical models of packed bed thermal energy storage systems. *Appl. Therm. Eng.* 50 (1), 384–392.
- Oztop, H., Bayrak, F., Hepbasli, A., 2013. Energetic and exergetic aspects of solar air heating (solar collector) systems. *Renew. Sustain. Energy Rev.* 21, 59–83.
- Ozturk, H., Bascetinçelik, A., 2003. Energy and exergy efficiency of a packed-bed heat storage unit for greenhouse heating. *Biosyst. Eng.* 86 (2), 231–245.
- Pacheco, J.E., Showalter, S.K., Kolb, W.J., 2002. Development of a molten-salt thermocline thermal storage system for parabolic trough plants. *J. Solar Energy Eng.* 124 (2), 153–159.
- Pan, Z., Zhao, C., 2017. Gas-solid thermochemical heat storage reactors for high-temperature applications. *Energy* (130), 155–173.
- Pardo, P., Anxionnaz-Minvielle, Z., Rougé, S., Cognet, P., Cabassud, M., 2014a.  $\text{Ca}(\text{OH})_2/\text{CaO}$  reversible reaction in a fluidized bed reactor for thermochemical heat storage. *Solar Energy* 107, 605–616.
- Pardo, P., Deydier, A., Anxionnaz-Minvielle, Z., Rougé, S., Cabassud, M., Cognet, P., 2014b. A review on high temperature thermochemical heat energy storage. *Renew. Sustain. Energy Rev.* 32, 591–610.
- Pelay, U., Luo, L., Fan, Y., Stitou, D., Rood, M., 2017. Thermal energy storage systems for concentrated solar power plants. *Renew. Sustain. Energy Rev.* 79, 82–100.
- Prieto, C., Cooper, P., Fernández, A.I., Cabeza, L.F., 2016. Review of technology: thermochemical energy storage for concentrated solar power plants. *Renew. Sustain. Energy Rev.* 60, 909–929.
- Rady, M., 2009a. Granular phase change materials for thermal energy storage: experiments and numerical simulations. *Appl. Therm. Eng.* 29 (14), 3149–3159.
- Rady, M., 2009b. Thermal performance of packed bed thermal energy storage units using multiple granular phase change composites. *Appl. Energy* 86 (12), 2704–2720.
- Rees, A., Davidson, J., Dennis, J., Fennell, P., Gladden, L., Hayhurst, A., Mantle, M., Müller, C., Sederman, A., 2006. The nature of the flow just above the perforated plate distributor of a gas-fluidised bed, as imaged using magnetic resonance. *Chem. Eng. Sci.* 61 (18), 6002–6015.
- Rodríguez, J.M., Sánchez, D., Martínez, G.S., Ikken, B., et al., 2016. Techno-economic assessment of thermal energy storage solutions for a 1 mwe csp-orc power plant. *Solar Energy* 140, 206–218.
- Rodríguez-Sánchez, M.R., Soria-Verdugo, A., Almendros-Ibáñez, J.A., Acosta-Iborra, A., Santana, D., 2014. Thermal design guidelines of solar power towers. *Appl. Therm.*

- Eng. 63 (1), 428–438.
- Rosen, M.A., 2001. The exergy of stratified thermal energy storages. *Solar Energy* 71 (3), 173–185.
- Rougé, S., Criado, Y.A., Soriano, O., Abanades, J.C., 2017. Continuous cao/ca (oh) 2 fluidized bed reactor for energy storage: first experimental results and reactor model validation. *Indust. Eng. Chem. Res.* 56 (4), 844–852.
- Saez, A.E., McCoy, B.J., 1982. Dynamic response of a packed bed thermal storage system—a model for solar air heating. *Solar Energy* 29 (3), 201–206.
- Saitoh, T., Hirose, K., 1986. High-performance phase-change thermal energy storage using spherical capsules. *Chem. Eng. Commun.* 41, 39–58.
- Salatino, P., Ammendola, P., Bareschino, P., Chirone, R., Solimene, R., 2016. Improving the thermal performance of fluidized beds for concentrated solar power and thermal energy storage. *Powder Technol.* 290, 97–101.
- Saxena, A., Varunb, El-Sebaili, A., 2015. A thermodynamic review of solar air heaters. *Renew. Sustain. Energy Rev.* 43, 863–890.
- Schaube, F., Kohzer, A., Schütz, J., Wörner, A., Müller-Steinhagen, H., 2013. De-and re-hydration of ca (oh) 2 in a reactor with direct heat transfer for thermo-chemical heat storage. part a: Experimental results. *Chem. Eng. Res. Des.* 91 (5), 856–864.
- Schumann, T., 1929. Heat transfer: a liquid flowing through a porous prism. *J. Frank. Inst.* 208 (3), 405–416.
- Singh, H., Saini, R., Saini, J., 2010. A review on packed bed solar energy storage systems. *Renew. Sustain. Energy Rev.* 14 (3), 1059–1069.
- Singh, H., Saini, R., Saini, J., 2013. Performance of a packed bed solar energy storage system having large sized elements with low void fraction. *Solar Energy* 87 (1), 22–34.
- Singh, P., Deshpandey, S., Jena, P., 2015. Thermal performance of packed bed heat storage system for solar air heaters. *Energy Sustain. Develop.* 29, 112–117.
- Singh, R., Saini, R., Saini, J., 2006. Nusselt number and friction factor correlations for packed bed solar energy storage system having large sized elements of different shapes. *Solar Energy* 80 (7), 760–771.
- Singh, R., Saini, R., Saini, J., 2009. Models for predicting thermal performance of packed bed energy storage system for solar air heaters - a review. *Open Fuels Energy Sci. J.* 2, 47–53.
- Solé, A., Martorell, I., Cabeza, L.F., 2015. State of the art on gas–solid thermochemical energy storage systems and reactors for building applications. *Renew. Sustain. Energy Rev.* 47, 386–398.
- Sozen, Z.Z., Grace, J.R., Pinder, L.P., 1988. Thermal energy storage by agitated capsules of phase change material. 1. Pilot scale experiments. *Indust. Eng. Chem. Res.* 27, 679–684.
- Srivastva, U., Malhotra, R., Kaushik, S., 2017. Review of heat transport properties of solar heat transfer fluids. *J. Therm. Anal. Calor.* 130 (2), 605–621.
- Ströhle, S., Haselbacher, A., Jovanovic, Z., Steinfeld, A., 2016. The effect of the gas–solid contacting pattern in a high-temperature thermochemical energy storage on the performance of a concentrated solar power plant. *Energy Environ. Sci.* 9 (4), 1375–1389.
- Ströhle, S., Haselbacher, A., Jovanovic, Z., Steinfeld, A., 2017. Upgrading sensible-heat storage with a thermochemical storage section operated at variable pressure: an effective way toward active control of the heat-transfer fluid outflow temperature. *Appl. Energy* 196, 51–61.
- Ströhle, S., Haselbacher, A., Jovanovic, Z.R., Steinfeld, A., 2014. Transient discrete-granule packed-bed reactor model for thermochemical energy storage. *Chem. Eng. Sci.* 117, 465–478.
- Suárez, F., Luzzi, C.D., Mariani, N.J., Barreto, G.F., 2017. Effective parameters for conductive contributions to radial heat transfer in fixed beds under stagnant conditions. *Chem. Eng. Res. Des.* 119, 245–262.
- Tomar, V., Tiwari, G., Norton, B., 2017. Solar dryers for tropical food preservation: thermophysics of crops, systems and components. *Solar Energy* 154, 2–13.
- Tregambi, C., Chirone, R., Montagnaro, F., Salatino, P., Solimene, R., 2016. Heat transfer in directly irradiated fluidized beds. *Solar Energy* 129, 85–100.
- Tyagi, V., Panwar, N., Rahim, N., Kothari, R., 2012. Review on solar air heating system with and without thermal energy storage system. *Renew. Sustain. Energy Rev.* 16 (4), 2289–2303.
- Van Antwerpen, W., Du Toit, C., Rousseau, P., 2010. A review of correlations to model the packing structure and effective thermal conductivity in packed beds of mono-sized spherical particles. *Nucl. Eng. Des.* 240 (7), 1803–1818.
- Wakao, N., Kagueli, S., Funazkri, T., 1979. Effect of fluid dispersion coefficients on particle-to-fluid heat transfer coefficients in packed beds: correlation of Nusselt numbers. *Chem. Eng. Sci.* 34 (3), 325–336.
- Wang, T., Mantha, D., Reddy, R.G., 2013. Novel low melting point quaternary eutectic system for solar thermal energy storage. *Appl. Energy* 102, 1422–1429.
- Webb, R.L., 1979. Toward a common understanding of the performance and selection of roughness for forced convection. *Stud. Heat Transfer: Festschrift ERG Eckert* 257–272.
- Wei, G., Wang, G., Xu, C., Ju, X., Xing, L., Du, X., Yang, Y., 2018. Selection principles and thermophysical properties of high temperature phase change materials for thermal energy storage: a review. *Renew. Sustain. Energy Rev.* 81, 1771–1786.
- White, A., McTigue, J., Markides, C., 2014. Wave propagation and thermodynamic losses in packed-bed thermal reservoirs for energy storage. *Appl. Energy* 130, 648–657.
- White, A.J., 2011. Loss analysis of thermal reservoirs for electrical energy storage schemes. *Appl. Energy* 88 (11), 4150–4159.
- White, A.J., McTigue, J.D., Markides, C.N., 2016. Analysis and optimisation of packed-bed thermal reservoirs for electricity storage applications. *Proc. Inst. Mech. Eng., Part A: J. Power Energy* 230 (7), 739–754.
- Wokon, M., Kohzer, A., Linder, M., 2017. Investigations on thermochemical energy storage based on technical grade manganese-iron oxide in a lab-scale packed bed reactor. *Solar Energy* 153, 200–214.
- Wu, M., Xu, C., He, Y., 2014. Dynamic thermal performance analysis of a molten-salt packed-bed thermal energy storage system using PCM capsules. *Appl. Energy* 121, 184–195.
- Wu, M., Xu, C., He, Y., 2016. Cyclic behaviors of the molten-salt packed-bed thermal storage system filled with cascaded phase change material capsules. *Appl. Therm. Eng.* 93, 1061–1073.
- Wu, S., Fang, G., 2011. Dynamic performances of solar heat storage system with packed bed using myristic acid as phase change material. *Energy Build.* 43 (5), 1091–1096. < <http://www.rubitherm.eu> >, 2017 (last accessed october, 2017).
- Xia, L., Zhang, P., Wang, R.Z., 2010. Numerical heat transfer analysis of the packed bed latent heat storage system based on an effective packed bed model. *Energy* 35 (5), 2022–2032.
- Xu, B., Li, P.-W., Chan, C., 2012a. Extending the validity of lumped capacitance method for large Biot number in thermal storage application. *Solar Energy* 86 (6), 1709–1724.
- Xu, C., Zhifeng, W., He, Y., Li, X., Bai, F., 2012b. Sensitivity analysis of the numerical study on the thermal performance of a packed-bed molten salt thermochemical storage system. *Appl. Energy* 92, 65–75.
- Yadav, D., Banerjee, R., 2016. A review of solar thermochemical processes. *Renew. Sustain. Energy Rev.* 54, 497–532.
- Yagi, S., Kunii, D., 1957. Studies on effective thermal conductivities in packed beds. *AIChE J.* 3 (3), 373–381.
- Yagi, S., Kunii, D., Wakao, N., 1960. Studies on axial effective thermal conductivities in packed beds. *AIChE J.* 6 (4), 543–546.
- Yan, J., Zhao, C., 2016. Experimental study of cao/ca (oh) 2 in a fixed-bed reactor for thermochemical heat storage. *Appl. Energy* 175, 277–284.
- Yang, Z., Garimella, S.V., 2010a. Molten-salt thermal energy storage in thermoclines under different environmental boundary conditions. *Appl. Energy* 87, 3322–3329.
- Yang, Z., Garimella, S.V., 2010b. Thermal analysis of solar thermal energy storage in a molten-salt thermocline. *Solar Energy* 84, 974–985.
- Yang, Z., Garimella, S.V., 2013. Cyclic operation of molten-salt thermal energy storage in thermoclines for solar power plants. *Appl. Energy* 103, 256–265.
- Yataganbaba, A., Ozkahraman, B., Kurtbas, I., 2017. Worldwide trends on encapsulation of phase change materials: a bibliometric analysis (1990–2015). *Appl. Energy* 185, 720–731.
- Yu, N., Wang, R., Wang, L., 2013. Sorption thermal storage for solar energy. *Prog. Energy Combust. Sci.* 39 (5), 489–514.
- Zanganeh, G., Khanna, R., Walser, C., Pedretti, A., Haselbacher, A., Steinfeld, A., 2015a. Experimental and numerical investigation of combined sensible – latent heat for thermal energy storage at 575° C and above. *Solar Energy* 114, 77–90.
- Zanganeh, G., Pedretti, A., Haselbacher, A., Steinfeld, A., 2015b. Design of packed bed thermal energy storage systems for high-temperature industrial process heat. *Appl. Energy* 137, 812–822.
- Zanganeh, G., Pedretti, A., Zavattoni, S., Barbato, M., Steinfeld, A., 2012. Packed-bed thermal storage for concentrated solar power–pilot-scale demonstration and industrial-scale design. *Solar Energy* 86 (10), 3084–3098.
- Zavattoni, S.A., Barbato, M.C., Pedretti, A., Zanganeh, G., 2015. Single-tank TES system-transient evaluation of thermal stratification according to the second-law of thermodynamics. *Energy Proc.* 69, 1068–1077.
- Zhang, H., Benoit, H., Gauthier, D., Degrevè, J., Baeyens, J., López, I.P., Hemati, M., Flamant, G., 2016. Particle circulation loops in solar energy capture and storage: Gas–solid flow and heat transfer considerations. *Appl. Energy* 161, 206–224.
- Zhang, H., Benoit, H., Perez-Lopez, I., Flamant, G., Tan, T., Baeyens, J., 2017. High-efficiency solar power towers using particle suspensions as heat carrier in the receiver and in the thermal energy storage. *Renew. Energy* 111, 438–446.
- Zhao, B.-c., Cheng, M.-s., Liu, C., Dai, Z.-m., 2017. Cyclic thermal characterization of a molten-salt packed-bed thermal energy storage for concentrating solar power. *Appl. Energy* 195, 761–773.
- Zhao, C.Y., Wu, Z.G., 2011. Thermal property characterization of low melting-temperature ternary nitrate salt mixture for thermal energy storage systems. *Solar Energy Mater. Solar Cells* 95, 3341–3346.
- Zondag, H., van Essen, M., Bleijendaal, L., Cot, J., Schuitema, R., van Helden, W., Planje, W., Epema, T., Oversloot, H., 2008. Comparison of reactor concepts for thermochemical storage of solar heat. In: *Proceeding of IRES*; 24–25 November, 2008. Berlin, Germany.